Louisiana State University
LSU Digital Commons

LSU Master's Theses | Graduate School

2004

Effects of corrosion prevention compounds and overload induced residual stress field on fatigue life in aluminum alloy

Jin Hee Park
Louisiana State University and Agricultural and Mechanical College

Follow this and additional works at: https://digitalcommons.lsu.edu/gradschool_theses

 Part of the Mechanical Engineering Commons

Recommended Citation
Park, Jin Hee, "Effects of corrosion prevention compounds and overload induced residual stress field on fatigue life in aluminum alloy" (2004). *LSU Master's Theses*. 554.
https://digitalcommons.lsu.edu/gradschool_theses/554

This Thesis is brought to you for free and open access by the Graduate School at LSU Digital Commons. It has been accepted for inclusion in LSU Master's Theses by an authorized graduate school editor of LSU Digital Commons. For more information, please contact gradetd@lsu.edu.

EFFECTS OF CORROSION PREVENTION COMPOUNDS AND OVERLOAD INDUCED RESIDUAL STRESS FIELD ON FATIGUE LIFE IN ALUMINUM ALLOY

A Thesis

Submitted to the Graduate Faculty of the
Louisiana State University and
Agricultural and Mechanical College
in partial fulfillment of the
requirements for the degree of
Master of Science in Mechanical Engineering

in

The Department of Mechanical Engineering

by
Jin Hee Park
B.E., Andong National University, Korea, 2001
August 2004

ACKNOWLEDGMENTS

I would like to express my sincere gratitude to my major professor, Dr. Muhammad A. Wahab for his technical advice, support and guidance throughout this thesis work. His wisdom is really recognized. Many thanks are also owed to Dr. Su-Seng Pang for his support during my thesis work. I thank them for their belief in my abilities and their unweavering support from the beginning. I also would like to thank Dr. Dorel Moldovan for serving on my committee.

A special thanks is also owed to Dr. Samuel Ibekwe and Dr. Parviz S. Razi for allowing me to use their experimental facilities in the Department of Mechanical Engineering of Southern University and A&M College. Also, I want to thank Ms. Diane Morgan, the Departmental graduate secretary and Mr. Charles Smith, a research specialist in Mechanical Engineering for their kindness & support. Special thanks goes to the senior graduate students for their help from the day I arrived here. This work would not have been completed without their help. I appreciate their support. This work was sponsored by Louisiana Board of Regents LaSPACE Grant. Financial support received from both LaSPACE Grant and Louisiana State University is acknowledged with thanks.

Last but not least, I would like to thank my parents, as well as my younger brother, Sehee Park, for their constant understanding and love. In addition, I want to thank Yoonhee Lee for her patience, understanding and standing by me throughout my studies.

TABLE OF CONTENTS

LIST OF TABLES

LIST OF FIGURES

GLOSSARY OF SYMBOLS

Roman Notations

a	half crack length
a_i	initial crack length
a_f	final crack length
$\Delta a/\Delta N$	crack growth rate (crack length per cycle)
b	half width of specimen, maximum possible crack length
C	fatigue crack growth coefficient in Paris's equation
CA	constant amplitude
CPC	corrosion-prevention-compounds
E	elastic modulus
f	frequency
FCG	fatigue crack growth
h	half height of test specimen
K	stress intensity factor, a fracture mechanics parameter
K_c	plane stress fracture toughness
K_{IC}	plane strain fracture toughness
k_t	stress concentration factor
ΔK	range of stress intensity factor
ΔK_{eff}	effective stress intensity range
m	fatigue crack growth exponent in Paris's equation
N	number of cycles
N_f	final fatigue life
OL	overload
OLR	overload ratio
R	stress ratio for cyclic loading (minimum stress/ maximum stress)
r_p	radius of plastic zone at the crack tip
S	nominal stress, based on gross area
S_{op}	crack opening stress
ΔS	range of nominal stress
ΔS_{eff}	effective stress range
t	thickness
VA	variable amplitude loading
Y	geometric crack configuration factor

Greek Notations

α	relative crack length aspect ratio ($\alpha = a / b$)
β	geometry correction factor
σ	normal stress at a point
σ_y	yield strength
σ_u	ultimate tensile strength

Subscripts;	**meaning**
a	amplitude
c	critical
f	final
i	initial
m	mean
max	maximum
min	minimum

ABSTRACT

Corrosion-Prevention Compounds (CPC) are commonly used to prevent corrosion in the aircraft industry. The presence of corrosive environment (salt-fog, water-fog, even dry air) on aircraft structures has detrimental effects on the integrity of aircraft components which reduces the fatigue life and may accelerate the crack growth rate in the structures. This thesis work is aimed at identifying the effect of CPC and corrosion fatigue on the fatigue life of test specimen. This study describes the results of an experimental study on aluminum alloy 2024-T3 with center-crack specimen to investigate the effect of CPC on fatigue life. Generally, these compounds contain a volatile solvent, corrosion inhibitors, and a barrier film such as grease or wax. The mechanism of corrosion fatigue is studied with the application of CPC. The corrosion fatigue with the presence of water-vapor reduces the total fatigue life. The fatigue life with the CPC treatment is shown to increase the fatigue life due to the protection from the corrosive environment (water-vapor). Test results are obtained for various stress ratios and frequencies; with and without the CPC treatment, under constant amplitude fatigue loading in water vapor.

Second objective of thesis work is to investigate the effect of periodic overloads on the fatigue life under constant amplitude fatigue loading. The results show that the fatigue life increases due to the periodic overloads in 2024-T3 aluminum alloy. The interactions between overloads that are controlled by the spacing cycles between overloads and overload ratios are also examined. The maximum interaction to achieve a maximum increase in fatigue life is observed that the best spacing cycle between overloads has been found to be in the range from 400 to 2000 cycles for an overload ratio of 1.7.

Micrograph of the failed specimen surface is examined by using Scanning Electron Microscope (SEM) to investigate the failure processes and the formation of crack surface along the crack front in the crack growth surface. It is indicated that two distinct failure modes are found. These are ductile fracture and brittle fracture. The transition from the ductile mode to brittle mode is observed in this thesis work.

CHAPTER 1. INTRODUCTION

1.1 History of Corrosion Fatigue and Overload Induced Residual Stress Field

Twenty to thirty years ago, a major focus was on maintaining aircraft structures in their prime (Rolfe and Barsom, 1977, & Schijve, 1976 etc.); today, the emphasis is on the care of the aged and extension of service lives beyond their design life (Newman, 1997, Tür and Vardar, 1996, & Schijve, 1985, etc.). Life extension of aircraft structures has become the major growth sector of the aerospace industry. The bulk of that sector is concentrated on two major fronts: the fight against fatigue and the control of corrosion. The coupled effects of fatigue and corrosion largely determine the service life of our transportation system and infrastructure complex.

Over the years, structural engineers and corrosion scientists have made significant inroads into understanding, predicting and monitoring both corrosion and fatigue. Unfortunately there are many parts of the airframe structure, e.g. fuselage lap joints and wing spar caps, that are subject to simultaneous corrosion and fatigue. The effect of their combined attack on the durability of the structure is still a relatively unknown factor.

One important example is the case of mechanically fastened joints, such as wing and fuselage lap splices, which are treated with Corrosion Prevention Compounds (CPC) on the inner faying surfaces of the panels. Experimental studies indicate that while Corrosion Prevention Compounds (CPC) are very effective in preventing corrosion within joint, in many instances they have also significantly reduced their fatigue life (Hinton, et al., 1996 & Komorowski, et al., 1996 & Rudy Dhamari, et al., 1999 & Krishnakumar Shankar, 2002). This is due to the lubricative effect of oil and wax based Corrosion Prevention Compounds that reduce the friction between faying surfaces, consequently increasing the bearing load on the fasteners, which reduces the fatigue life of the joints. However, there is still debate on this issue. In some cases no reduction in fatigue life has been observed. These disparities have been attributed to variations in frequency or load range and so on. But, there is also a beneficial effect of Corrosion Prevention Compounds on fatigue life. The presence of Corrosion Prevention Compounds at the crack tip can influence the rate of crack growth in the specimens directly by dispelling moisture from environment.

The second part of this thesis work relates to the effect of periodic overloads during constant cycling amplitude loadings on the fatigue life. The loading condition is varied significantly in real service condition. Overload can occur in service situations. Overload is a high peak stress under variable amplitude loading. The residual stress induced by overload has a beneficial effect on crack growth. The crack growth retardation due to one overload has been widely investigated (Dahl and Roth, 1979, & Schijve, 1973) in those studies. The crack growth rate was reduced after overload. In other words, the fatigue life was increased due to overload. Crack growth analysis for variable amplitude loadings is not possible without an account of retardation effects. But, few studies relating to periodic overloads are available. Therefore, in this thesis work an experimental program was undertaken to study the effect of periodic overloads on fatigue life.

1.2 Mechanism of Corrosion Fatigue

The combined effect of treatment with CPC on the corrosion fatigue life would be a compromise between the beneficial effect (exclusion of moisture and prevention of oxidation at the crack tip) and the detrimental effect of the reduced friction between fraying surfaces (due to the lubricative effect of the corrosion prevention itself). To understand this complex conflicting phenomena, this research will study the effect of CPC on the crack growth behavior in center pre-crack aluminum alloy (2024-T3) specimens under environmental conditions (water-vapor) and the influence of stress level, frequency and stress ratios on this effect. These studies about the synergistic actions of corrosion and fatigue, however, have produced diverse and wide range results. The reason is partly due to the large number of variables involved with this type of material behavior. The exact degree to which corrosion affects fatigue life depends on factors that influence fatigue such as stress level, frequency, stress amplitude, stress ratio and stress history, as well as on corrosion parameters such as the type of environments (vacuum, dry air, water-vapor, salt-vapor), and exposure time. Their mutual interactions on fatigue life will be mentioned in Chapter 2.

But, in general the exposure to corrosive environment either prior to fatigue or during the cyclic loading significantly reduces the life of the component. The primary characteristics of corrosion fatigue life are that the crack growth rates can be substantially higher in the corrosive environment, because it reduces the fatigue life of crack initiation or it increases the crack growth rate or both.

A general survey of a fatigue prediction scenario is given in Figure 1.1. All aspects of the input information have to be used for predictions on fatigue life and crack growth. A pertinent question is: Do we have reliable prediction models? If so, do we obtain accurate indications of the fatigue behavior of a structure in service? Is it desirable to verify the predictions by laboratory fatigue experiments? Are the results from standard fatigue specimens good to use in real structures? If not, what modification do we need? An evaluation of these questions requires a fundamental understanding of the fatigue mechanisms occurring in structural materials under conditions applicable to the real structure in service conditions.

The aim of this thesis work is to develop further understanding of fatigue life and to predict fatigue life. The emphasis is on the effect of environments (dry air, water vapor with or without Corrosion Prevention Compounds) and loading conditions (frequency, stress ratio) on the fatigue life. Also, the effect of CPC (LPS-3 Heavy duty corrosion inhibitor) on fatigue life under corrosive environment is being studied. The above work has been carried out experimentally in this thesis work. It is useful to consider the fatigue life as consisting of two periods:

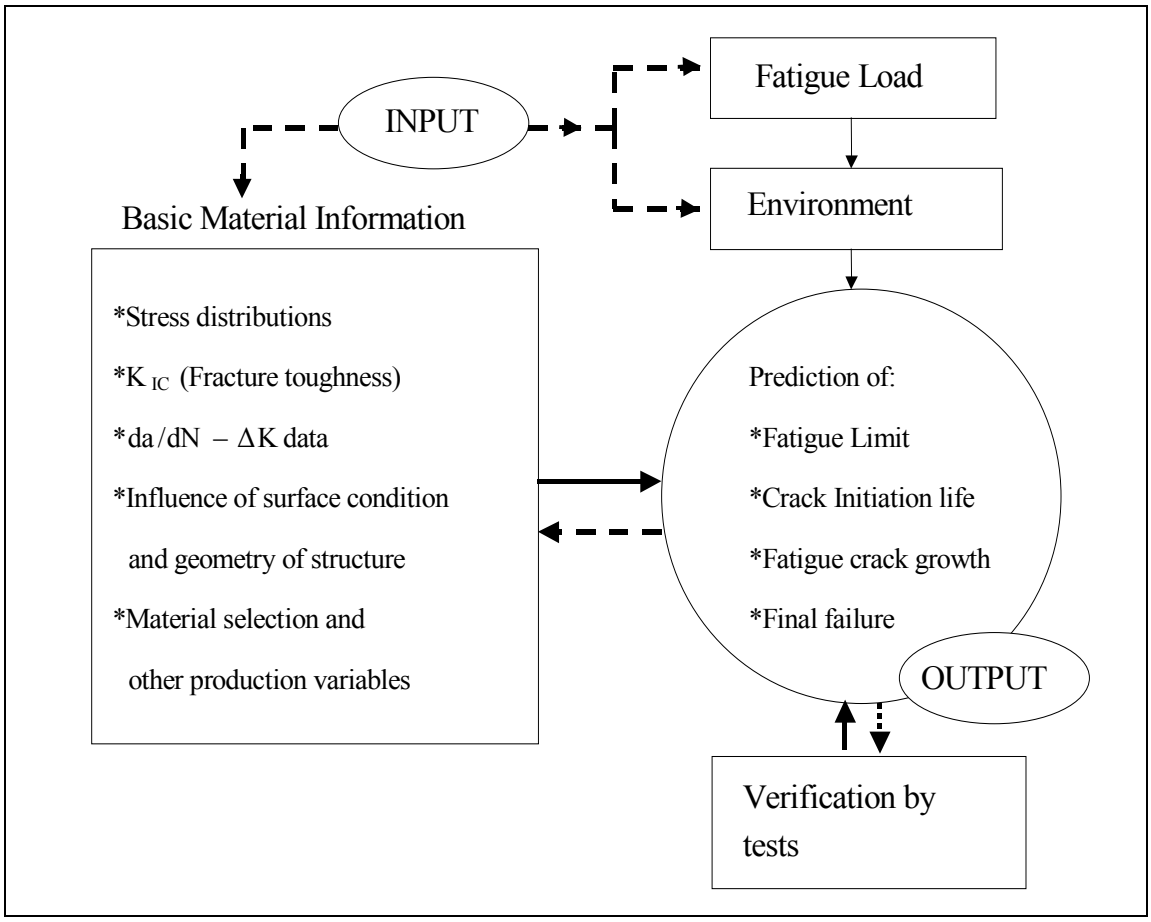

Figure 1.1 Diagram of the fatigue prediction problem in practical applications. (Schijve, 1996)

- The crack initiation period, including crack nucleation and micro-crack growth.
- The crack growth period, covering the growth of a visible crack.

There is an obvious question of defining the transition from the initiation period to the crack growth period. The transition from the micro-crack growth period to the macro-crack growth period depends on the type of material, structure and structural dimensions. Different phases of fatigue life and relevant factors are shown in Figure 1.2.

Corrosion fatigue refers to the phenomenon of cracking in materials under the combined actions of fatigue (cyclic) loading and a deleterious corrosive environment (gaseous or aqueous). This phenomenon has been recognized as an important cause for a failure of engineering structures (Barsom, 1971, & Gangloff and Wei, 1977).

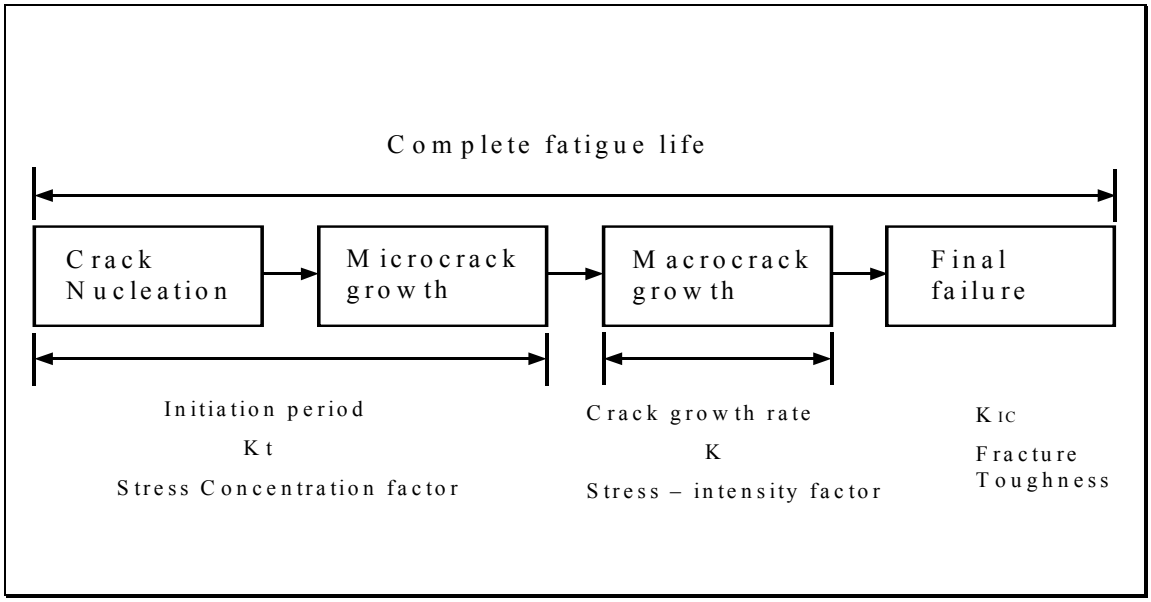

Figure 1.2. Different phases of fatigue life and relevant factors

Understanding of the corrosion fatigue mechanism is essential to service life prediction, and fracture control. The concept is shown schematically in Figure 1.3. Engineering analysis of crack growth is often required and can be done using the stress intensity concept, K, of fracture mechanics. The fracture mechanics parameter K quantifies the severity of the combination of crack length, loading, and geometry that exists around the crack tip. This equation can be expressed by

$$K = YS\sqrt{\pi a} \tag{1.1}$$

where "a" is half-crack length, and S is nominal stress, usually defined based on the gross area of the uncracked member, and Y is a geometry factor. Basically, crack growth is the geometrical consequence of sharpening and crack tip blunting. A growing crack increases its length by a Δa due to the application of a number of cycles, ΔN. The rate of growth with cycles can be represented by the ratio Δa/ΔN. From the above equation, $\Delta S = S_{max} - S_{min}$ is related to the stress intensity range ΔK, by

$$\Delta K = Y\Delta S\sqrt{\pi a} \tag{1.2}$$

Assume that the applied loading is cyclic with constant values of the stresses S_{max} and S_{min}. It is conventional to use the stress range ΔS and the stress ratio $R = S_{min} / S_{max}$, which can be defined as shown in Figure 1.3. The ΔK increases with crack length during constant amplitude stressing ΔS, and since the crack growth rate da/dN depends on ΔK, the crack growth rate is not constant, but increases with crack length. Therefore, the crack accelerates as it grows. This situation of changing da/dN necessitates the use of an integration procedure to obtain the fatigue life until the complete failure. Crack growth rates da/dN for a given combination of material and R-ratio are given by the equation shown in Figure 1.3.

Various forms of crack growth rate equations (Paris's or Walker's equations, etc.) that are normally used are given in Chapter 2. By solving the equation for dN and integrating both sides, fatigue life N_f is obtained. This integral gives the number of cycles required for the crack to grow from an initial size a_i to a final size a_f at cycle number N_f. The primary variable affecting the fatigue life is the range of the stress, stress ratio, frequency, and corrosion environment. So, fatigue life prediction is related to quantifying the fatigue problem in terms of crack growth rate and integration.

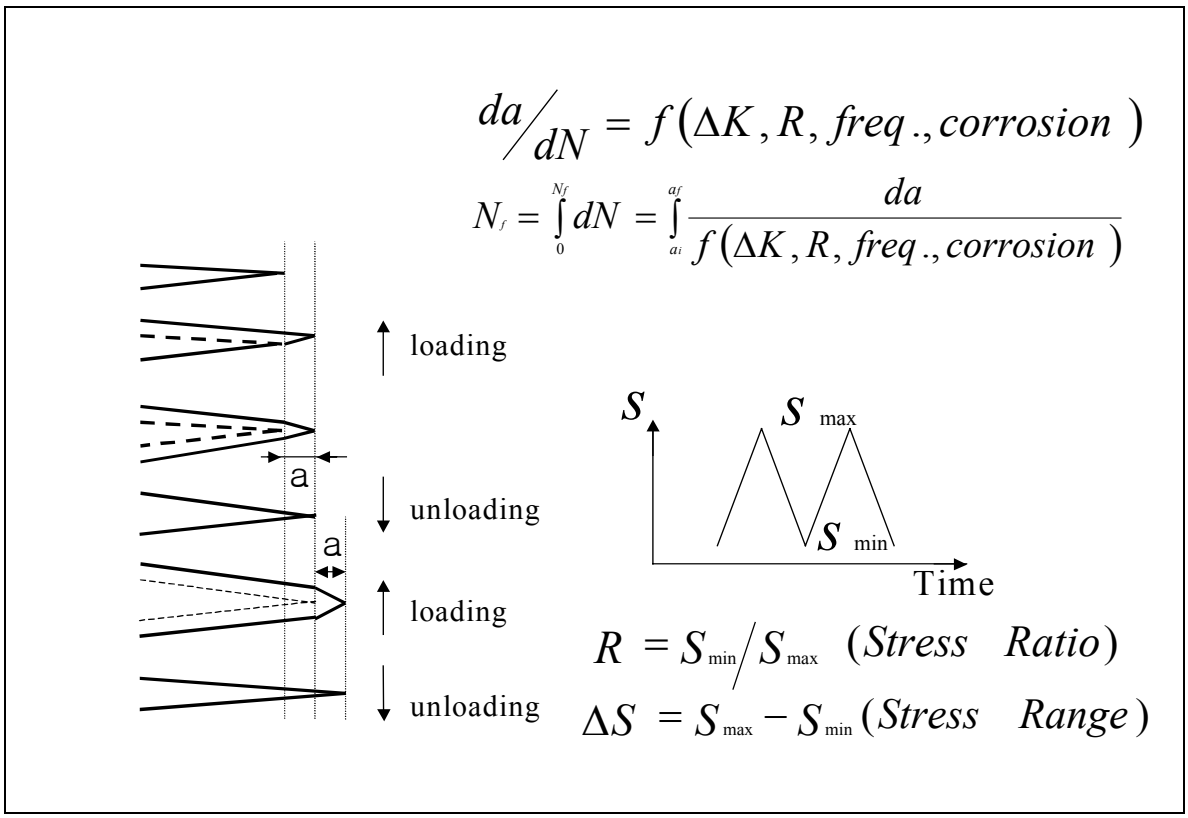

Figure 1.3. Concept of fatigue crack growth and fatigue life

Fatigue is a practical problem for all kinds of structures with many load cycles. A repetition of many load cycles can initiate a fatigue crack. The crack will grow until total fracture of the structure, unless it is found by inspection. Fatigue failures can have significant consequences in practice, which can be highly undesirable for reasons of economy and safety. As a consequence, the concept of designing against fatigue has attracted much attention from industry, universities, and research institutes to protect society against catastrophic accidents. Therefore, designing against fatigue is a matter of serious concern. Various design-options, experience and engineering judgment are essential for a safe design against fatigue failure.

The general interrelationships associated with environmentally assisted cracking (Corrosion Fatigue), which can encompass crack growth rates of more than 10 mm/s to less than 10^{-10} mm/s, are shown in Figure 1.4.

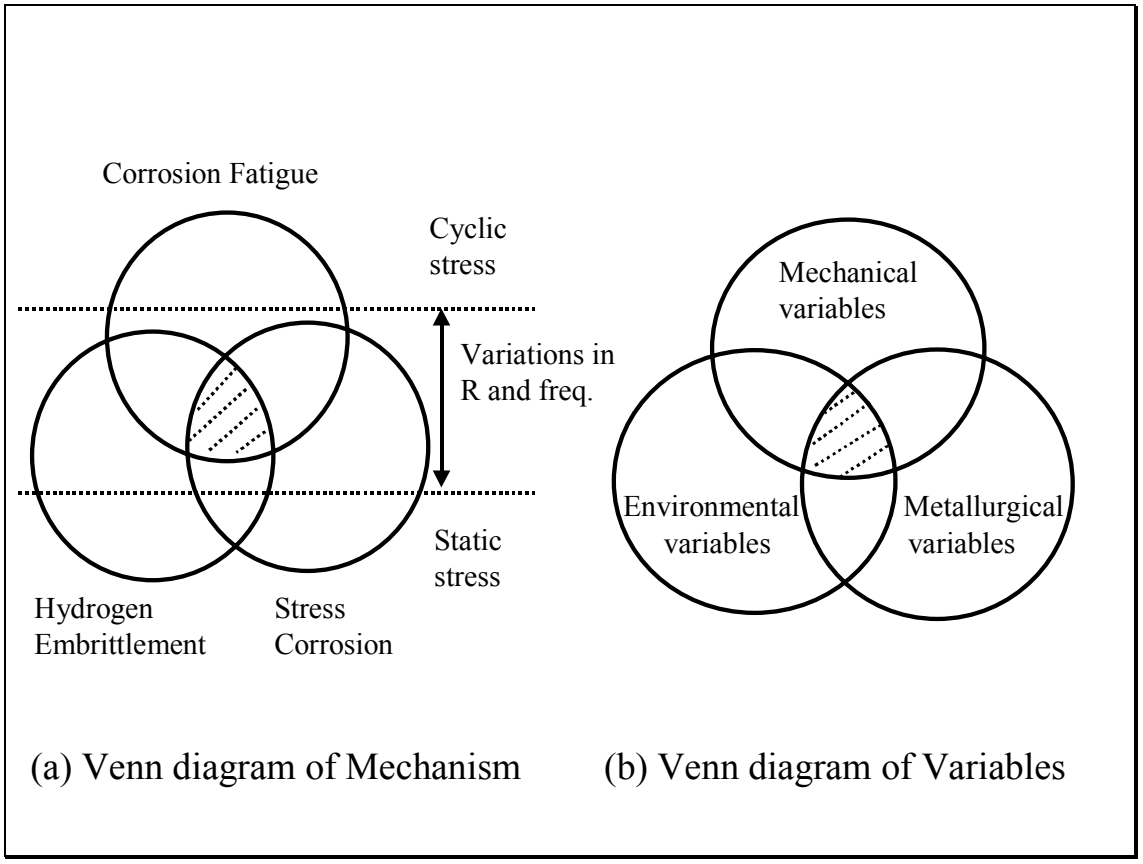

Figure 1.4. General interrelationships associated with environmentally assisted cracking (a) Venn diagram of Mechanism, (b) Venn diagram of Variables (Andresen, 1996)

The generalized corrosion fatigue cracking mechanism involves the single or mutual occurrence of hydrogen embrittlement with the different stress type depending on the variations of the stress ratio and frequency. The variables can be divided into four categories (mechanical, geometrical, metallurgical and environmental variables). The influences of some of the variables on the corrosion fatigue life are described briefly below.

Mechanical Variables

- Fatigue load frequency
- Fatigue load ratio
- Fatigue load waveform
- Maximum stress or stress-intensity factor
- Cyclic stress or stress-intensity range
- Load interactions in variable amplitude loading (over/ under/ spectrum load)
- State of stress
- Residual stress
- Stress ratio

Geometrical Variables

- Crack size and shape, and their relation to component size and geometry
- Crack geometry
- Specimen thickness (plane strain versus plane stress)

Metallurgical Variables

- Alloy composition
- Microstructure and crystal structure
- Heat treatment
- Grain boundary structure
- Grain shape and size
- Texture
- Distribution of alloy elements and impurities
- Preferred orientation of grains and grain boundaries (texture)
- Deformation mode (slip character, twining, cleavage)
- Mechanical properties (strength, toughness, etc.)

Environmental variables

- Type of environments (gaseous or liquid)
- Partial pressure of damaging species in gaseous environments
- Concentration of damaging species in aqueous or other liquid environments
- Temperature
- pH level
- Electrochemical potential
- Viscosity of the environment
- Coatings, inhibitors, etc.

Among the above factors, the following factors and their interdependence are crucial in most investigations of corrosion fatigue life. Therefore, only the following factors will be considered in this thesis work.

1. Stress Intensity Amplitude (ΔK)
2. Effect of Fatigue Frequency
3. Effect of Stress Ratio
4. Effect of Environment

An experimental program is carried out to examine the degree of corrosion prevention by using a Corrosion-Prevention-Compound (LPS-3 Heavy-Duty Rust Inhibitor compound) in a water vapor environment with the above different four factors. This compound meets Boeing BMS-3-23F Type Ⅱ, MIL-C-0083933A para.3.2-3.16, MIL-C-16173D Grade 2 Class I, Airbus TN A. 007.10138 Type Ⅰ grade 2 and DMS 2150. Typical results of use are to protect against rust and corrosion, provide anti-seize coating, and provide non-sling lubrication for up to two years. Unfortunately, the product ingredients of LPS-3 are a trade secret and it remains unknown.

Corrosion-Prevention-Compounds have both beneficial and detrimental effects on crack growth and fatigue. This investigation is aimed at identifying the mechanisms by which CPC influence fatigue life in Aluminum Alloy, 2024-T3. Aluminum alloy is widely used in industry because of its light weight and corrosion resistance. Al-2024-T3 is widely used for aircraft structures, offshore structures, truck wheels and screw-machine products, etc. Aluminum alloys are employed for the structural framework of fuselage and wing assemblies in aircraft structures. Therefore, Al-2024-T3 has been used in this thesis work. In real service situation, there are variations in random loading condition in the aerospace industry. Overload is sometimes caused by wind gusts. These overloads should be considered carefully to predict the fatigue life of the wing when the wing is designed. The second part of this thesis investigates the effect of periodic overloads on fatigue life.

Specifically, the technical objectives can be summarized as follows:

Task#1: Study of fatigue life under water vapor environment (different frequencies and stress ratios) with and without Corrosion-Prevention-Compounds (CPC: LPS-3)

Task#2: Study of the significance of periodic overloads and interactions under constant amplitude loading.

1.3 Mechanism of Overloads

Service loads are mostly random in nature. Most structures like airplanes, bridges experience some form of variable amplitude loading. One high peak stress can also occur during variable loading. This stress is called overload. This load fluctuation can lead to fatigue crack propagation, the rate of which depends on the interaction of loads. High peak overload can cause large immediate incremental growth, but sometimes can disturb the crack tip parameters leading to retarded growth in the following cycles depending on the overload ratio (OLR = $S_{overload}$ / $S_{constant\ amplitude}$) and the number of spacing cycles between overloads. The underlying mechanisms for this retardation need to be studied to investigate the fatigue life effectively. At the crack tip, the elastic stress would become very large due to the stress concentration factor. However, in practice large stresses do not occur because in a ductile material this region becomes plastically deformed. This causes a plastic zone at the crack tip. After unloading, the remainder of material will be elastic. I.e., the bulk of material returns to zero strain after unloading. But, the plastic zone cannot return to the original size due to plastic deformation. This plastic zone will be squeezed back to its original size. This causes the compressive residual stress to occur at the crack tip. Therefore, after high peak overload, at the crack tip the compressive residual stress will be present. During subsequent cycling this compressive residual stress will have to be added to the applied stress. The crack growth accounts for this compressive residual stress. The crack growth rate will be slower or retarded during the following cyclic loading due to the compressive residual stress along the crack plane. Once the crack has grown through the overload plastic zone, the original crack growth rate will be resumed.

The phenomenological behavior under various load combinations needs to be studied. Single overload and interaction between periodic overloads induce such behavior. Periodic tensile overloads superposed on constant amplitude load history are studied by using Al-2024-T3. After each periodic overload, the crack growth rate is reduced due to the compressive residual stress field induced by overloads. Typically, crack closure does play a predominant role, but several other mechanisms also contribute to retardation such as residual compressive stresses ahead of the crack tip, shear lip effects, strain hardening, etc. The detail about crack closure is mentioned in Chapter 2.

1.4 Scope of Research Work

The first task will investigate the fatigue life behavior of Al-2024-T3 in a corrosive environment (also, different frequencies and stress ratios) with and without Corrosion-Prevention-Compounds (CPC: LPS-3). Corrosion affects fatigue life depending on various factors such as stress level, frequency, stress amplitude, stress ratio and stress history, as well as on corrosion parameters such as the type of environment, exposure time and so on. An experimental matrix, with different frequencies and two stress ratios, taking into consideration of corrosive environment with or without Corrosion-Prevention-Compounds (CPC: LPS-3), has been evaluated through various testing.

The ways to extend the fatigue life of Al-2024-T3 by overloads has been investigated. The second part of the research program is to develop new techniques for fatigue life extension of Al-2024-T3. The loading history dependence has a profound influence on fatigue life. This approach needs to be assessed to investigate the total fatigue damage on fatigue life. It is reported that the fatigue life can be increased by periodic tensile overloads (Tür, et al., 1996, Tür. and Vardar, 1996). If the overload is repeated at just the correct intervals, there is a significant increase in the fatigue life. This correct interval (spacing cycles between overloads) is needed to be determined with the proper overload ratio.

The retardation associated with the interaction between overloads controlled by the periodicity (spacing cycles between overloads) of the overloads is examined. The periodicity is varied roughly between 50 and 2000 cycles for different overload ratio. The objective of this part is to find out the optimum periodicity spacing cycles between overloads to lead to maximum fatigue life for different overload ratio. The periodic tensile overloads are superposed on constant amplitude load cycles in this work. A overload ratio of 1.7 is used in this research. The objective of this part is to investigate the optimum overload ratio and spacing cycles for maximum fatigue life of the test specimen.

Fracture surfaces need to be scanned by Scanning Electron Microscope (SEM) to investigate the fatigue damage along the crack front. Some selected samples of tested specimens are studied using a Scanning Electron Microscope (SEM).

The scope of this thesis is as follows:

The background of corrosion fatigue and life extension due to periodic overloads, and literature review is briefly mentioned in Chapter 2. Numerical work by ANSYS is addressed in Chapter 3. The crack growth retardation by overload is modeled by using ANSYS 5.7. The experimental methodology to carry out the experiments is addressed in Chapter 4. The results and conclusions are mentioned with some discussions in Chapter 5. Finally, the conclusions and recommendations for the future work are mentioned in Chapter 6.

CHAPTER 2. BACKGROUND & LITERATURE REVIEW

2.1 General Introduction

The background and literature review section discuss the importance of corrosion fatigue, variables affecting corrosion fatigue, the effects of Corrosion-Prevention-Compounds (CPC) on fatigue crack growth, and crack growth retardation due to single or periodic overload. At the end of chapter 2, various crack growth models to predict fatigue life are discussed. The corrosion under hostile environment affects the fatigue crack growth, in other words, the fatigue life. To protect from this environment, CPC is used for this thesis work. Relations between these mechanisms are discussed in this chapter. In actual service situation, overload sometimes occurs in the aerospace industry. The overload effect on fatigue crack growth rate is discussed as well. In this chapter, mechanisms of corrosion fatigue and crack growth retardation due to overloads are primarily focused on. In this thesis work, corrosion fatigue with or without CPC is carried out in task #1. In task #2, the effect of overloads on fatigue life is evaluated.

2.2 Mechanisms of Corrosion Fatigue

The generalized corrosion fatigue cracking mechanism involves the single or mutual occurrence of hydrogen-induced cracking or anodic dissolution at the crack tip. Hydrogen embrittlement (hydrogen-induced cracking or hydrogen-assisted cracking) can be divided into five types of mechanisms:

1) Decohesion
2) Pressure
3) Adsorption
4) Deformation
5) Brittle hydride

Anodic dissolution can be divided into four possible mechanisms.

1) Slip-dissolution
2) Brittle film-rupture
3) Corrosion-tunneling
4) Selective-dissolution

Both processes (dissolution and hydrogen-assisted cracking) can occur simultaneously at the crack tip.

2.2.1 Hydrogen-Assisted Cracking

In corrosion fatigue, hydrogen is generated by the reaction of environmental species such as gaseous hydrogen, water vapor, seawater, and so forth, with the newly cracked material at the crack tip. This hydrogen is absorbed at the metal surface and then transported by diffusion into the highly stressed region (plastic zone) at the crack tip,

where it causes localized damage and increases the fatigue crack growth rate. Figure 2.1 illustrates various processes that might be involved in corrosion fatigue crack growth by hydrogen-assisted cracking mechanism. Several hydrogen-assisted cracking mechanisms have been proposed to explain how hydrogen enhances corrosion fatigue crack growth rates. Some of the principles are briefly discussed below. These three principles are the lattice decohesion mechanism, surface adsorption mechanism and hydrogen enhanced plasticity mechanism.

These three are explained in detail below:
(1) The lattice decohesion mechanism postulates that the hydrogen as a solute decreases the cohesive bonding forces between metal atoms. Crack growth occurs when the local tensile stress in the crack tip region exceeds the hydrogen-weakened inter-atomic cohesive strength. This mechanism is difficult to prove on the atomic scale.

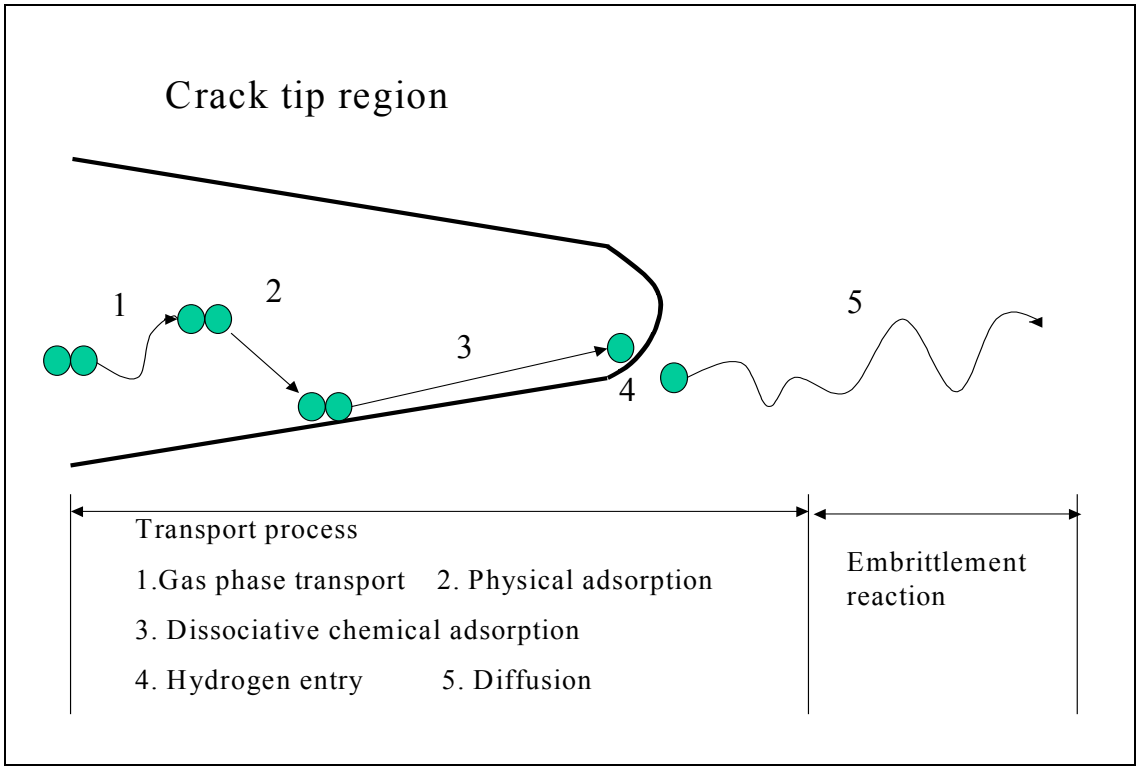

Figure 2.1 Various sequential process involved in corrosion fatigue crack growth in alloys exposed to aggressive environments (Gangloff and Wei, 1977).

(2) The surface adsorption mechanism proposes that strongly adsorbed hydrogen at the surface serves to lower the surface energy of the metal needed for crack extension. If the classic theory of the Griffith criteria for crack propagation is adopted, it facilitates crack extension and increases the crack growth rate. The end results of these two mechanisms are the same in that the critical crack-tip drive force required for advancing the crack is reduced by the presence of hydrogen.

One of the major deficiencies in the surface adsorption mechanism is centered on the generally large amount of plastic deformation energy that accompanies crack growth. The plastic deformation energy is usually much larger than the relatively small surface energy (about 1000 to 1). Thus, even a large reduction in surface energy due to hydrogen adsorption should not markedly affect the fracture stress. Another discrepancy is that other environmental species, such as oxygen and nitrogen, are also strongly adsorbed to the clean metal surfaces and have the potential to reduce surface energy to a greater extent than hydrogen. Yet, neither oxygen nor nitrogen accelerates crack growth rates like hydrogen does.

(3) Hydrogen enhanced plasticity mechanism: In contrast to previous hydrogen-assisted cracking mechanisms that suggest hydrogen "embrittles" the material and thus reduces that driving force required for crack extension, the hydrogen enhanced plasticity mechanism proposes that hydrogen assists the process of plastic flow by enhancing the dislocation mobility at the crack tip. By recognizing that the three major categories of fracture paths, namely micro-void coalescence, cleavage, and intergranular cracking, which are observed in benign environments are also produced in environmentally assisted cracking, it is argued that hydrogen in the lattice merely assists these fracture processes.

2.2.2 Anodic Dissolution

Anodic dissolution is commonly referred to as active path dissolution, slip dissolution, strain/stress enhanced dissolution, and surface film rupture dissolution. Crack growth rates are enhanced by these mechanisms along susceptible paths such as grain boundaries. In corrosion fatigue cracking, the anodic dissolution mechanism depends on the rupture of the protective film at the crack tip and the subsequent repassivation of the newly exposed fresh metal surface. Corrosion fatigue crack growth rates will be controlled by the bare surface anodic dissolution rate, the rate of repassivation, the rate of oxide film rupture, mass transport rate of reactant to the dissolving surface.

Under fatigue loading, a slip step forms at the crack tip and ruptures the protective surface film. The freshly created surface reacts with the environment and partly dissolves until the crack tip region is completely repassivated. Then, the protective surface film is repaired. But, it's difficult to apply this mechanism to corrosion fatigue in a gaseous environment (such as water vapor or water fog) or in distilled water where the electrochemical reaction necessary for dissolution at the crack tip is unattainable. Anodic dissolution also fails to account for several phenomenological observations, especially the fractographic features of materials. The brittle-like appearance of fatigue fracture surfaces and brittle striations are difficult to reconcile with the lateral dissolution velocity concept that is an integral part of the anodic dissolution mechanism description (Cullen, Gabetta, and Hanninen, 1985). The hydrogen assisted cracking mechanism has the advantage that it can account for the fractographic features in materials. But, it's difficult to quantify the hydrogen effect.

Another concern is that the dissolution mechanism cannot account for the frequency dependence of fatigue crack growth rate without invoking a strong competitive process.

For low load ratios (R (= S_{min} / S_{max}) ~ 0.1 to 0.2), it has been demonstrated that very long cyclic periods (lower frequency) produce much larger environmental effect on fatigue crack growth (Van Der Sluys and Emanuelson, 1985). But, for very high load ratios (R ~ 0.8 to 0.9), the maximum in growth rate enhancement comes at high frequencies, up to about 10 or 20 Hz. On its own, anodic dissolution would predict a continuing increase in growth rates for increasing cyclic periods.

2.3 Variables Affecting Corrosion Fatigue

In corrosion fatigue crack growth analysis, the mechanical driving force is normally characterized in terms of the fracture mechanics parameters such as the crack-tip stress intensity factor, K, or stress intensity factor range, ΔK (Refer to equation (1.1)).

The stress intensity concept, K, of fracture mechanics which is called the stress intensity factor, quantifies the severity of the combination of crack length, loading, and geometry that exists, being expressed by where "a" is crack length, and S is nominal stress, usually defined based on the gross area of the uncracked member, and Y is a dimensionless function of geometry. Two of the following interrelated loading variables are commonly used for characterizing corrosion fatigue crack growth: stress intensity factor range, ΔK (ΔK = Kmax – Kmin), where Kmax is maximum stress intensity factor; and stress ratio or load ratio, R (= Smin / Smax), where Smin is the minimum stress in a load cycle. The following factors are crucial in most investigations of corrosion fatigue.

2.3.1 Range of Stress Intensity Factor (ΔK)

Engineering analysis of crack growth is often required and is done by using the stress intensity factor K. The rate of fatigue crack growth is controlled by K. Therefore, under constant amplitude cyclic loading, the dependence of K on crack length "a" and Y causes the crack to accelerate as it grows. While environmental crack growth rates increase with increasing ΔK, the specific dependency varies greatly. There is often a profound shift in the dependence of ΔK, typically producing reduced ΔK dependence in aggressive environments, at least in the intermediate region where power law behavior is observed. It is always important to examine the entire relevant ΔK regime, not assuming the observed enhancement at a specific ΔK (Refer to equation (1.2)).

2.3.2 Effect of Fatigue Frequency

Figure 2.2 shows that the environmental effect is much more pronounced at lower cyclic frequencies than that at higher frequencies. The fatigue crack growth rates at 0.1 Hz are higher than those obtained at 4 Hz at a load ratio R=0.1. The effect on growth rate per cycle of a given hostile environment is usually greater at slower frequencies, where the environment has more time to act. Fractographic examination of the fracture surfaces also indicated that, at lower frequencies, where the environmental effect was significant, the fracture path in water vapor was primarily intergranular along the prior austenite grain boundaries, similar to those observed in hydrogen and in water under sustained load conditions. At higher test frequencies, the fracture path was primarily transgranular with

respect to the prior austenite grains in specimens. Figure 2.2 is tested in inert argon environment.

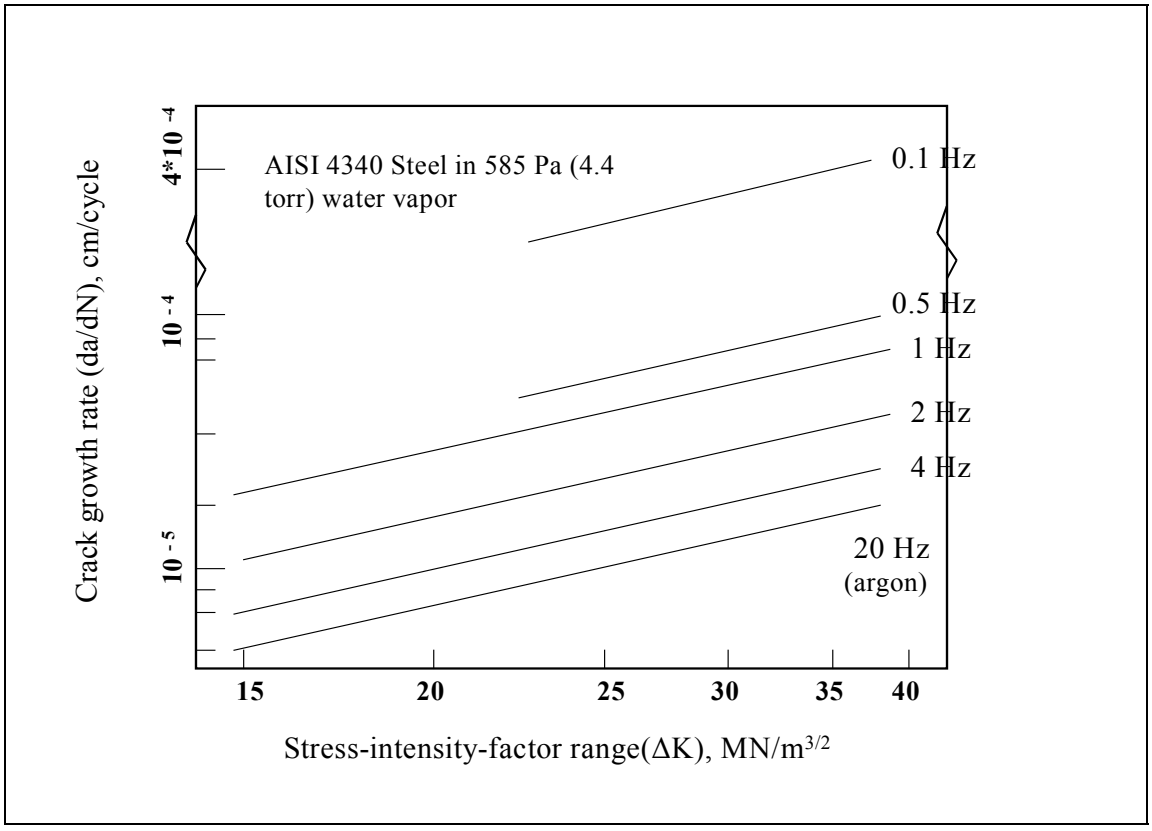

Figure 2.2 Room-temperature fatigue crack growth kinetics of AISI 4340 steel in dehumidified argon and in water vapor (585 Pa) at R=0.1 (Pao and Wei, 1979)

2.3.3 Effect of Environment

Crack growth is caused by hostile chemical environment. Hostile chemical environments often increase fatigue crack growths, with certain combinations of material and environment. The term corrosion fatigue is often used when the environment involved is a corrosive medium, such as seawater. Even the gases and moisture in air can act as a hostile environment, which can be demonstrated by comparing test data in vacuum.

Stress corrosion cracking, where material removal by corrosion in water, water vapor, salt water, or other liquid assists in growing the crack. In other cases, no corrosion is involved, as in cracking of steels due to hydrogen embrittlement, or cracking of aluminum alloys due to liquid metal embrittlement caused by mercury. As mentioned above, the embrittling substance appears to enhance the breaking of chemical bonds in the highly stressed region of the crack tip. Embrittlement and hence crack growth can occur even where the harmful substance is not present as an external environment. For example, it is

sometimes the case for hydrogen cracking of metals. Even the moisture and gases in air can cause environmental crack growth in some materials.

The use of most engineering materials relies on the presence of a kinetic surface barrier (passivity) to reduce the oxidation rate to manageable proportions. When passivity is disturbed (e.g., by local strains in the underlying material), the reaction (oxidation) rate of the exposed metal is generally very high as the protective film is reformed (as repassivation occurs). Many environmental effects on crack growth are associated with the direct loss (oxidation/dissolution) of metal (known as the slip oxidation mechanism); deformation, absorption, and transport of hydrogen (hydrogen embrittlement). The maximum environmental contribution can be predicted by measuring the dissolution rate in a bare metal surface. Figure 2.3 shows that, compared to vacuum, the crack propagation rate of a high-strength steel is 4 times higher in moist air, 100 times higher in sodium chloride solution, and 1000 times higher in gaseous hydrogen.

The important observation (Ford, 1988) is that the environment enhancement is not uniform, for example across the entire range of loading conditions. Environmental enhancement reaches a maximum under intermediate ΔK, R, and frequency conditions. Indeed, the environmental enhancement tends to decrease at very high loading rates (e.g., at high frequency and ΔK values).

Other concerns for the environment include:

1. Specimen and grip design (e.g., to avoid failure at crevices by minimizing stress in creviced regions).
2. Proper design of environmental chamber (e.g., to avoid contamination).
3. Maintenance of proper chemistry, which often requires refreshed or flowing systems for controlling the chemistry in gases or liquids.
4. Proper and thorough monitoring or recording of all relevant chemical and electrochemical parameters.

2.3.4 Effect of Stress Ratio (R)

An increase in the stress-ratio, R, of the cyclic loading causes growth rates for a given ΔK to be larger. In general, higher stress ratios will result in higher corrosion fatigue crack growth rates and lower corrosion fatigue crack growth thresholds. This can be viewed as a mean stress effect. The effect is generally more pronounced for more brittle materials. In contrast, mild steel and other relatively low-strength, highly ductile, structural metals exhibit only a weak R effect in the intermediate growth rate region of the da/dN vs. ΔK curve.

For example, the corrosion fatigue crack growth rates of MF-80- HSLA steel in 3.5% NaCl solution at $R = 0.67$ are about two times higher than the rates obtained at $R = 0.1$ at similar stress intensity levels (Gill and Crooker, 1990). The effect of load ratio is shown in Figure 2.4.

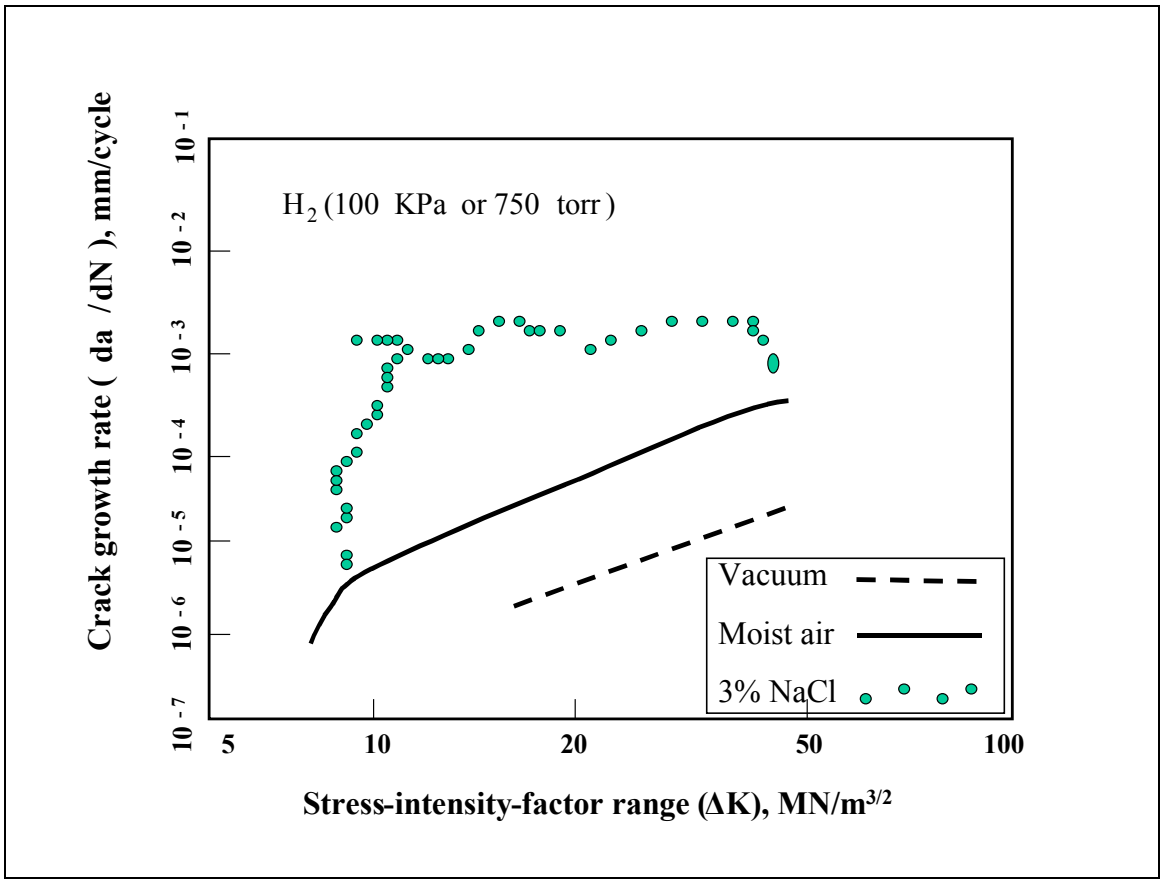

Figure 2.3 Room-temperature corrosion fatigue crack growth rates (effect of environment on fatigue crack propagation in 4130 steel with a yield strength of 1330 MPa. Temp. 23˚C, Freq. 0.1 Hz, load ratio = 0.1: Gangloff, 1984)

A special case of corrosion fatigue cracking is "ripple load" cracking. "Ripple loading" refers to a loading profile where relatively small amplitude cyclic loads are superimposed on a large sustained load. A typical ripple load profile is schematically shown in Figure 2.5 where the stress ratio often exceeds R = 0.9. The significance of ripple load cracking is its relation to stress-corrosion cracking (SCC), where the applied load is assumed to be constant. However, in the real world, structures rarely experience a constant load condition, but are far more apt to see a combination of very small amplitude cyclic loads and a large constant load. A typical example is an offshore platform structure. Under ripple loading conditions, if a structure is designed solely based on the SCC threshold without considering the possibility of ripple loads, cracking or fracture may occur prematurely.

2.3.5 Effect of Waveform

While cyclic load waveform has little effect on the fatigue crack growth rates in benign environments, available data indicates that corrosion fatigue crack growth rates in aggressive environments is highly dependent on the shape of the cyclic load waveform.

Corrosion fatigue crack growth rates in a 3% NaCl solution under both square and negative saw-tooth waveforms, which have very short rising load periods, are identical and are equal to the fatigue crack growth rates in ambient air. However, the corrosion fatigue crack growth rates of 15Ni-5Cr-3Mo steel in 3% NaCl solution under sinusoidal, triangular, and positive saw-tooth waveforms, which all have long rising load periods, are about three times higher than the fatigue crack growth rates under square and negative saw-tooth waveforms in the same 3% NaCl environment and in air (Rolfe and Barsom, 1977). The longer the load rise time during each load cycle, the greater the influence of an aggressive environment. In case of the square cyclic waveform that has a very short rising load period, the aggressive environment has little effect on the fatigue crack growth rates. Generally, a sine or sawtooth shape waveform is used during a fatigue test. Both waveforms generate similar data at room temperature. In this thesis work, sine waveforms are used, because sine waveforms are easier for the MTS 810 testing machine (servo-hydraulic-system) which was used in this study to control. Sawtooth should be used when elevated-temperature fatigue crack growth and creep-fatigue interactions are of interest.

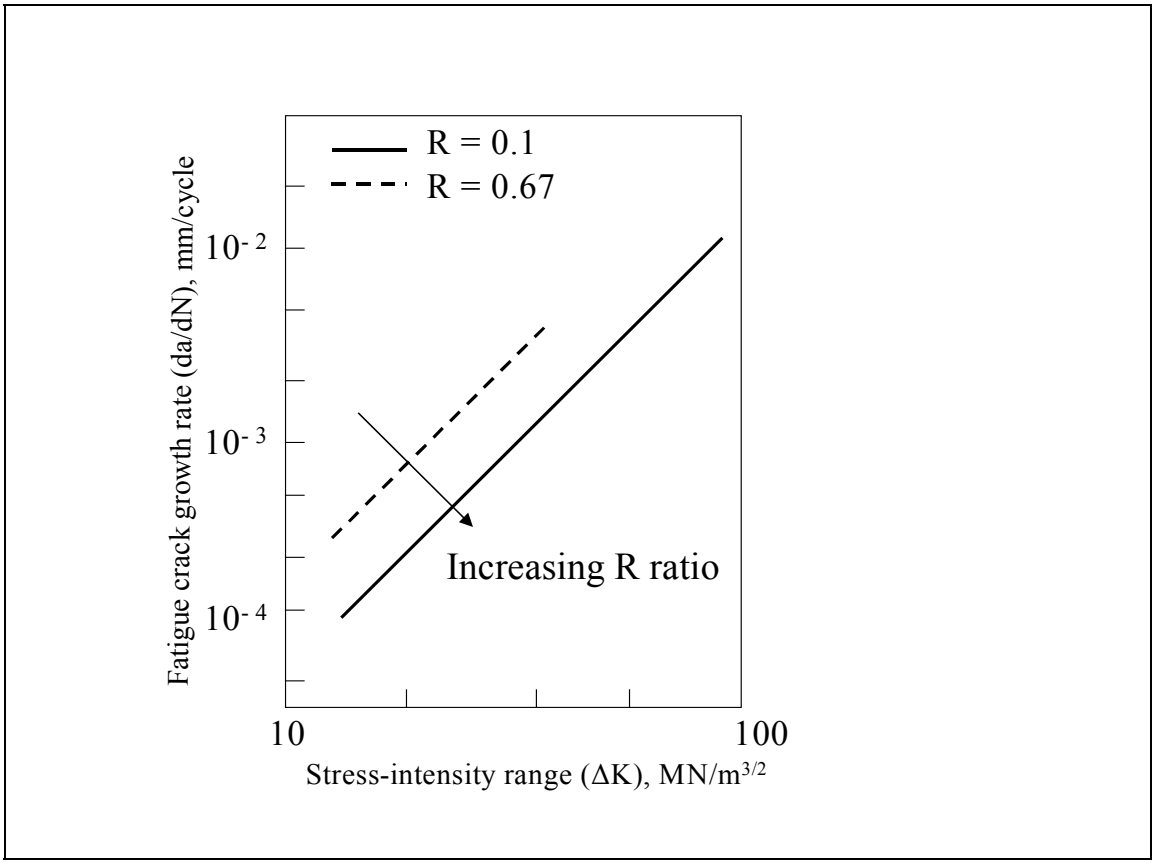

Figure 2.4 Effect of load ratio on the corrosion fatigue crack growth rates of MF-80-HSLA steel in 3.5% NaCl solution (Pao, 1996)

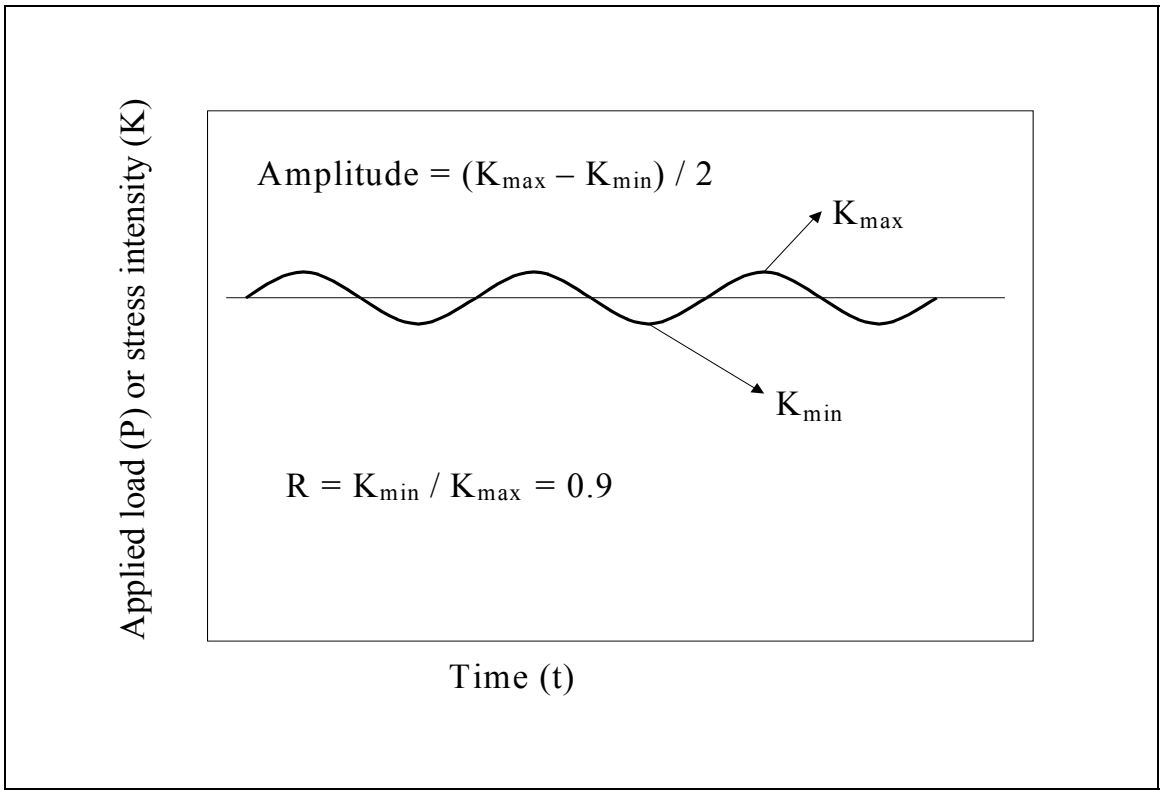

Figure 2.5 Ripple load profile (Pao, 1996)

2.3.6 Effect of Temperature

Temperature may influence the environment/metal surface reactions. Temperature is expected to affect corrosion fatigue crack growth rates. In general, corrosion fatigue crack growth rates increase with increasing temperature. In this study, the effect of temperature on fatigue crack growth is disregarded and all tests are carried out at constant room temperature.

2.3.7 Metallurgical Variables

Microstructure and alloy strength influence fatigue crack propagation in embrittling gases and liquids. In general, brittle corrosion fatigue cracking is accentuated by impurity (e.g., phosphorus or sulfur) segregation at grain boundaries

1. Planar deformation associated with ordering or peak aged coherent precipitates
2. Increased yield strength or hardness
3. Surface treatment

The effects of alloy composition, grain size, and microstructure vary with environment and brittle cracking mechanism. Laboratory experiments are necessary to establish specific trends. Machining and surface treatments such as shot peening can significantly

affect cracking. Shot peening and related treatments that produce surface compressive stresses are beneficial on the crack growth rate.

2.3.8 Crack Closure Effects

Premature crack surface contact during unloading, or "crack closure," can greatly reduce rates of fatigue crack propagation. The true (or effective) crack tip driving force is reduced below the applied ΔK because of the reduced crack tip displacement range. Closure phenomena are produced by a variety of mechanisms and are particularly relevant to fatigue crack propagation in the near-threshold regime, after large load excursions, or for corrosive environments. The engineering significance of beneficial crack closure influences depends on the stability of the corrosion product during complex tension-compression loading and fluid conditions. Oxides form on crack surfaces through a fretting mechanism during cycling in air. Crack growth rates are reduced by oxide-induced closure. Thus, crack growth at low frequencies may be increased by hydrogen (or chemical) embrittlement but be decreased from increased oxide formation and closure.

2.3.9 General Comments about Corrosion Fatigue Crack Growth

Corrosion fatigue is a function of the chemistry of the environment or material system, the microstructure, and the applied loading conditions. Because environmental susceptibility is a complex phenomenon occurring at the atom/molecular level, it is difficult to predict or verify using specific models or tests. For the present, it is necessary to characterize materials using appropriate real time loading profiles in the service environment to ensure adequate service lives. It has long been known that the applied cyclic amplitude (ΔK) can be attenuated at the crack tip by crack closure, which can be attributed to a variety of phenomena that promote premature contact of the crack flanks, including fracture surface roughness, oxide growth on the walls of the crack, plasticity or phase transformation in the crack wake. The significance of crack closure is large, making it difficult to determine a "real" stress intensity range ΔK at the crack tip. In many engineering systems, cracks are observed to grow at stress intensities dramatically lower than the observed K_I in laboratory data. There is also increasing awareness that there is a subtle, delicate, and complex interdependence between sustained strain at the crack tip (which locally disrupts passivity) and the crack advance process itself.

So far, fully integrated approaches to mechanistic understanding and life prediction of environmentally assisted cracking are being developed for a variety of systems and some of the interesting work are presented in the Proc. Life Prediction of Structures Subject to Environmental Degradation, 1996 & Proc. Int. Symp. on Plane Aging and Life Prediction of Corrodible Structures, 1995.

2.4 Effect of Corrosion-Prevention-Compounds (CPC) on Fatigue Crack Growth

Crack growth data generated under constant amplitude fatigue loading of center pre-crack tension specimens at various stress ratios, frequencies and exposure levels are employed to study the influence of Corrosion-Prevention-Compounds (CPC: LPS-3 Heavy duty

corrosion inhibitor) on fatigue life under corrosive environments (water-vapor). The product description of LPS-3 is mentioned in chapter 4.9.

It has generally been assumed that if a structure is fully protected against corrosion it will maintain the same fatigue life as it would have if there were no corrosive environment present. Specimens treated with Corrosion-Prevention-Compounds (CPC) have been found to exhibit crack growth rates and fatigue lives in distilled water and acidic environment similar to those of specimens tested in ambient air environment (Bellinger, 1994 & Komorowski, 1993).

2.5 Fatigue Crack Growth under Overloads or Variable-Amplitude Loading

The observation of cycle-by-cycle crack extension has simulated various prediction models on fatigue crack growth. It is a basic concept for models on crack growth under variable amplitude (VA) loading. Another important concept used in these models is crack closure. Plasticity-induced crack closure was discovered by Elber (Elber, 1971). It implies that fatigue cracks can be fully or partly closed while the material is still under tension. It occurs as a consequence of plastic deformation left in the wake of the crack along the crack flanks. The plastic deformation remains from crack-tip plasticity of previous load cycles. As long as the crack tip is still closed, there is no stress singularity at the physical crack tip.

To quantify this crack closure, the crack opening stress level S_{op} should be introduced. During cycling, the crack opening stress level, $S_{op,}$ can be between S_{min} and $S_{max.}$ The crack tip is fully open if $S > S_{op.}$ Elber defined an effective stress range $\Delta S_{eff} = S_{max} - S_{op,}$ and similarly an effective value by:

$$\Delta K_{eff} = \beta Y \Delta S_{eff} \sqrt{\pi a} \tag{2.1}$$

Where β is the geometry correction factor. According to Elber:

$$\Delta K_{eff} / \Delta K = U(R) \tag{2.2}$$

where U(R) is a function of the stress ratio $S_{min} / S_{max..}$ Several U(R) relations have been proposed in the literature (Kumar, 1992). They conclude empirical U(R) relations could describe the effect of the R-ratio in crack growth under constant amplitude loading by using $\Delta K_{eff..}$ Plasticity-induced crack closure significantly contributed to our understanding fatigue crack growth under variable amplitude loading.

2.5.1 Fatigue Phenomena in Metallic Materials

Fatigue cracks generally start at the material surface. Micro-crack initiation is a surface phenomenon. So, the micro-crack initiation life primarily depends on the surface conditions of the material. It thus can be sensitive if the surface conditions do not represent a constant surface quality. Generally, micro-cracking depends on the microstructure, crystallography, crystal lattice orientation (texture) and the grain size and

Table 2.1 Types of variable-amplitude tests and main variables

Type of test	Main variables
Simple test: Constant amplitude with overload	Single Overload (OL)
	Repeated Overloads
Block tests	2 blocks, Hi-Lo and Lo-Hi sequence
	Repeated blocks
Moderate complexity Program tests	Sequence of amplitude
	Size of period of blocks
Complex tests Random load test	Irregularity loads
Service simulation test	Variable of service load history

so on. As a result, crack nucleation and the micro-crack growth cannot be expected for different materials. But, the macro-crack growth depends on the crack-growth resistance of the material, which then is considered to be a bulk property of the material. Continued crack growth occurs away from the material surface; it does not depend on the material surface quality. Actually, the applicability of fracture mechanics to small micro-cracks is questionable, but it can be a useful tool for describing macro-crack growth. In this thesis, fatigue cracks are referred to as macro-cracks if crack growth has become a regular growth process along the entire crack front. They are not necessarily visible cracks.

2.5.2 Variable Amplitude (VA) Load Sequences

The increased complexity of load histories applied in VA fatigue tests became possible by the development of modern fatigue machines (closed-loop computerized load control). In general, such a test by fatigue machine cannot be considered a realistic simulation of a service load history. Many loads in service have a random character, although there are different types of randomness. In tests on other types of structures, it is now recognized that a realistic simulation of the service load sequence is essential to obtain a similar fatigue damage accumulation. Actually, there are many inherent problems to simulate the real service load history. A well-known and easily recognized problem of service simulation fatigue tests is that they must be completed in a limited time period. As a consequence, the service simulation fatigue test is an accelerated fatigue test. If there are time-dependent effects in fatigue, a problem arises. The classical one is fatigue in a corrosive environment. This obviously applies to welded offshore structures in salt water. It now can be questioned whether such accelerated tests can still give reliable information. The time scale has been considerably modified. Time-dependent significantly affects (and thus frequency-dependent effects) on fatigue crack extension. The compression of the time scale should have an influence on the test result. For fatigue of aluminum alloys in air and in other gaseous environments the water vapor content has a significant influence on fatigue (Hartman, 1965, & Bradshaw and Wheeler, 1969, & Broek, 1972).

Under normal humidity, cyclic loads with frequencies of about 10 Hz and lower give the same maximum environmental contribution to fatigue crack growth. Flight simulation tests have been carried out on 2024-T3 and 7075-T6 sheet specimens with test

frequencies of 10 Hz, 1Hz, and 0.1 Hz (Schijve, 1972). The results have confirmed that the same crack growth rates are found for the three frequencies. This limited experimental verification indicates that time-dependent effects may not be significant, because under both low- and high-frequency load histories, there is sufficient time for the same environmental damage contribution to crack growth. However, the situation can be quite different for other materials and other environments. As an example, for fatigue of steel in salt water, a systematic frequency effect was clearly observed long ago (Endo and Miyao, 1958). A detrimental saltwater effect has also been found in random-load frequency tests on steel for offshore structures tested under a sea wave spectrum (Heywood, 1956).

2.5.3 Crack Growth Retardation due to Overloads (OL)

Most structures like airplanes and bridges experience some form of variable amplitude loading. One high peak stress can also occur during variable amplitude loading. This stress is called overload. The residual stress induced by overload has a beneficial effect on crack growth rate. Generally, residual stress can be produced mechanically by shot peening, hammer peening, or overloads.

Fatigue crack usually grows through the material in load cycle. Crack growth is the geometrical consequence of sharpening and crack tip blunting. In theoretical calculation for fatigue crack growth, it is assumed that crack grows "Δa" per cycle. During cyclic loading, the crack length increases at a constant rate. There are other parameters such as the corrosive environments, frequency, metallurgical variables, loading conditions and so on. However, this growth rate per cyclic loading is generally a function of two parameters, stress ratio (R) and stress range ($\Delta\sigma$). In real structures, high peak stress can be produced within the material. For example, the wing of the airplane experiences the high peak load due to a sudden gust or wind. So, crack growth analysis for variable amplitude loading is not possible without an account of retardation effects. The crack growth rate can be reduced after proper overloads. Theoretically, at the crack tip, the elastic stress would become very large due to the stress concentration factor. However, in practice, large stresses do not occur because in a ductile material this region becomes plastically deformed. This causes a plastic zone to occur near the crack tip. After unloading, the remainder of the material will be elastic. So, the bulk of material return to zero strain after unloading. But, the plastic zone cannot return to the original size. This plastic zone will be squeezed back to its original size. This causes the compressive residual stress to occur at the crack tip.

Thus, after high peak overload, at the crack tip the larger plastic zone will be formed. A more extensive residual stress will be present at the crack tip. During the subsequent cycling this compressive residual stress will have to be added to the applied stress. The crack growth rate response accounts for this compressive residual stress. The crack growth rate will be slower or retarded during the following cyclic loading due to the compressive residual stress along the crack plane. Once the crack has grown through the overload plastic zone, the original crack growth rate will be resumed. The size of plastic zone for plane stress (Figure 2.6) can be found by the following equation (Irwin, 1960).

$$2r_p = \frac{1}{\pi}\left(\frac{K_I}{\sigma_y}\right) \tag{2.3}$$

After each periodic overload, the crack growth rate was reduced due to the compressive residual stress field induced by overload. This beneficial residual stress effect on crack growth is called crack growth retardation. If the overload is repeated at just the correct intervals, there is a significant increase in the figure life. So, the fatigue life can be extended mechanically by overloads. More than half a dozen models have been proposed in order to explain the retardation. The Wheeler model (Wheeler, 1972) is widely used. For constant amplitude fatigue, the Wheeler model works well. After second overload, the plastic zone was increased further. This second overload will reduce the crack growth rate again. Overload ratio is the ratio of overload amplitude to constant cyclic amplitude. The crack growth retardation varied a lot depending on the value of overload ratio. Sometimes, the crack growth rate stops if the overload ratio is 2 (David, 1988).

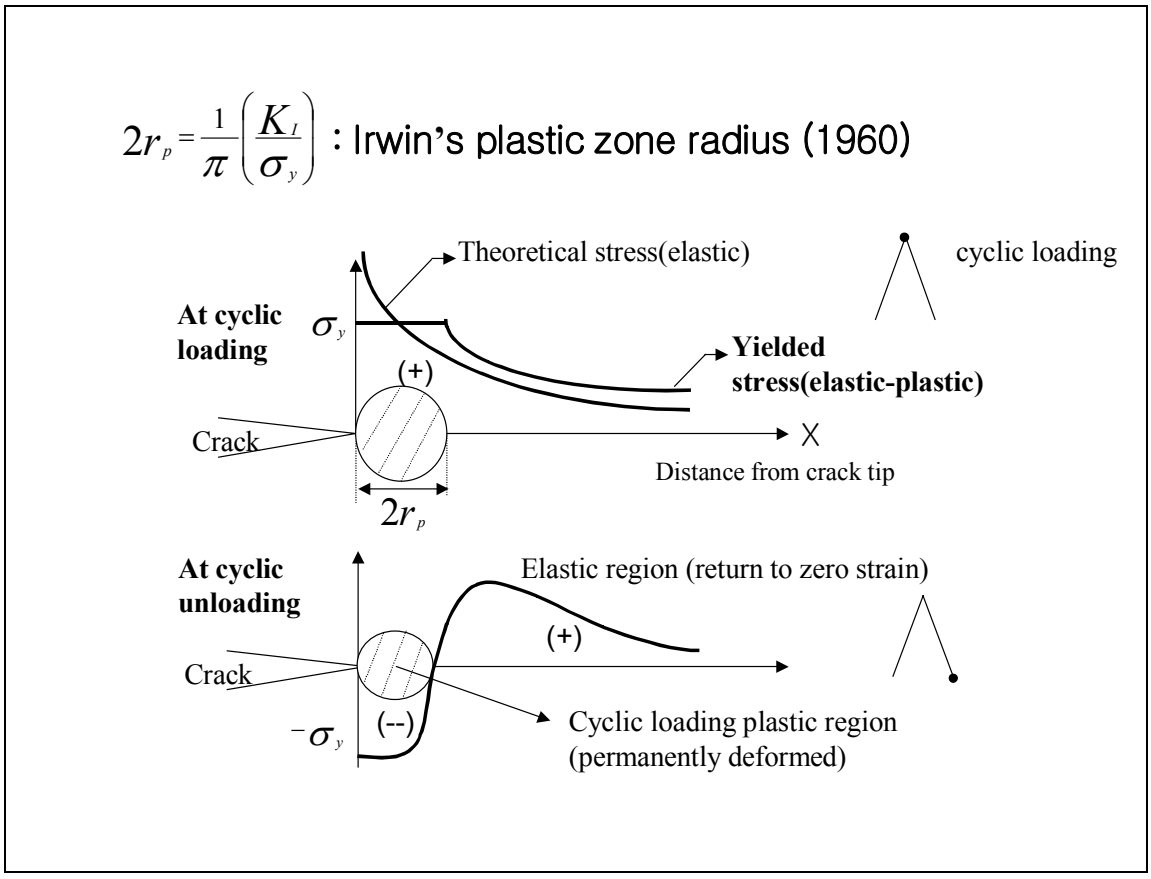

Figure 2.6 Plastic zone size for plane stress (Irwin, 1960)

The overload cycle starting with the minimum peak, followed by the maximum peak (−/+) OL cycle caused a very large retardation of the fatigue crack growth. The maximum peak load caused a large plastic zone at the crack tip, which left compressive residual stresses in this zone. That will retard subsequent crack growth when the crack grows

through this zone. The explanation can also be formulated in terms of the plasticity induced crack closure phenomenon (Elber, 1970). Due to the plastic deformation of the OL, more crack closure will occur after the OL has been applied. The S_{op} (stress when crack opens) is increased and $\Delta S_{eff} = S_{max} - S_{op}$ is reduced. Some elementary tests on crack closure before and after an OL have been carried out (Schijve, 1976). The schematic test is shown in Figure 2.7. The delay caused by the OL can easily be observed from the crack growth curve. The crack closure measurements carried out before the application of the OL indicated $S_{op} \sim 62$ MPa. Directly after the OL the S_{op} level was reduced to about 45 MPa. Because the OL opens the crack by crack-tip plasticity, such a trend should be expected. Crack closure measurements made after the OL application indicated S_{op} values above S_{min} of the CA cycles. However, S_{op} decreased later below $S_{min.}$ At the moment that $S_{op} = S_{min,}$ the crack growth delay had finished. This should also be expected because crack closure no longer occurred during the CA cycles at R = 0.67.

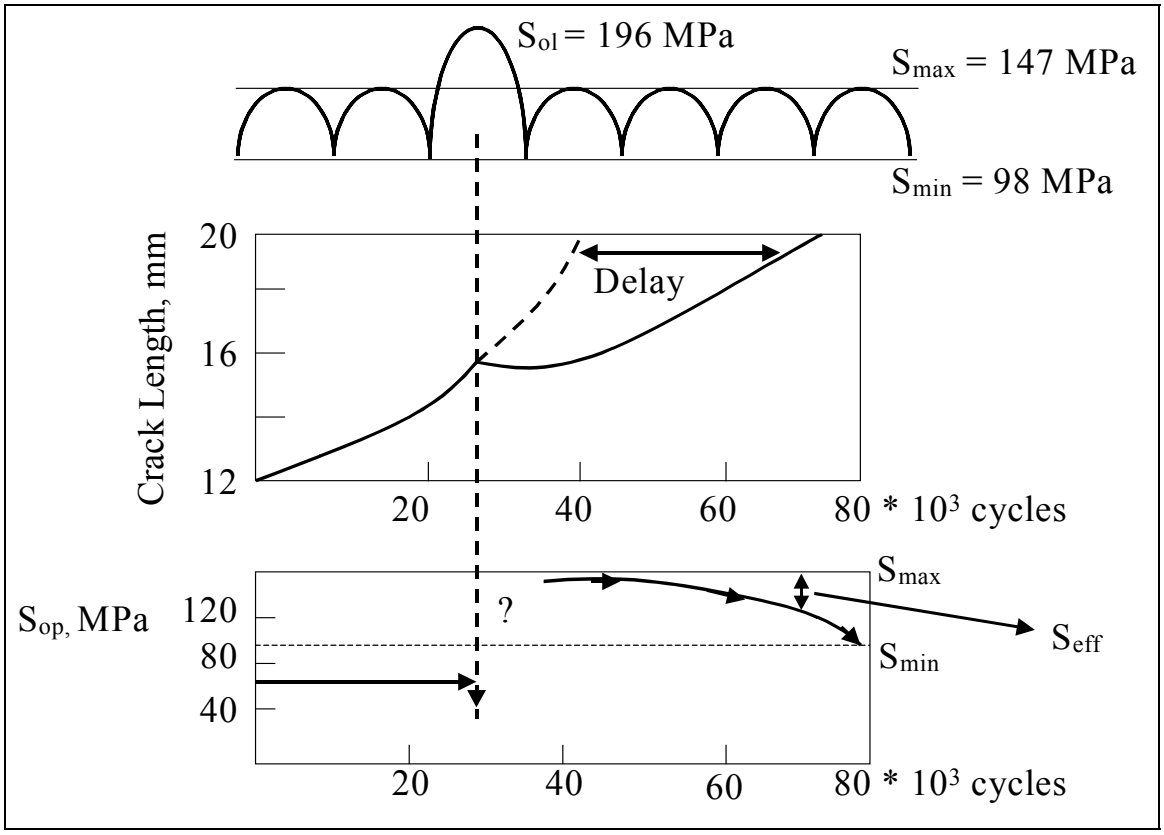

Figure 2.7 Crack growth delay after an overload and the influence on S_{op} in 2024-T3 sheet (Schijve, 1976)

Crack growth retardation after an OL is generally related to the size of the plastic zone, because crack closure results from the crack tip plasticity induced by the OL. Unfortunately, the size of the plastic zone is different for plane strain and for plane stress. In a thin sheet the state of stress at the crack tip is predominantly plane stress, whereas in a thick plate it is predominantly plane strain. It then should be expected that the retardation effects are different for fatigue cracks in thin sheets and thick plates. This is

confirmed by the results of Mills and Hertzberg (Mills and Hertzberg, 1975). Crack growth delay period can be defined in a simple way. The delay period is larger for thinner materials (larger plastic zone) and the delay period increases at higher stress intensities (also lager plastic zone). Both trends agree with the effect of the plastic zone size on crack growth delay.

The 2024-T3 aluminum alloy has a relatively low yield stress (i.e., $S_{0.2}$ = 377 MPa, as compared to $S_{0.2}$ = 473 MPa for the 7075-T6 material). As a consequence, the crack-tip plastic zone sizes were considerably larger in the 2024-T3 sheet specimens than in the 7075-T6 specimens. That explains the larger retardation effect observed in the 2024-T3 experiments. In the 7075-T6 specimens, the plastic zones were smaller and so the retardation effects were less significant (Schijve, Vlutters, Ichsan, and ProvoKluit, 1985). An increased thickness leads to more plane strain at the crack front, and so to smaller plastic zones and less crack growth retardation, thus, the crack growth lives are smaller. The life for the thin sheet material was about 10 times longer than for the thick plate material.

2.5.4 Periodic Overloads & Delayed Retardation

It has also been observed that more overload cycles give a larger delay for a carbon steel (Dahl and Roth, 1979). The test results show that the delay period is larger for higher overloads. However, it is noteworthy that larger numbers of OL cycles increased the crack growth delay period. The latter trend may be explained by considering that crack extension occurs during the OL cycles. More OL cycles then will leave more plastic deformation in the wake of the crack, behind the crack tip (Elber, 1970, & Elber, 1971).

A related problem was investigated by Mills and Hertzberg (Mills and Hertzberg, 1976). They considered the effect of two OL cycles in constant-ΔK tests, with a certain number of cycles (spacing cycles) between the two overloads as a variable (Figure 2.8). The second OL cycle can be applied at the moment that the crack growth retardation of the first one is still effective. The results indicate that the delay of second OL cycle is dependent on the interval between the two overloads. According to Mills and Hertzberg, the maximum interaction between the two single overloads is obtained when the crack growth increment between the overloads is about 25% of the plastic zone of the first OL.

The multiple OL effect has recently been confirmed by Tür and Vardar (Tür and Vardar, 1996). They applied periodic overloads in constant amplitude load tests, with the number of periodicity spacing cycles between the overloads as a variable. Initially the retardation increased for increasing number of periodicity spacing cycles, but for a larger number of spacing cycles it decreased again. In other words, the retardation interactions associated with periodic overloads controlled by the periodicity spacing cycles between overloads was examined. The maximum interaction, and thus the maximum fatigue life, is observed when overload spacing is around half of the delay cycles (N_d) of single overload application. It is reported by, Tür and Vardar, 1996 that the maximum fatigue life at overload ratio = 1.65 has occurred every 5000 spacing cycles, for overload ratio = 1.3 the longest fatigue life occurred every 600 spacing cycles. Generally, retardation increases as

periodicity is increased until a peak is reached, followed by a decrease in retardation afterwards.

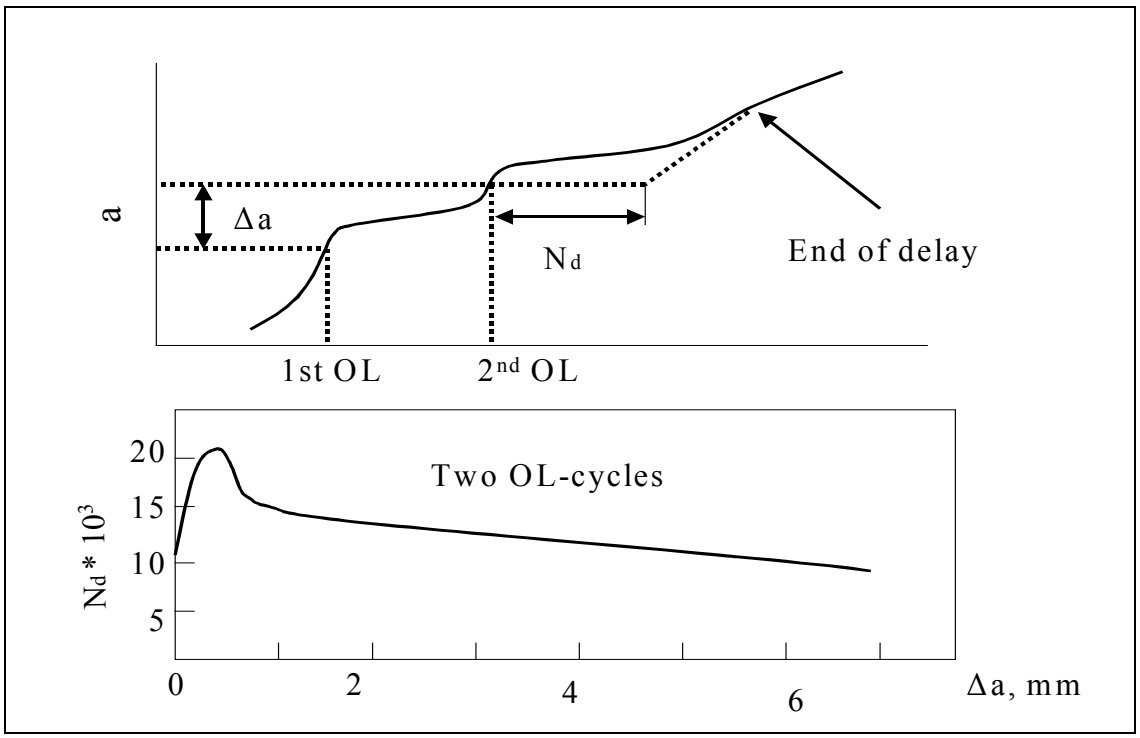

Figure 2.8 Crack growth delay after two overloads cycles as affected by the number of cycles between the overloads (Mills and Hertzberg, 1976)

The fatigue lives for various overloads ratios are studied by Newman, 1997. The longest fatigue life occurred at overload ratio of 2. When the overload ratio reached 3.75, the specimen failed on the first application of overload. When overloads are applied periodically, interaction between overloads becomes possible and retardation is enhanced. Certainly, too closely spaced overloads lead to acceleration rather than retardation; but there is a large range in between where the best retardation occurs. The enhanced retardation due to overloads interactions is well documented, but a systematic study of the periodicity spacing cycle has not been well studied. The fatigue lives for overload ratio of 1.7 and also, for various spacing cycles between overloads (from 20 to 5000 cycles) is investigated in this study.

The spacing between overloads can be stated in terms of crack length as well. In fact, most studies use "Δa" as the measure of spacing between overloads since retarded crack growth is compared with the plastic zone size at the crack tip. The "Δa" between overloads is normalized by plastic zone size of the overload ($2r_y^{OL} = 1/3\pi(K_{OL}/S_y)^2$). The trend is the same which is at $\Delta a = 0.2(2r_y^{OL})$ for constant load control test. It means that the maximum retardation occurs at the same $\Delta a / 2r_y^{OL} = 0.2$ independent of the overload ratio applied. So, the overload induced plastic zone governs the retardation behavior. This maximum retardation occurring at Δa = 0.2 * (overload induced plane strain plastic zone size) for 2024-T3 is reported in the literature, Tür and Vardar, 1996. De Koning (De

Koning and Dougherty, 1981) has introduced the terms *primary plastic deformation* and *secondary plastic deformation*. Primary plastic deformation occurs at the crack tip if plastic deformation penetrates into elastic material that has not been plastically deformed by previous load cycles. Secondary plastic deformation refers to crack-tip plasticity that remains inside a primary plastic zone. More recently, De Koning and Dougherty (De Koning and Dougherty, 1989) have proposed that crack extension during primary plastic deformation is much more effective than during secondary plastic deformation. The first peak load caused a good deal of primary plastic deformation. The second one gave a much smaller contribution of primary plastic deformation, due to the primary plastic zone of the first high load. Similar confirmation was obtained by considering striation spaces in fatigue tests, as discussed in reference (Schijve, 1992). The corresponding plastic zones for this case are schematically indicated in Figure 2.9.

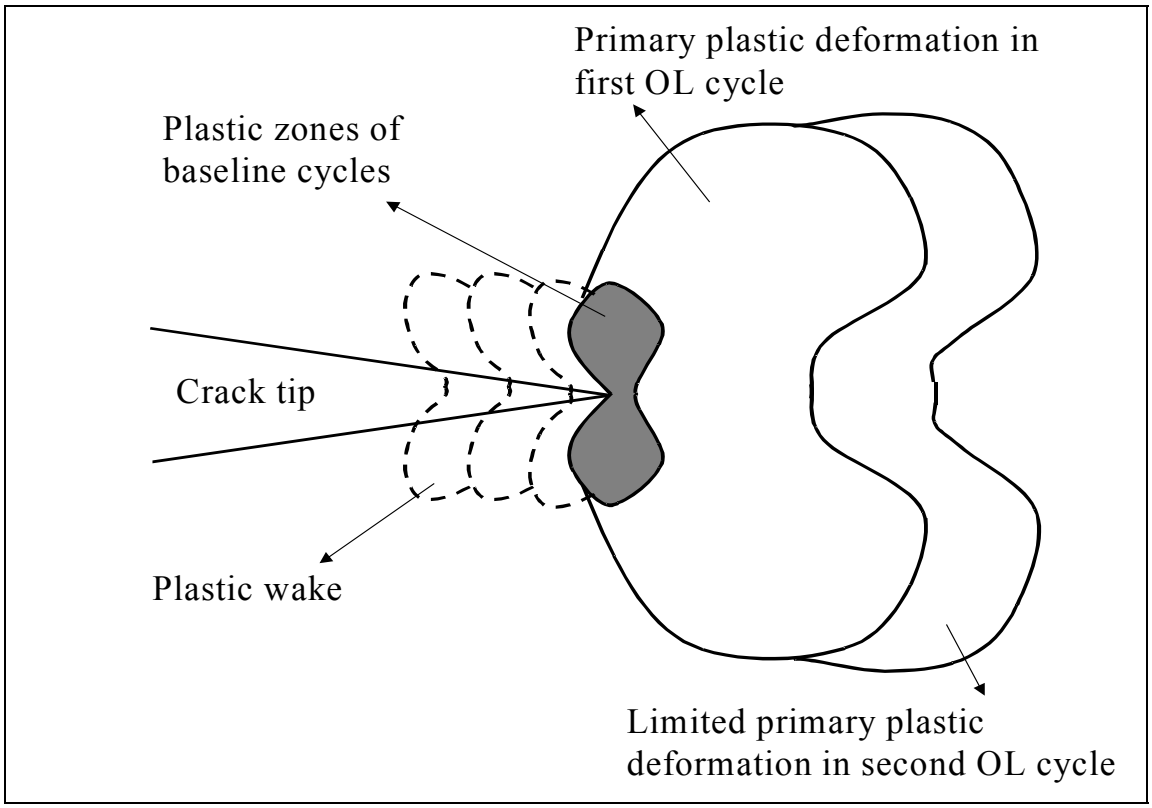

Figure 2.9 Plastic zones in crack growth test with overload cycles (Schijve, 1992)

2.5.5 Crack Closure & Residual Stress in Crack-tip Plastic Zone

Dahl and Roth (Dahl and Roth, 1979) have raised the question whether crack growth delay after an overload is due only to crack closure, or whether there is also an effect of the residual compressive stress in the plastic zone of the crack tip. Interesting experiments were carried out in 1970 by Blazewicz (Schijve, 1979). It simply suggests that the crack growth retardation should be explained by crack closure only. The efficiency of creating a crack length increment (Δa) depends on the plasticity right at the crack tip, not on residual stresses ahead of the crack tip. The residual stress in the crack-

tip plastic zone can have an indirect effect on the cyclic plasticity at the crack tip, but opening the crack tip is the decisive mechanism to have crack extension.

At the surface of a material the crack tip is loaded under plane-stress conditions. Depending on the material thickness, the state of stress at mid-thickness approached plane-strain conditions. The plastic zone size under plane stress is significantly larger than under plane strain. It thus should be expected that crack closure will be more significant near the material surface and will occur to a lesser degree at mid-thickness. The large crack growth retardations induced by overload cycles are a prominent illustration of interaction effects. Interaction effects imply that fatigue damage accumulation in a certain load cycle is affected by fatigue in the preceding load cycles of a different magnitude. In other words, a fatigue cycle will affect damage accumulation in subsequent load cycles.

2.5.6 Results of Simple Variable Amplitude Fatigue Test

Overloads that lead to more favorable residual stresses can extend the fatigue life considerably. These effects are demonstrated in many investigations, and surveyed in reference (Schijve, 1985). Unfortunately, the life enhancement of such loads may give

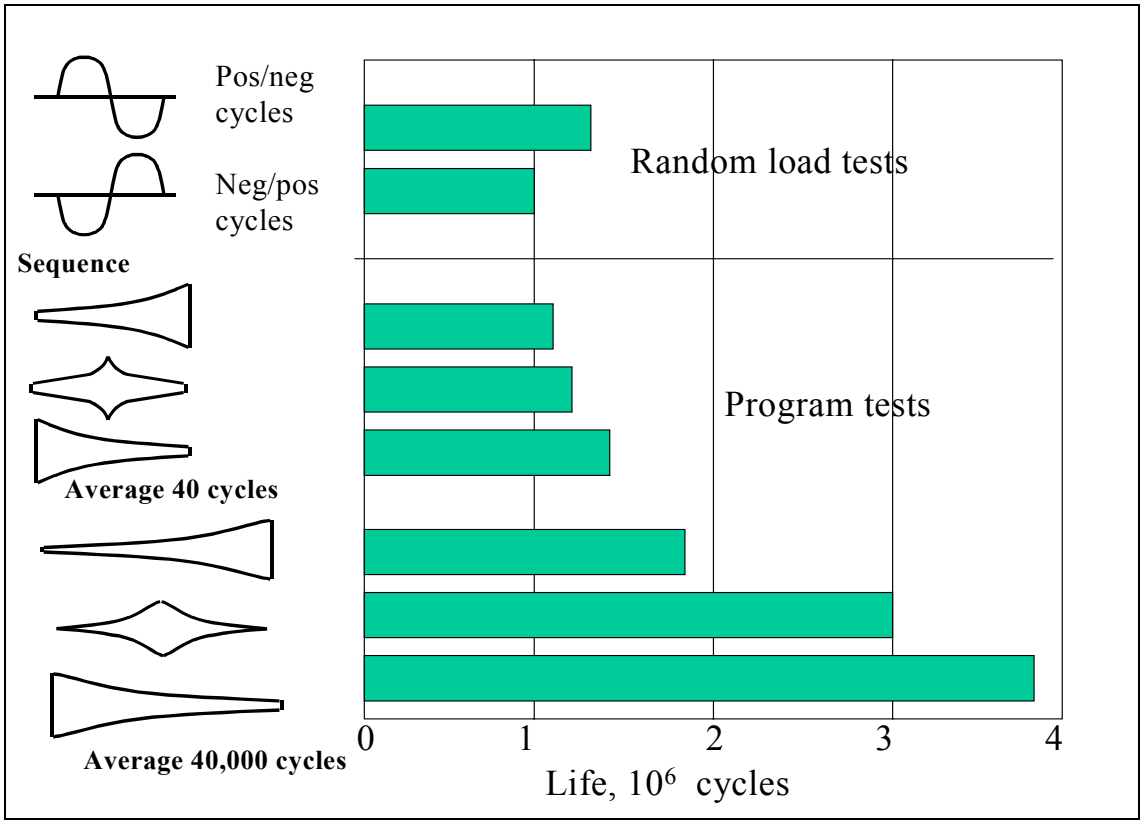

Figure 2.10 Comparison between fatigue crack growth under random loading and different types of program loading in 2024-T3. t (thickness) =2 mm; a (half crack length) =12~50 mm (Schijve, 1973)

unconservative fatigue life results. An illustrative test program was carried out on fatigue crack growth in 2024-T3 sheet material in Figure 2.10 (Schijve, 1973). The load spectrum used was a gust load spectrum of 40,000 cycles with seven different amplitudes.

Two random sequences were applied with full cycles, and the difference between the crack growth lives was rather small. In the program tests with the full spectrum in one period (40,000 cycles), the results indicate two remarkable trends: (a) there was a systematic sequence effect with the longer crack growth life for the Hi-Lo sequence. (b) the crack growth lives were considerably longer than for the random sequence (i.e., about three times longer than for the Lo-Hi-Lo sequence). This is an unconservative result. Fractographic observations indicated that the fracture surfaces of the specimens tested in programmed sequences were rougher than those of specimens tested in random sequences. This test shows that a load spectrum with a random load sequence in service should not be simulated by a programmed sequence with a long period. The programmed sequence is an artificial simulation that cannot be accepted as a simplification. Another specific study was conducted by Newman Jr., Dawicke, 1989. A brief description of load type and results is given here in Table 2.2.

Load type 1: Single spike overload repeated every 50 cycles.
2: Single spike overload repeated every 100 cycles.
3: Five spike overloads repeated every 50 cycles.
4: Five spike overloads repeated every 100 cycles.
5: Single overload-underload cycle repeated every 39 cycles
6: Single underload-overload cycle repeated every 39 cycles

Table 2.2 A brief description of load type (Newman Jr. and Dawicke, 1989)

Load type	Test life cycles	Closure model (α = constraint factor)	
		α = 1.7	α = 1.9
1	474,240	1.4	1.10
2	637,730	1.19	0.97
3	251,210	1.36	1.19
4	409,620	1.28	1.09
5	179,320	1.03	0.95
6	251,050	0.78	0.68

The plane-stress condition is with constraint factor (α = 1), and plane-strain condition with α = 3. The opening stresses during the constant-amplitude loading for load type 3, 4 (five overloads) were slightly higher than those for load type 1, 2 (single overload). These results show that the closure model predicts more delay in crack growth during the constant-amplitude portion for larger number of overloads. This is because five overloads cause a larger zone of residual plastic deformation to remain along the crack surfaces than a single overload. However, the five overloads are more damaging to crack growth than the single overload. Thus, the overall life for load type 3, 4 was shorter than that for load type 1, 2. Also, the opening stresses after the overload-underload were lower for load type 5 than those for load type 6 where the overload and underload were reversed.

Thus, the underload eliminated some of the plastic deformations that were caused during the overload. More details can be found in Newman Jr. and Dawicke, 1989. The following specific observations on fatigue crack growth under VA loading are listed in Table 2.3.

Table 2.3 Specific interaction phenomena during crack growth under variable-amplitude loading

Observation	Related aspects
1. Crack growth retardation or acceleration after overloads	-Delayed retardation
2. Plane strain/plane stress transition	-Effect of thickness -Differences between crack closure at the material surface and at mid-thickness
3. Multiple overload effect	-Initial decreasing growth rate if a crack starts from a notch
4. Incompatible crack front orientation	-Tongue-shaped crack extension during high loads -Accelerated crack growth in mode I

2.6 Fatigue Damage Evaluation and Models to Predict Fatigue Life

For the fatigue life estimates under constant amplitude loading, the fatigue life was represented by the P.C. Paris equation (Paris, 1964). In addition to design applications, analysis of crack growth life is also useful in situations where an unexpected crack has been found in a component of a machine, vehicle, or structure. The remaining life can be calculated to determine whether the crack may be ignored, or whether repair or replacement is needed immediately.

In general, prediction models published in the literature employed basic material fatigue data as a reference. Such data can be fatigue limits, S-N data, fatigue diagrams, crack growth data, and the fracture toughness for final failure. The data are supposed to be characteristic fatigue properties of a material, characterizing the fatigue resistance or the fatigue crack growth resistance. These data are used as the material data to predict the fatigue under VA load histories.

Fracture mechanics offers an attractive way for fatigue life prediction, if fatigue crack growth in metal can be characterized by a simple function, such as the commonly used Paris' Law. This approach works well, if a relatively long fatigue crack has been formed and regular cyclic stresses are involved. The fatigue crack growth is severely affected by overloads or low cycle fatigue proceeding high cycle fatigue (Newman Jr., 1997 & Tür.

Yahya, 1996). Another concern with long crack measurements is that fatigue crack growth characterized by Paris' Law only accounts for a certain fraction (50 to 90%) of total fatigue life. The crack initiation life could be as high as 10 to 50% of total life. The problem of metal fatigue life prediction cannot be solved if the influence of complex loading history on short cracks or fatigue crack initiations is not well understood.

Prediction models in principle adopt a similarity approach (also called similitude): similar stress cycles or similar strain cycles should give the same fatigue damage. Also, similar ΔK_{eff} cycles should give similar crack length increments. This approach implies that fatigue data for most simple conditions are extrapolated to more realistic engineering conditions. But, the extrapolation steps can be quite large. As a consequence, prediction models require empirical verifications. However, to judge the reliability of model, a physical understanding of a model is essential. Because problems involved with crack initiation and crack growth are different, models will be discussed in two categories: models for the crack initiation period and models for fatigue crack growth. In this project, models for the fatigue crack growth are discussed.

Observations on crack growth retardation after overloads and the occurrence of crack closure have stimulated the development of several prediction models in crack growth under variable amplitude loading. Most literature sources on prediction models give verification test data of crack growth in aluminum alloy sheet, mainly because variable amplitude loading and fatigue crack growth are important for aircraft structures. Acceleration and retardation must also both be considered. Inspections for cracks can be done by a variety of means, including visual examination, x-ray photography, reflection of ultrasonic waves, and application of electric currents.

2.6.1 Crack Growth Models to Predict Fatigue Life

Consider a growing crack that increases its length by an amount "Δa" due to the application of a number of cycle ΔN. The rate of growth with cycles can be characterized by the ratio Δa/ΔN, or for small intervals, by the derivative da/dN. If the applied loading is constant, the corresponding gross section nominal stresses S_{max} and S_{min} are also constant. For fatigue crack growth, the stress range ΔS is defined as S_{max} - $S_{min.}$ The primary variable affecting the crack growth rate is the range of the stress intensity factor. This is calculated from the stress range ΔS. The equation is given in [2.2]. The value of Y depends only on the geometry and the relative crack length (a/b), where "b" is a width dimension of the specimen. In this thesis work, Paris' and Walker's equations are used to consider the effect of stress ratio R. However, the effect of frequency is not considered when predicting the fatigue life.

a) Paris' equation

For a given material, the crack growth behavior can be described by the relation between cyclic crack growth rate da/dN and stress intensity range ΔK. The relationship representing this crack growth behavior is given by Paris' equation (Paris, 1964).

$$\frac{da}{dN} = C(\Delta K)^m \tag{2.4}$$

where C is a constant and m is the slope on the log-log plot (da/dN vs. ΔK).

b) Walker equation

The above equation doesn't consider the effect of the stress ratio R. For characterizing the effect of R on da/dN vs. ΔK curves, the Walker's relationship (1970s) is used.

$$\frac{da}{dN} = \frac{C1}{(1-R)^{m1(1-\gamma)}}(\Delta K)^{m1} \tag{2.5}$$

where γ is a constant for the material. Constants C and m for equation (2.5) are thus

$$C = \frac{C1}{(1-R)^{m1(1-\gamma)}} \qquad \text{m = m1} \tag{2.6}$$

Hence, constant C is predicted to be a function of R, but the slope m is unaffected by R. Constants for the Paris, and Walker equations are given for several materials in Dowling, 1993. The crack growth rate exponent m is higher for brittle materials. For ductile metals, m is typically in the range 2 to 4.

A variety of mathematical expressions have been proposed to represent da/dN vs. ΔK curves. Some of them are quite complex. Sometimes, as many as ten empirical constants may be required to accurately represent the behavior of a given material. Some of these are not merely empirical, but are based on attempts to include modeling of plasticity induced crack closure of the crack, and other physical phenomena (effect of retardation) that affect crack growth. For example, Forman-Metu (NASGRO 1992) equation is one of the latest. It considers the effect of crack closure and retardation.

2.6.2 Life Estimates for Constant Amplitude Loading

As mentioned in Chapter 1, from the crack growth rate da/dN the fatigue life can be calculated by numerical integration. To perform the integration for a particular case, it is necessary to substitute the specific da/dN equation for the material and R of interest, and also the specific equation for ΔK for the geometry of interest. Some useful closed form solutions exist, but numerical integration is necessary in many cases.

Consider a situation where the crack growth rate is given by Paris' equation and where Y = Y (a / b) is constant, or can be approximated as constant, over the range of crack length a_i to a_f. The value of C used can include the effect of the Stress ratio R, as from the Walker approach using equation (2.6). Assume that S_{max} and S_{min} are constant, so that ΔS and R are also both constant. Therefore, C, F, ΔS, R, and m are all constant. The only variable is a, and integration can be expressed by

$$N_f = \int_{a_i}^{a_f} \frac{da}{f(\Delta K, R)} = \int_{a_i}^{a_f} \frac{da}{C(\Delta K)^m} = \int_{a_i}^{a_f} \frac{da}{C(Y \Delta S \sqrt{\pi a})^m} \quad (2.7)$$

$$= \int_{a_i}^{a_f} \frac{1}{C(Y \Delta S \sqrt{\pi a})^m} \frac{da}{a^{m/2}}$$

If m = 2, this equation (2.7) is mathematically indeterminate.

Other crack growth rate equations can be obtained by the same method. In using the above equation to estimate the crack growth life, the final crack length a_f equation (2.8) is often unknown and should be determined before the equation (2.7) is applied. It is also necessary to determine $Y_f = Y(a_f / b)$, so that it can be confirmed that this value does not differ excessively form $Y_i = Y(a_i / b)$. If Y_f and Y_i differ by more than about 10 to 15%, the resulting error in N_f due to using a constant value will be very large. In that case, numerical integration is then usually needed. Under constant amplitude cyclic loading, the value K_{max} corresponding to S_{max} increases as crack grows. When K_{max} reaches the fracture toughness K_c, for the material and thickness of interest, failure is expected at the length a_f that is critical for the failure.

$$a_f = \frac{1}{\pi}\left(\frac{K_c}{YS_{max}}\right)^2 \quad (2.8)$$

Since, Y varies as crack grows, an iterative solution is needed to obtain a_f.

This above closed form of equation (2.7) is for the crack propagation life. It doesn't include the crack initiation life. Actually, the fatigue life results from this thesis work include both the crack initiation life and crack growth life until failure. Therefore, the results from this work need to be divided into two parts (fatigue crack initiation life and fatigue crack growth life). But, the transition from crack initiation to crack growth is not clear. In this thesis work, the total fatigue life is used instead of crack growth life. As crack accelerates during their growth, most cycles are exhausted while the crack is short, and few cycles are spent while the crack is near its final length.

2.7 Summary and Gaps in the Knowledge

The critical point in this work is the investigation of the effect of Corrosion-Prevention-Compounds on fatigue life of center pre-crack specimen (middle tension specimen) Al-2024-T3 with or without water vapor. Unfortunately, limited laboratory or field research has been undertaken to investigate the effect of the usage of CPC with center pre-crack specimen. Most research has been done to investigate the fatigue behavior of bolted joints, or double lap joints to see the effect of CPC on fatigue life. When aircrafts are operated in real service, a crack whether it is small or large is existent in the material or on the

material in a corrosive environment such as salt fog, or water vapor. An obvious method for preventing corrosion is to exclude the environment from the metal surface.

The CPCs are inexpensive and easily applied, and widely used throughout the aircraft industry. Therefore, in this thesis work, center per-crack specimen is used to investigate the effect of CPC on fatigue life in water vapor environment. Generally, the CPC provides significant corrosion protection for aluminum alloys. The corrosion protection performance of the CPC depends on the type of the test environment. In this thesis, the water vapor is considered as a corrosive environment.

In the past, most work didn't consider the effect of stress ratio and frequency. In this thesis work, task #1 tests are run with CPC considering the effect of different stress ratio and frequency. The actual mechanisms of corrosion fatigue with CPC is still unclear, obviously more work is required with a center pre-crack specimen in a corrosive environment. In the second part of this thesis work, tests are run to measure the effect of periodic overloads on fatigue life of aluminum alloy 2024-T3. Much is available in the literature in the case of single overloads and their effect on the crack growth retardation. Interactions between periodic overloads need to be determined to increase the fatigue life of test specimen. Therefore, it is important to control the spacing cycles between overloads and overload ratio to achieve the maximum fatigue life of aluminum alloy 2024-T3. In this work, the spacing cycles is controlled approximately from 50 to 4000 cycles to find out the optimum spacing cycle between overloads to achieve the maximum fatigue life. At this optimum number of spacing cycle, the interactions between overloads become the maximum, in other words, the crack growth retardation due to overloads becomes maximum. Therefore, the maximum fatigue life should be achieved at this optimum spacing cycle. Experimental methods for corrosion fatigue and periodic overloads are addressed in chapter 4.

CHAPTER 3. NUMERICAL ANALYSIS

3.1 Scope of Numerical Work

This thesis work includes numerical analysis to simulate the crack growth retardation due to periodic overloads induced residual stress field at the crack tip and to calculate the stress intensity factor for the plane strain and plane stress cases at different applied loading conditions for 2-D & 3-D modeling. The first part of the numerical analysis provides a significant insight to understand the mechanism of overload induced residual stress field in spite of its limitation. In further work, cyclic strain hardening, node release method, fracture criteria and non-linear material behavior should be considered in the future work.

In this work, the crack tip displacement is recorded as the crack growth length. Instead of the real crack growth modeling, elastic strain and plastic strain are recorded at the crack tip. In second part of the numerical work, modeling crack region and calculating the fracture parameter (stress intensity factor: K_I) are focused on. The most important region in modeling the fracture region is the region around the crack. The singularity at the crack tip should be picked up when modeling the crack. The PREP7 KSCON command, which assigns element division sizes around a key-point, is used in a 2-D model to create 2-D crack tip elements with nodal singularity. This command removes the nodal singularity at the crack tip.

3.2 Crack Growth Retardation due to Overload Induced Residual Stress Field

In this study, a finite element analysis using ANSYS 5.7 was conducted to simulate the crack-growth retardation due to the single-peak overload under cyclic loadings. The objective of simulation is to predict the crack-growth retardation due to the influence of overload in Aluminum Alloy with a center pre-crack specimen. The compressive residual stress at crack-tip after the overload is the major factor causing retardation (Figure 3.1).

Residual stresses are produced when one region of a part experiences permanent plastic deformation while other regions of the same part either remain elastic or are plastically deformed to a different degree. The overload introduces a large plastic zone in which the material experiences permanent deformation. Upon unloading, the surrounding elastic material attempts to resume its original size (the plastic zone is permanently deformed) and by doing so, exerts compressive stresses on the plastically deformed material at the crack tip. When the crack has grown through the region (compressive plastic zone) of residual stresses after a further period of cyclic loadings, the crack growth resumes at the propagation rate expected under constant amplitude cyclic loadings. It means that if we can introduce compressive residual stress by the controlled yielding (overload), the fatigue life of a component will be significantly increased (Figure 3.2). This enhancement of fatigue life depends on the peak and magnitude of the overload ratio.

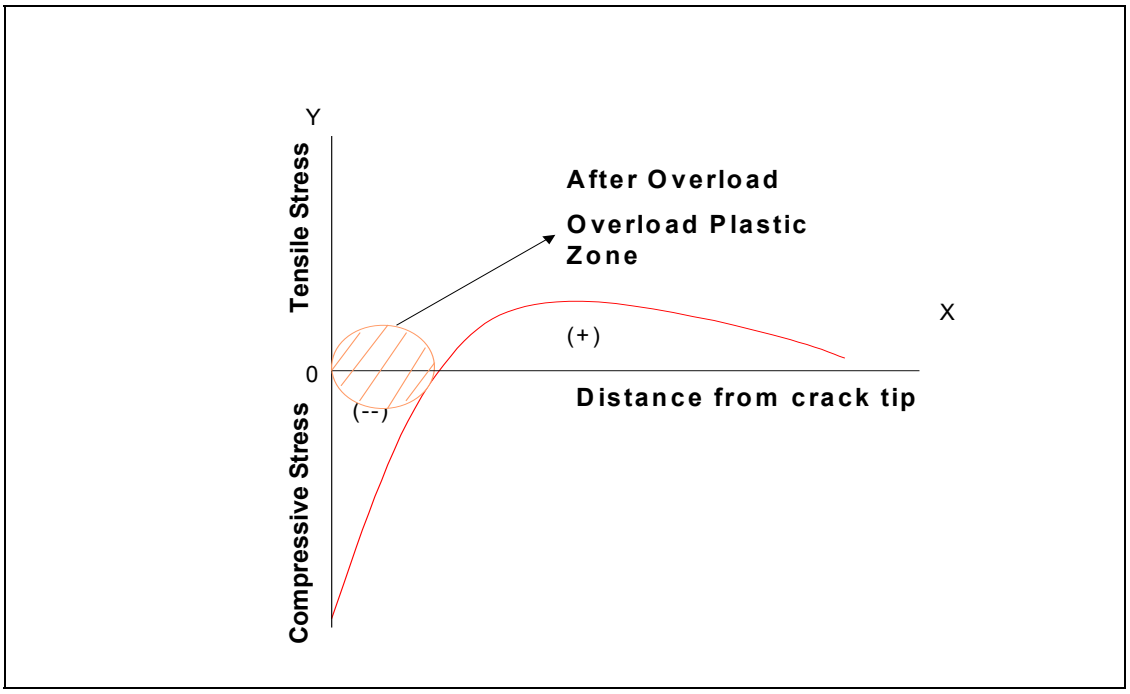

Figure 3.1 Residual compressive stresses ahead of crack tip

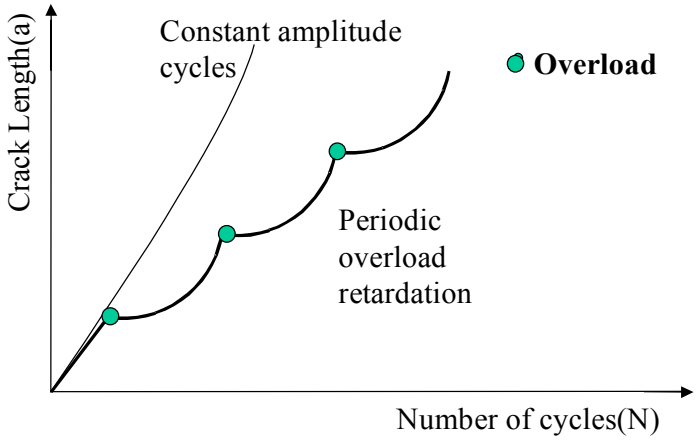

The slower crack growth continues until the crack grows beyond the overload plastic region(**The Wheeler model of crack growth inside an overload plastic zone)**. This beneficial residual stress effect of overload is called **crack growth retardation**.

Figure 3.2 Fatigue life enhancement due to overloads

During the crack propagation, the crack growth is affected by environmental conditions, material properties, and loading conditions including the magnitude and stress ratio of overload. Careful attention must be given to a series of critical decisions about element type, mesh method (Mapped mesh, Free mesh), element length size, the selection of material behaviors, model design (geometry of the specimen, symmetric boundary condition or loading condition) and crack tip modeling (singular point) if the analysis is to be reliable. A model for the elastic-plastic finite element simulation in plane stress is presented by running a nonlinear analysis with ANSYS 5.7. The bilinear inelastic isotropic hardening (an elastic-plastic model) is considered as element material behavior. Large deformation effects were also considered during the nonlinear analysis. The crack growth simulation was based on the stress-strain curve of the node point near crack-tip. The displacement near crack-tip, the stress-strain curve and stress redistribution along the crack plane after overload were investigated during cyclic loadings. The specific results that are being aimed for are the effects of overload induced residual compressive stresses on the crack growth near the crack tip.

3.3 Finite Element Modeling

In this study, 8 node PLANE82 was used as an element type with the plane stress option. Nonlinear analysis was performed with an elastic-plastic material model under the action of cyclic loadings when a single high peak overload was introduced. A bilinear inelastic isotropic hardening curve (an elastic-plastic model) was considered as material behaviors. The tangent modulus is taken as 0 GPa. Therefore, material behaves like an elastic-perfect plastic model. The mechanical properties of specimen (Aluminum) are shown in Table 3.1. The fracture toughness of Al-2024-T3 is 34MN/$m^{3/2}$.

Table 3.1 Mechanical properties of Aluminum Alloy

Elastic modulus (E)	Poisson Ratio (ν)	Yield Stress	Temperature (T)	Tangent modulus (H)
70 [GPa]	0.33	325 [MPa]	20 [°c]	0 [GPa]

The region around the crack tip that is under investigation needs to be finely meshed. In addition, the results are compared between the mapped and free mesh (with KSCON command which assigns element division sizes around a singular key point (crack tip)). It automatically generates singular elements around the specified key point.

To advance the crack, the crack tip advance scheme involving node release immediately after maximum load on each cycle is the preferred technique. The crack advancement at maximum loading was found to yield a closer representation of the actual crack phenomenon. The node release technique can also be carried out by using a series of nonlinear compression-only and tension-only springs along the crack plane or element

death option provided by ANSYS code. However, in this work, the node near the crack tip was employed to determine the crack growth or displacement. The displacement and stress-strain curve of the node near the crack tip are recorded.

The mesh refinement study was also conducted to determine the size of element length (L_e) required along the crack plane. The parameter selected for rating mesh size was the ratio of the element length (L_e) to the plastic zone size (r_p). The equation of the plastic zone radius given by Irwin's expression assuming plane stress condition is given in equation (2.3).

The value of K_I (Stress Intensity Factor) was chosen as 35 [$MN/m^{3/2}$]. To avoid the discontinuity between the crack stress and strain, element size less than L_e/r_p =0.1 are required to appropriately capture the crack plasticity effects. The element length size could be obtained as 0.5mm. Symmetry boundary conditions were adopted (Figure 3.3). The boundary conditions used for the specimen were as follows.

(1) All nodes along the crack plane were constrained from the crack tip to the right bottom edge along the crack plane.
(2) All nodes were constrained along the left plane.

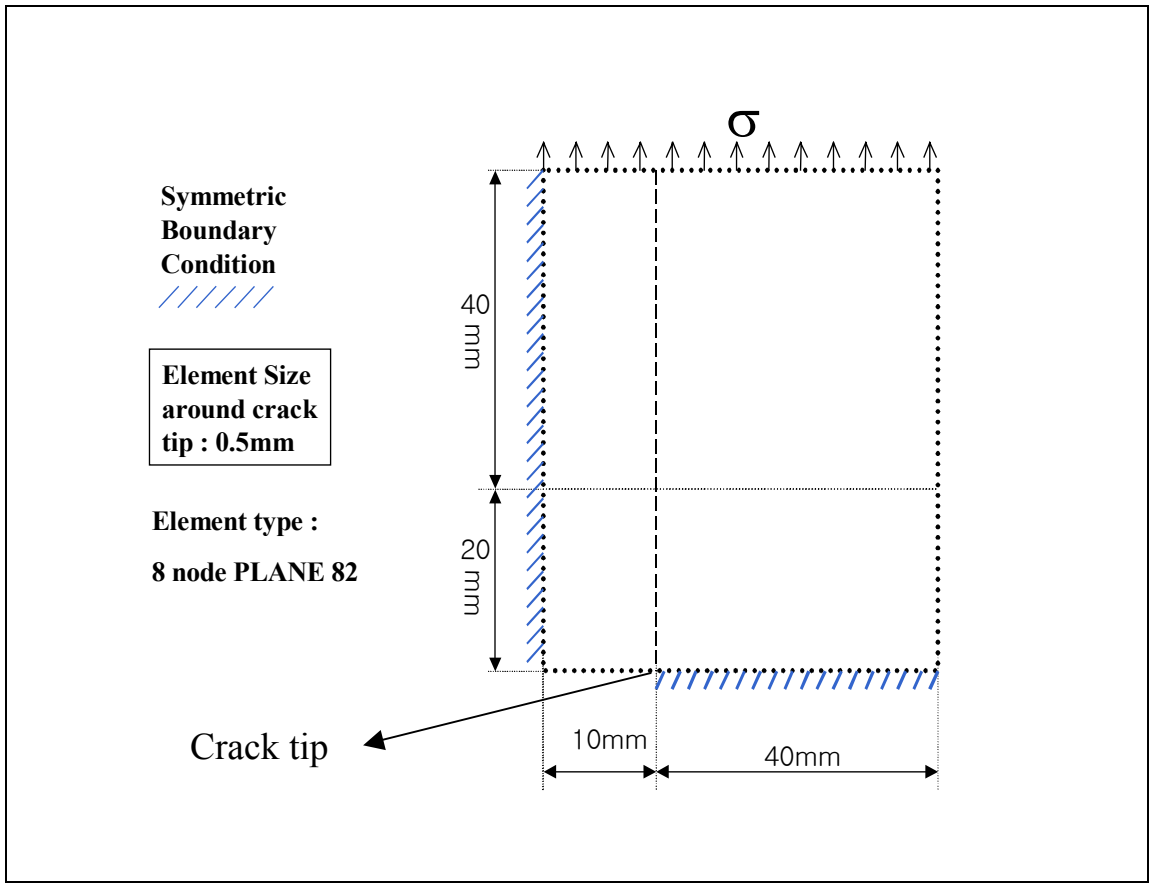

Figure 3.3 Geometry and dimension of finite element modeling

The external load within a load step was applied in increments over a certain number of sub-steps. The size of the load increment is controlled by defining these subsequent sub-steps. For the cycling loading steps, 5 sub-steps were specified, with a maximum of 25 and a minimum of 3 sub-steps. For the overload step, 10 sub-steps were specified, with a maximum of 50, and a minimum of 5 sub-steps. Since, the specimen exhibits a severe nonlinear behavior during the overload, the load increment was increased up to $1/10^{th}$ of the size of the overload. In order to investigate stress relaxation after overload, constant cyclic loadings after the peak high overload have also been applied (Figure 3.4).

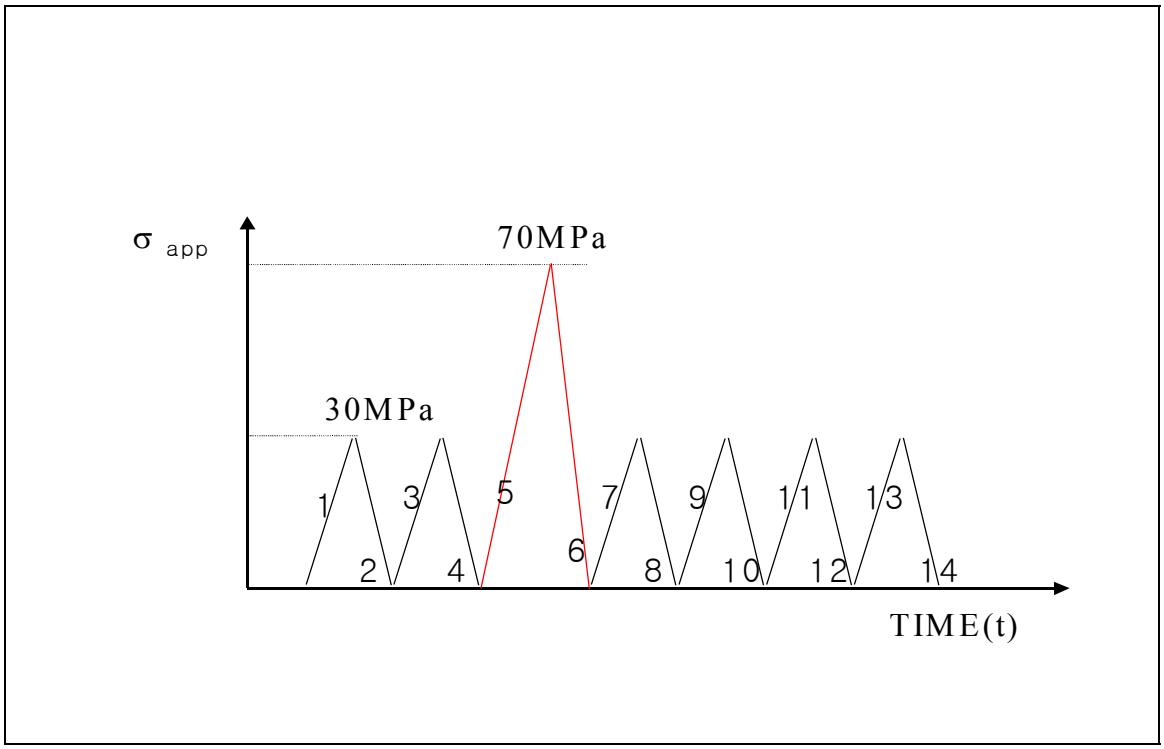

Figure 3.4 Applied cyclic loading conditions with a high peak overload. (The number of load step is shown on the load line.)

In order to investigate the effect of residual stresses in fatigue crack growth, it is necessary to know (1) the magnitude and shape of the residual stress field, and (2) the combined effect of the residual stress and applied stresses on the fatigue crack growth rate. Therefore, the displacement of the node near crack tip was monitored over the entire solution. Furthermore, the reaction forces at the same node were monitored. The crack tip stress-strain curve at the same node was also plotted. The strain was obtained by adding elastic and plastic strain. Combined residual stresses and applied stresses along the crack plane were shown by using the path operation command. The results showed the influence of overload induced compressive residual stresses on the crack plane. These compressive residual stresses will decrease the crack growth rate. Overloads ratio, strain hardening, node release technique, creep and various loading conditions should be conducted in future work.

3.4 Results and Discussions

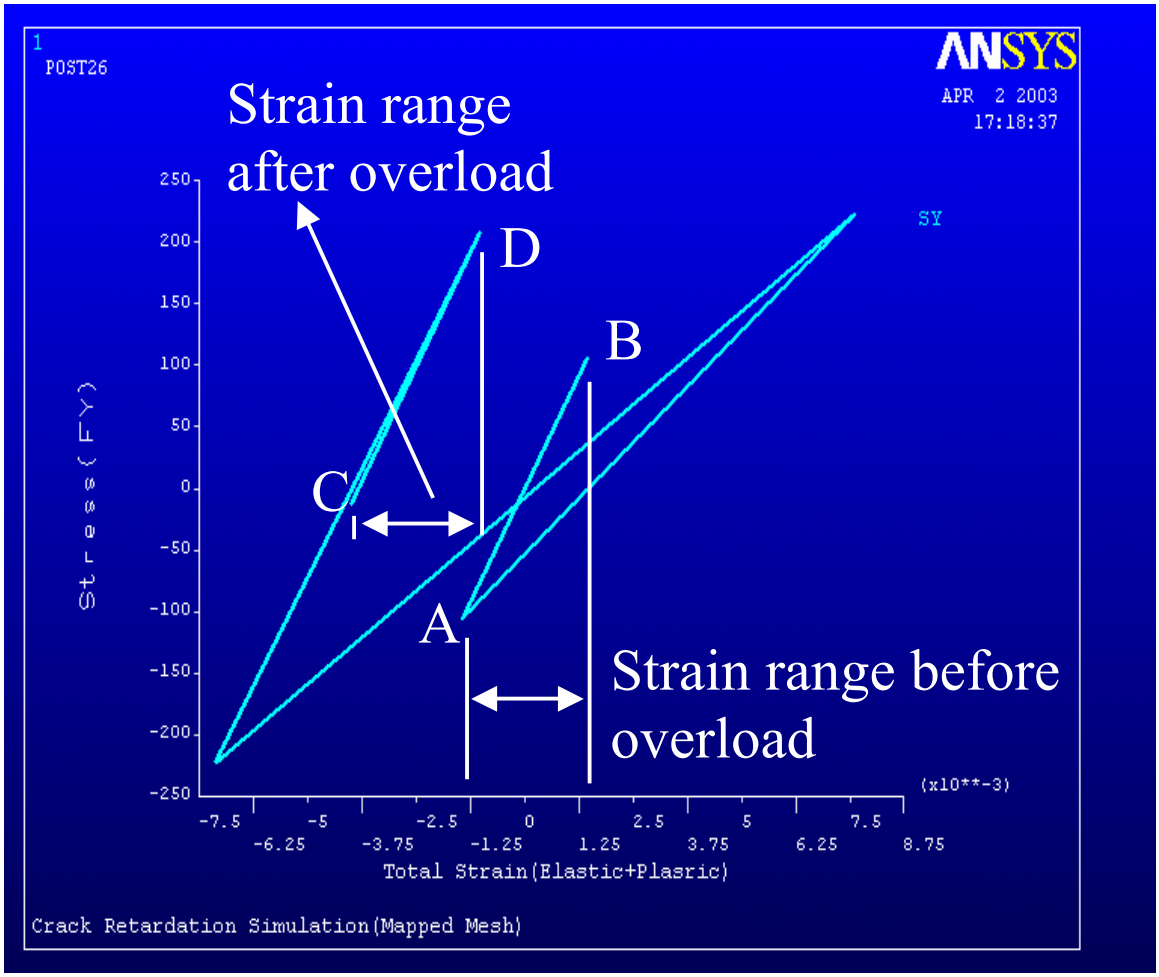

Figure 3.5 Stress-Strain Curve after one overload (80MPa)

In Figure 3.5, strain range before overload between A and B moves back to negative strain rage C-D after overload 80 MPa. Cyclic strain range is considerably reduced after one overload of 80 MPa. Therefore, the crack growth rate will decrease accordingly. Strain range becomes negative after overloading due to the residual compressive stress. This result might be considered crack growth retardation. This decreased strain will affect a change of displacement near crack tip. This graph shows the effect of overloading near crack tip displacement. The combined effect of the residual stress and applied stresses on the crack plane before overload and after overload was shown in order to know the effect of residual stresses in fatigue crack growth. The initial objective of this study is to investigate the influence of overload induced residual compressive stress field on fatigue crack growth. Accordingly, residual compressive stress is induced due to the overload when the model is stressed over yield point 200 MPa, but the stress-strain curve turns out to be unrealistic. The reason was a bilinear inelastic isotropic hardening (BISO) curve (an elastic-perfect-plastic model) was considered as a material behavior. Actually, the BISO

(material model behavior) cannot be used in order to simulate accurate rate-dependent plasticity as well as cyclic hardening or softening. Therefore, careful attention should be given to selections like element type, material model behavior. Further work needs to be carried out in the future. In order to simulate the actual crack growth, mesh at the crack-tip need to be re-meshed whenever the crack advances along the crack plane.

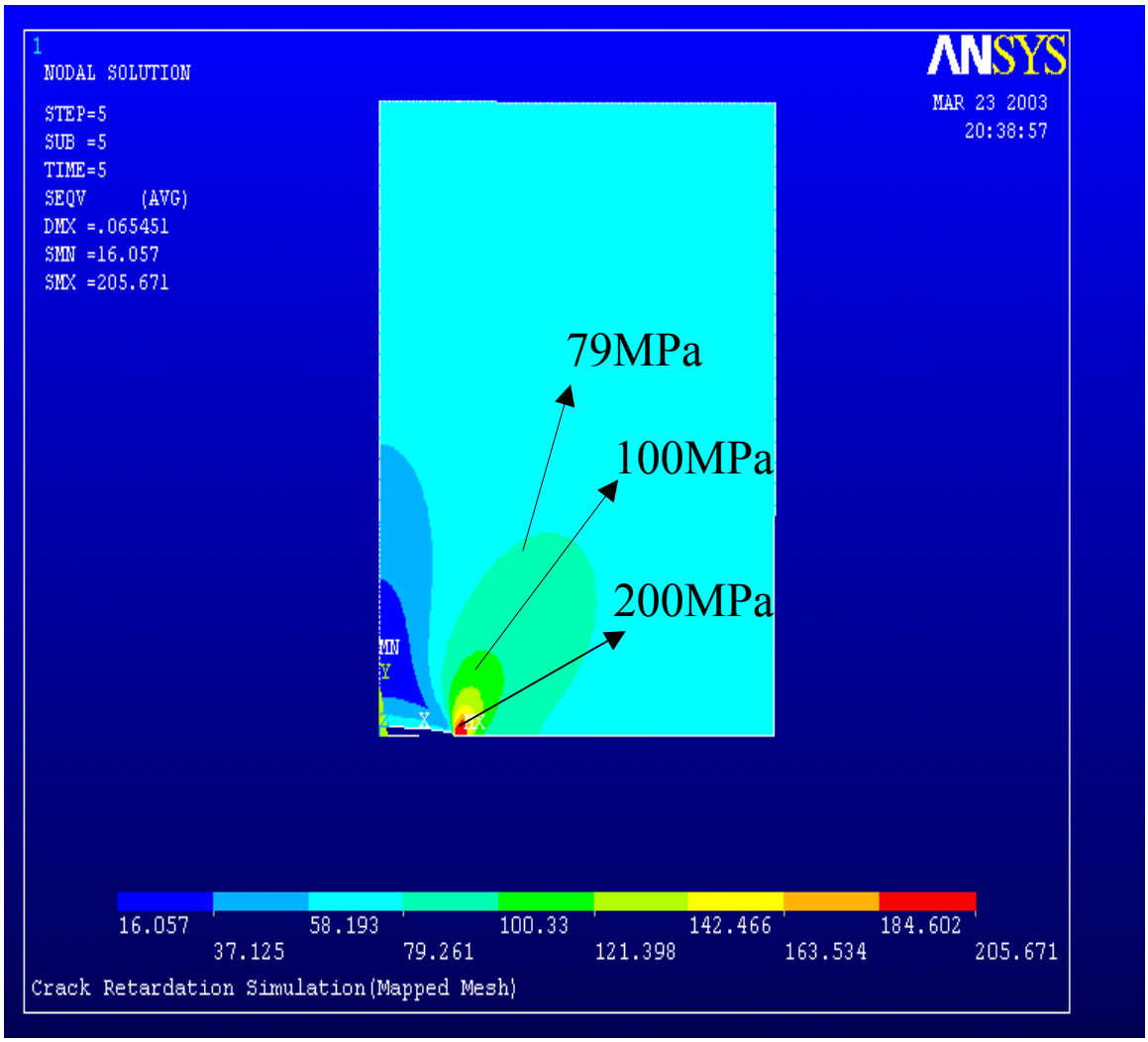

Figure 3.6 von-Mises Stress during overloading (after load step 5)

In Figure 3.6, the yield has occurred at the crack tip due to the stress concentration when overload of 70 MPa was applied. Therefore, the plastic deformation occurred at the crack tip. This plastic deformation at the crack tip was squeezed after overload and then, compressive residual stress field has been induced at the crack tip.

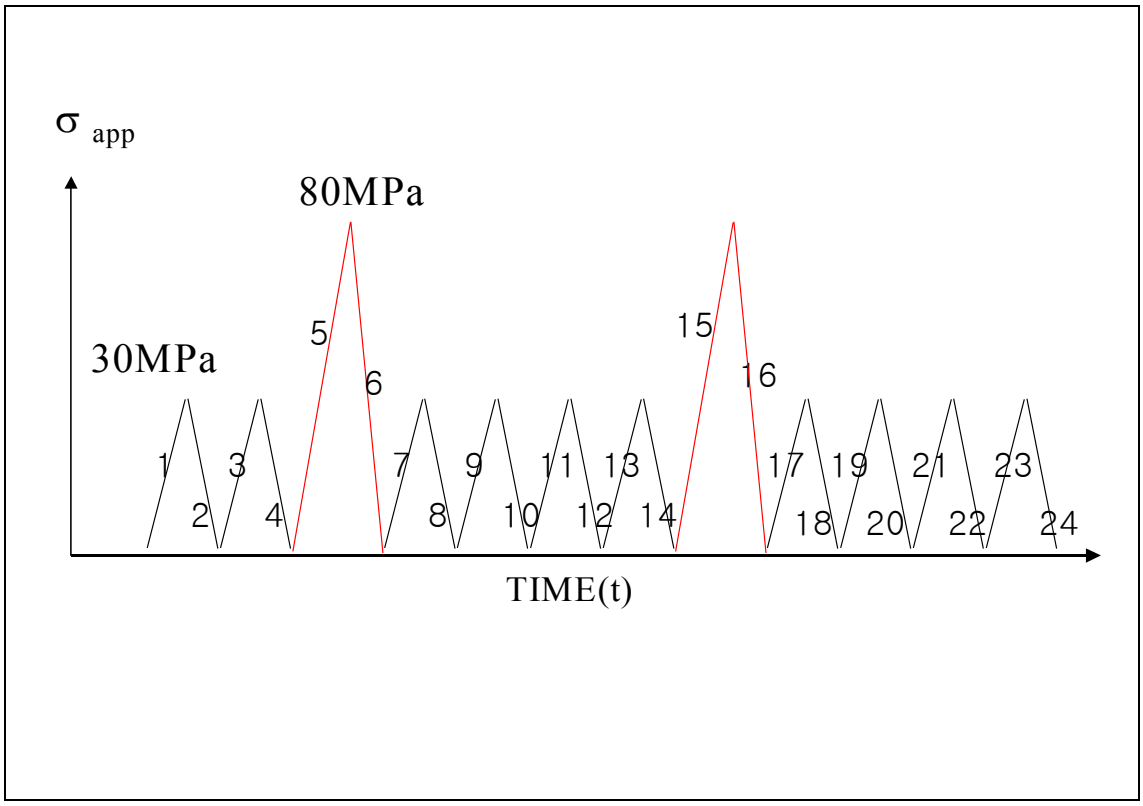

Figure 3.7 Applied cyclic loading conditions with two overloads condition (80MPa-80MPa)

To induce proper residual stresses, the peak and magnitude of the overload ratio are important, and therefore various loading conditions need to be conducted. Two overloads condition are carried out as shown in Figure 3.7.

The plot of total strain curve (Figure 3.8) didn't show any significant decreased in strain reading after second overloading for 80MPa-60MPa. After the second overload, the second reduced strain was recorded only in 80MPa-100MPa. In case of 80MPa-80MPa (Figure 3.7), the strain range after the second overload was plotted at the same strain range level following the first overload. This is because the material used in this study did not remember the load history. The effect of first overload was completely eliminated during the second overload.

Plasticity is a non-conservative, path-dependent, time-dependent and temperature-dependent phenomenon. Two overloads effects on the crack plane and crack growth rate were not well documented in this study, because the material did not remember the load history. Von-Mises stress redistribution along the crack plane after first overload (80MPa) was reduced as shown in Figure 3.9.

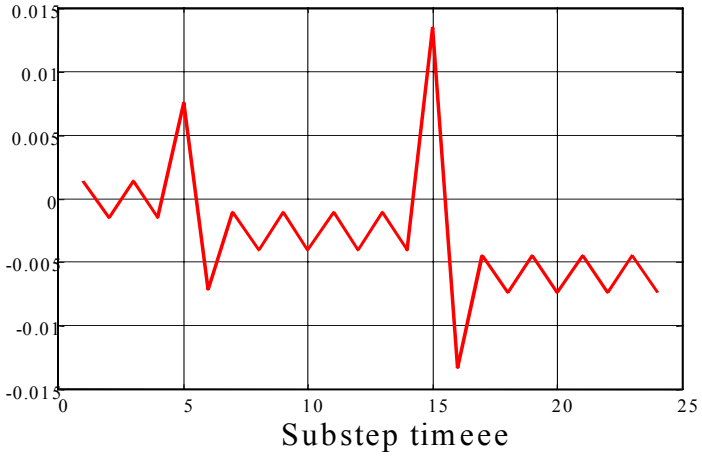
0.015
0.01
0.005
0
-0.005
-0.01
-0.015
0
5
10
15
20
25
Substep timeee

Real material doesn't behave like the elastic perfect-plastic model. Furthermore, in this study, the strain hardening was not considered. For more accurate modeling, appropriate material behavior should be considered, such as, cyclic strain hardening or softening and path or time dependent plasticity, which might remember the load history. Large deflection and large strain are associated with nonlinear analysis. Various loading conditions like overload ratio, stress ratio, and stress range should be conducted in the future. To advance the crack, the crack tip advance scheme (involving node release immediately after maximum load on each cycle) needs to be carried out. Further work is recommended.

The results of these studies vary depending on the following

- the type of nonlinear material behavior being defined
- the selection of appropriate element types
- the type of mesh (Mapped or Free)

3.5 Calculation of Stress-Intensity Factor in Center-Crack Specimen

Cracks and flaws occur in many structures such as bridges, aircrafts, and offshore structures, sometimes leading to disastrous failures. The engineering field of fracture mechanics was established to develop a basic understanding of such crack problems and the state of stress around the crack region. Fracture mechanics deals with the study of how a crack initiates and propagates through the material under applied loads. It involves comparing analytical predictions and simulations with experimental results. Typically, the crack length increases with application of cyclic load.

In order to estimate the exact crack growth rate analytically, fracture parameters such as stress intensity factor in the crack region should be known exactly. Crack growth rate (da/dN vs. ΔK) is based on the concept of the stress intensity factor that defines the near crack-tip driving forces for crack growth and thus, able to characterize crack growth for different geometries and loads.

Calculation of fracture parameters such as the stress intensity factor is important to fundamental studies of fracture mechanics, crack growth rate and fatigue mechanism. The objective of this study is to calculate the stress intensity factor (K_I) at the crack tip in the center-crack plate (2-D and 3-D) by Ansys 5.7, in the center crack plate specimen of Aluminum Alloy. This fracture parameter will be used as basic information to obtain the crack growth rate in the structure.

Some typical fracture parameters are:

- Stress intensity factors (K_I, K_{II}, K_{III}) associated with the three basic modes of fracture.
- J-integral, which may be defined as a path-independent line integral that measures the strength of the singular stresses and strains near a crack tip.

- Energy release rate (G), which represents the amount of work associated with a crack opening or closure.

3.6 Research Methodology

Modeling the crack region provides a sound basis to predict some typical parameters. Solving a fracture mechanics problem in ANSYS involves performing a linear elastic or elastic-plastic static analysis and then using specialized post-processing commands or macros to calculate desired fracture parameters. In this study, two main aspects have been concentrated on.

1. Modeling the crack region
2. Calculation of stress intensity factor K_I

The most important region in a fracture model is the region around the edge of the crack. To pick up the singularity around the crack, the crack faces should be coincident, and the elements around the crack tip (or crack front) should be quadratic, with mid-side nodes placed at the quarter points. Such elements are called singular elements. The recommended element type for a two-dimensional fracture model is 2-D plane strain elements (PLANE82), the 6-node triangular solid, and for three-dimensional model is SOLID95, the 20-node brick element. A one-quarter model is used because of symmetry. A long plate with a center crack is subjected to an end tensile stress σ as shown in Figure 3.11. The objective of this study is to determine the fracture mechanics stress intensity factor K_I in 2-D and 3-D model. Geometric properties are shown in Table 3.2 with loading conditions. The dimension is also shown in Figure 3.10.

Table 3.2 Geometric properties of specimen

Material Properties	Geometric Properties (Dimension as shown in Fig. 3.10)	Loading
E = 70 GPa	a = 5 mm	σ = 100 MPa
v = 0.3	b = 25 mm	
$K_I = 35$ MN/m$^{3/2}$	h = 25 mm	
	Thickness (t) = 5 mm (3-D) (Fig. 3.12)	

The simple 2-D model using PLANE82 is created by automatic (free) mesh generation. The PREP7 KSCON command, which assigns element division sizes around a key-point, is particularly useful in a 2-D model to create 2-D crack tip elements with nodal singularity. This command removes the nodal singularity at the crack tip. POST1 is used to get fracture mechanics stress intensity factor (K_I) by displacement extrapolation (KCALC command). The dimension of 2-D modeling is shown below with nodes. In fracture mechanics, the K_I value represents the resistance to failure. This stress intensity factor that is given in equation (1.1), is associated with the geometry of modeling, the crack size and the applied stress.

In middle-center crack specimen, the geometry factor "Y" is

$$Y = \sqrt{\sec(\pi a / 2b)} = 1.118 \qquad \text{ASTM Standard E 647 (ASTM, 95)} \qquad (3.1)$$

The applied stress (σ) is 100 MPa, the crack size (a) is 5 mm and the half width (b) is 25 mm. Hence, the calculated stress intensity factor at a center crack specimen (finite width plate) is 14 MN/$m^{3/2}$.

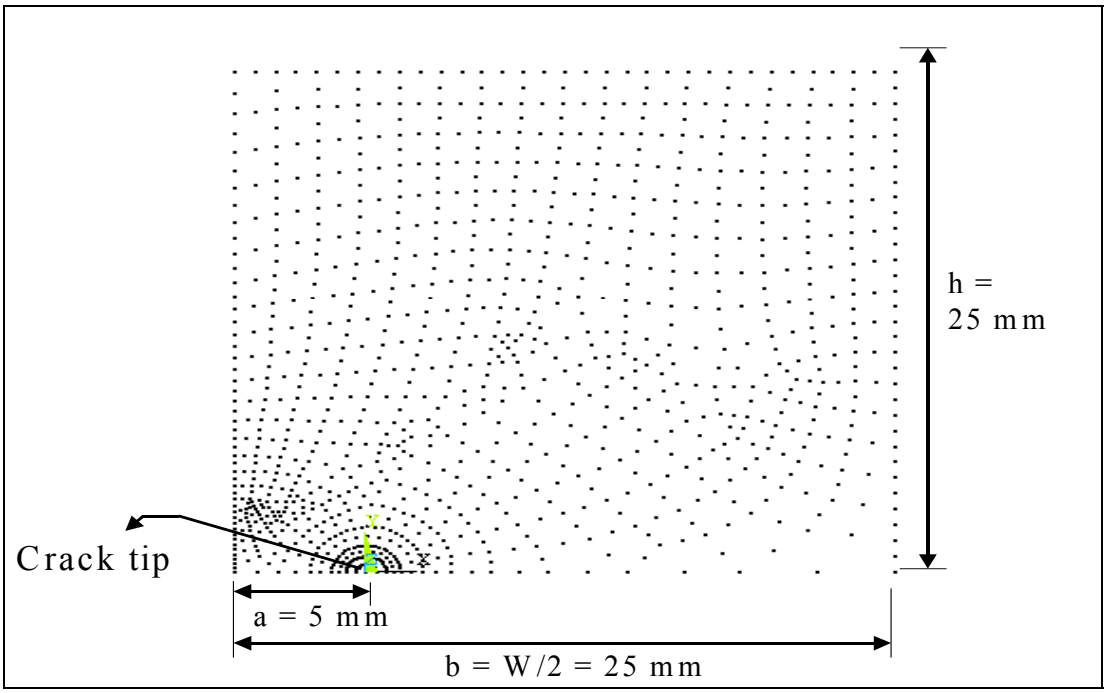

Figure 3.10 Dimension of finite element modeling

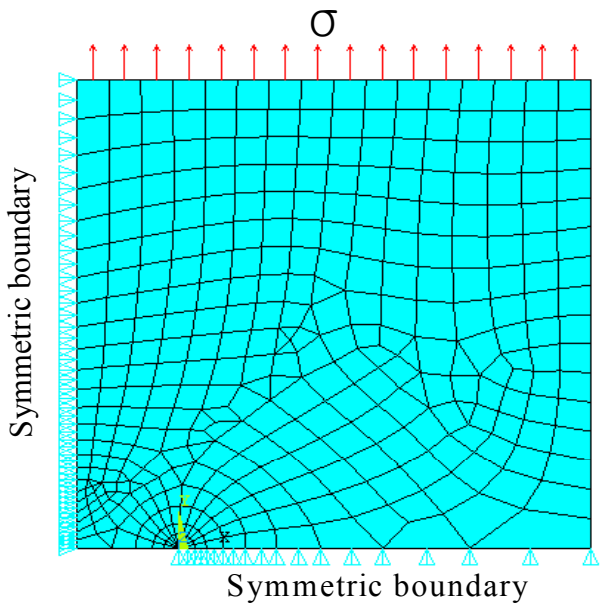

Representative finite element model with boundary conditions (2-D model with Plane82)

Figure 3.11 Element modeling with boundary conditions

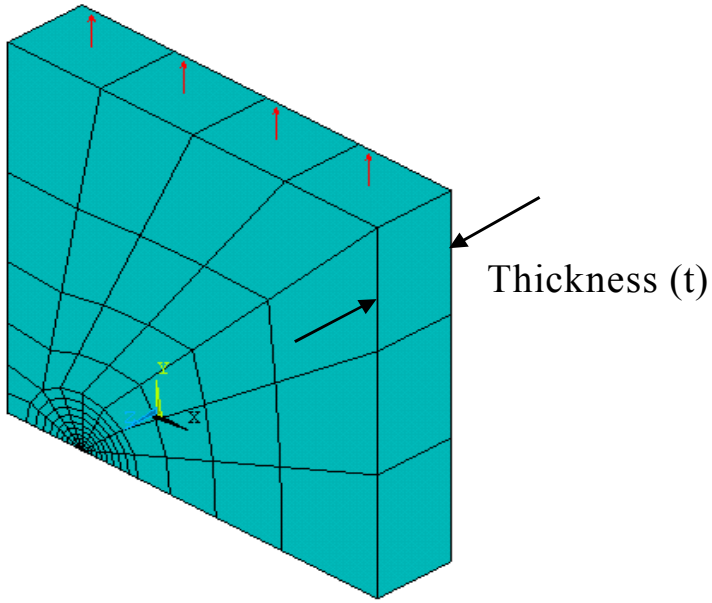

Representative finite element modeling (3-D model with Solid95)

Figure 3.12 Three-dimensional element modeling with applied stress

The element modeling is shown with symmetric boundary conditions in Figure 3.11. The stress is applied at the top of the specimen. Generating a 3-D fracture model is considerably more involved than a 2-D model. The KSCON command cannot be used. The 3-D solid (SOLID95 elements) is used to simulate the 3-D fracture model. In the 3-D analysis, the plane strain condition is achieved by constraining UZ degrees of freedom of all the nodes (displacements in the Z-direction). The 3-D element modeling is shown in Figure 3.12.

3.7 Results

(1) 2-D modeling

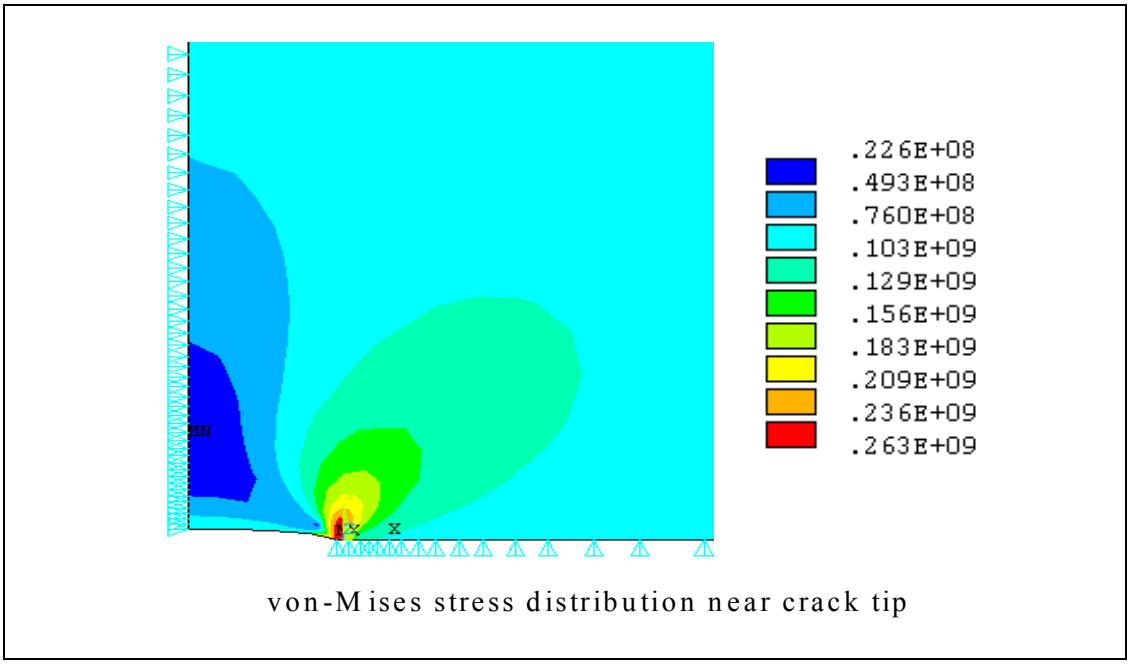

Figure 3.13 von-Mises stress distribution near the crack tip in 2-D modeling and K_I = 11.96 MN/m$^{3/2}$

Actually, the crack tip elements to designate singularity should be created by macro files to remove the singularity at the crack tip in 3-D modeling. But, in this study, singularity point at the crack tip was not removed. At the crack tip, the elements are disjointed. The reason is that the compatibility couldn't be maintained at the crack tip. Because the crack tip elements are not assigned to remove the singularity at the crack tip in 3-D modeling. This result shows the importance of the singularity at the crack tip element.

(2) 3-D modeling

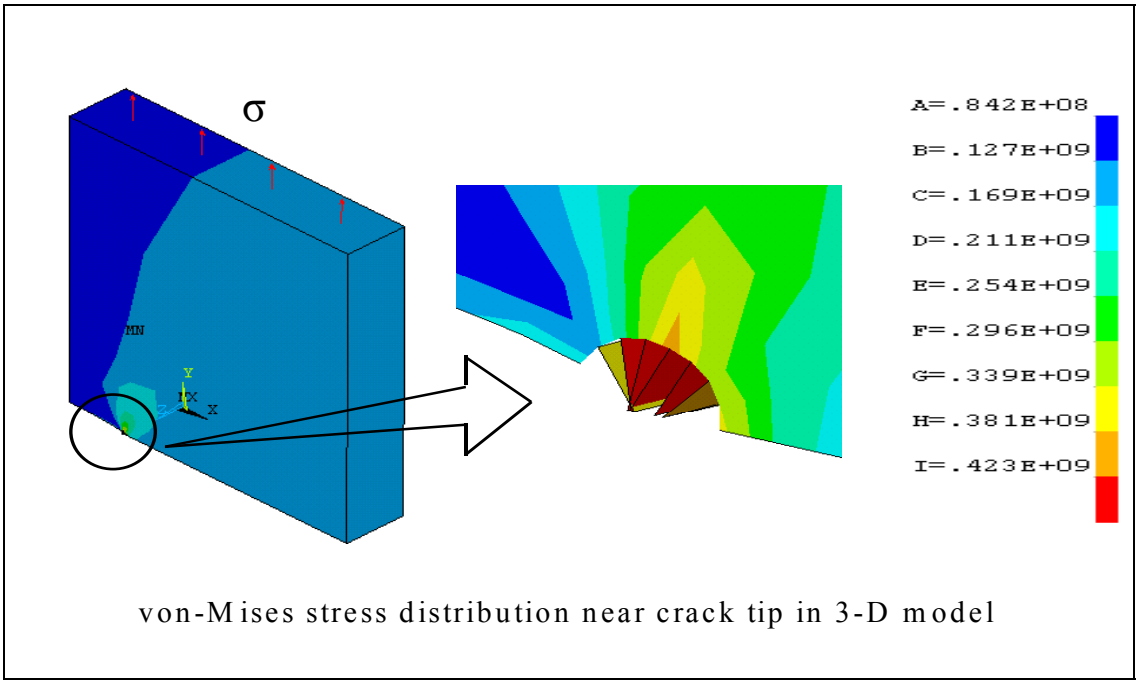

Figure 3.14 von-Mises stress distribution at the crack tip in 3-D modeling and K_I = 12.93 MN/m$^{3/2}$

(3) The results of K_I for the plane strain and plane stress cases at different applied loading conditions for 2-D & 3-D modeling are shown in Table 3.3 ~ Table 3.8. The column chart in Figure 3.15 shows all results. These data provides significant insights when calculating the fatigue life of the test material.

Table 3.3 Stress intensity factor (K) for the plane strain case, (σ = 100MPa)

	K_I (2-D model) MN/m$^{3/2}$	K_I (3-D model) MN/m$^{3/2}$	% variation from 2-D to 3-D
By Displacement Extrapolation (KCALC command)	11.96	12.93	8.11%
By the calculation of fracture mechanics	14	14	

Table 3.4 Stress intensity factor (K) for the plane strain case, (σ = 200MPa)

	K_I (2-D model) $MN/m^{3/2}$	K_I (3-D model) $MN/m^{3/2}$	% variation from 2-D to 3-D
By Displacement Extrapolation (KCALC command)	23.92	25.86	8.11%
By the calculation of fracture mechanics	28	28	

Table 3.5 Stress intensity factor (K) for the plane strain case, (σ = 250MPa)

	K_I (2-D model) $MN/m^{3/2}$	K_I (3-D model) $MN/m^{3/2}$	% variation from 2-D to 3-D
By Displacement Extrapolation (KCALC command)	29.9	32.32	8.09%
By the calculation of fracture mechanics	35	35	

Table 3.6 Stress intensity factor (K) for the plane stress case, (σ = 100MPa)

	K_I (2-D model) $MN/m^{3/2}$	K_I (3-D model) $MN/m^{3/2}$	% variation from 2-D to 3-D
By Displacement Extrapolation (KCALC command)	12.84	13.36	4.05%
By the calculation of fracture mechanics	14	14	

Table 3.7 Stress intensity factor (K) for the plane stress case, (σ = 200MPa)

	K_I (2-D model) $MN/m^{3/2}$	K_I (3-D model) $MN/m^{3/2}$	% variation from 2-D to 3-D
By Displacement Extrapolation (KCALC command)	25.67	26.71	4.05%
By the calculation of fracture mechanics	28	28	

Table 3.8 Stress intensity factor (K) for the plane stress case, (σ = 250MPa)

	K_I (2-D model) $MN/m^{3/2}$	K_I (3-D model) $MN/m^{3/2}$	% variation from 2-D to 3-D
By Displacement Extrapolation (KCALC command)	32.1	33.4	4.04%
By the calculation of fracture mechanics	35	35	

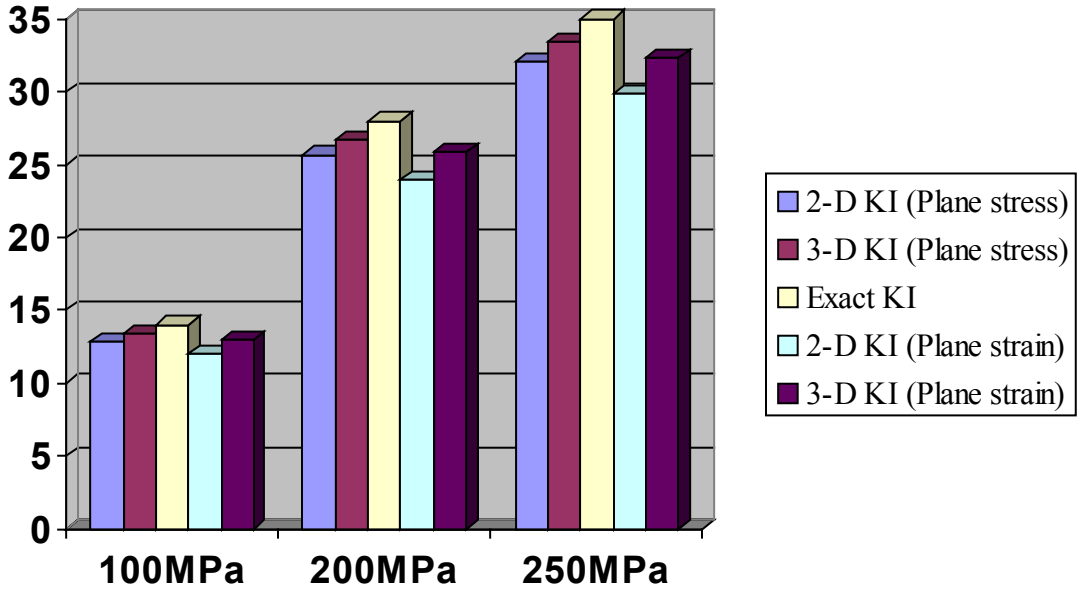

Figure 3.15 Stress intensity factor K_I in 2-D and 3-D for plane stress and strain conditions

3.8 Verifying Corrosion Fatigue Testing

The test for task #1 was conducted by using 1 specimen for each condition. There is a large range of region test results in this thesis work due to experimental constraints. To find out the fatigue life of test specimens theoretically, Walker (Walker, 1970) or Paris (Paris, 1964) equations are used in this thesis work. Finally, the theoretical results were compared with the experimental results of task #1. From the dimension of test specimen geometry, half width is b=24.5mm, the thickness t is 4.1 mm and an initial crack length a_i is 5 mm.

$$S = \frac{P}{2bt} = \frac{25000 \quad N}{2 \times 0.0245 \quad \times 0.0041} = 124 \quad MPa \qquad \text{at R = 0.2} \qquad (3.2)$$

The geometry factor Y is varying during the crack growth depending on the crack length. This value of Y in equation (3.1) can be obtained in ASTM Standard E 647. This approximation is accurate within 2% for (α = a / b) < 0.9. To find out the fatigue crack growth life by Paris or Walker equation, both the initial crack length a_i and final crack length a_f should be known. The final crack length a_f can be obtained from the trial and error method. Since, Y varies as crack grows, a iterative solution is needed to obtain a_f. The fracture toughness K goes close to K_{IC} = 34 MN/$m^{3/2}$ if the trial crack length is final crack length a_f. The procedure is shown in Table 3.9 for the case of R (stress ratio = 0.2). The fracture toughness K is close to K_{IC} = 34 MN/$m^{3/2}$ when the trial crack length (a) is 14.4 mm. Therefore, the final crack length a_f is assumed as 14.4 mm for R = 0.2 from the above analysis. Also, the real final crack length from experiments is 15 mm. For the case of R = 0.5, the same procedure can be used to find out the final crack length. In this case, the only difference is the gross stress S.

$$S = \frac{P}{2\,bt} = \frac{40000 \quad N}{2 \times 0.0245 \quad \times 0.0041} = 200 \quad MPa \qquad \text{at R = 0.5}$$

Table 3.9 Final crack length

Trial crack length "a" [mm]	$\alpha = \frac{a}{b}$	$Y = \sqrt{\sec\frac{\pi\alpha}{2}}$	$K = YS\sqrt{\pi a}$
5	0.20408	1.02648	15.9526
10	0.40816	1.11704	24.5508
11	0.44897	1.14598	26.4161
12	0.48979	1.17986	28.40649
13	0.53061	1.21959	30.562
14	0.57142	1.2664	32.933
14.4	0.58775	1.28752	33.95
14.5	0.59183	1.2930	34.219

In the case of stress ratio 0.5, at trial crack length a = 8 mm, the fracture toughness K = 33.967 is approximately close to K_{IC} = 34 MN/$m^{3/2}$. Therefore, we can assume that the final crack length a_f is 8 mm for R = 0.5. But, the real final crack length from this thesis work is about 10-11 mm. The result from this method is not the same in case of the stress ratio 0.5.

Consider the situation where the crack growth rate is given by the Paris's equation and where F = F (a / b) is constant, or can be approximated as constant, over the range of crack length a_i to a_f. The value of C used can include the effect of the Stress ratio R, as from the Walker approach (Walker, 1970) that is given in equation (2.6). The γ, C1, m1 are constants for the Al-2024-T3. These constants are determined from Dowling, 1993. The values are given below, γ = 0.68, C1 = 1.42*10^{-8}, m1 = m = 3.59.

The m1 in Walker's equation (Walker, 1970) is equal to m in Paris' equation (Paris, 1964). Assume that S_{max} and S_{min} are constant, so that ΔS and R are also both constant.

Therefore, C, Y, ΔS, R, and m are all constant. The only variable is "a", and integration can be expressed by the equation (2.7).

Equation (2.7) is for the crack propagation life that doesn't include the crack initiation life. Actually, the fatigue life results from this thesis work include both the crack initiation life and crack growth life until failure. Therefore, the results from experimental work need to be divided into two parts (fatigue crack initiation life and fatigue crack growth life). But, the transition from crack initiation to crack propagation is not clear. In this thesis work, the total fatigue life is used instead of fatigue crack growth life. As crack accelerates during their growth, most cycles are exhausted while the crack growth is non-exist, and few cycles are spent while the crack is growing. Experimentally, the fatigue crack growth part is observed as around 30% of the total fatigue life, and the remaining 70% is the fatigue crack initiation part of the total fatigue life. The result which is calculated from the closed form of equation is N_f = 3000 cycles. This fatigue crack growth result N_f = 3000 cycles is around 23% of the total fatigue life cycles 13466 cycles for the test case R=0.2, f=0.5.

In the case of R=0.5, the only difference is S_{max} = 240 MPa. The final crack length is taken as 8 mm, while the geometry factor Y is taken as 1.3. Thus, N_f from the same procedure is 2474 cycles. The fatigue crack growth result N_f=2474 cycles is 29 % of the total fatigue life cycle, 8550 cycles for R= 0.5, f=0.5.

3.9 Discussions of Numerical Work

The value of the stress intensity factor (K_I) from this study shows the valid results, if these results are compared with the exact value of K_I from fracture mechanics. The K_I in case of plane stress is close to the exact value of K_I from the fracture mechanics (% variation between result by KCALC command and result by fracture mechanics ranges from 4.5% to 8.3% depending on 2-D or 3-D). The difference in value for K_I between plane stress and plane strain results from the state of modeling. In plane stress, ductility dominates the state of modeling, while, in plane strain, brittleness dominates the state of modeling. Generally, K_I in ductile material (plane stress) is higher than that in brittle material (plane strain).

The difference between 2-D and 3–D results from the singularity at the crack tip was noted. In this study, the K_I in 3-D modeling has a higher value. The reason is that the singularity was not designated in this 3-D modeling. But, K_I in 2-D modeling shows valid values with the exact value from the fracture mechanics. The results show that the % variation of K_I (from 2-D to 3-D) depends on the plane stress or plane strain, not on the various stress level. The % variation for plane strain is 8%, and the % variation for plane stress is 4%. In this study, the importance of the singularity at the crack tip should be taken into consideration in fracture modeling. The obtained value of stress intensity factor (K_I) by using displacement extrapolation (KCALC command) in ANSYS shows the valid results in 2-D modeling. This data provides useful information in calculating fatigue life.

CHAPTER 4. EXPERIMENTAL TECHNIQUE

4.1 Corrosion Fatigue under Corrosive Environment with CPC

The experimental part of the project consisting of crack growth test under constant amplitude loading on middle center-crack specimen made of aluminum alloy (2024-T3) are carried out in two stages. One specimen is tested per simulated conditions. In order to study the influence of frequency and stress ratio on the effect of fatigue life with or without the CPC (Corrosion Prevention Compounds), tests are performed at two frequency ratios, 0.5 Hz and 1.0 Hz and two stress ratios of R=0.2 and R=0.5. LPS 3 Heavy-Duty Inhibitor is used in this study as a CPC. It is provided by LPS Laboratories, Atlanta Headquarters, an Illinois Tool Works Company. The test matrix is given below in Table 4.1.

Table 4.1 Test matrix for corrosive fatigue on fatigue life

	Test Program	Freq. 0.5 Hz		Freq. 1 Hz	
		R = 0.2	R = 0.5	R = 0.2	R = 0.5
Stage 1	Dry air	1	1	1	1
	Water Vapor	1	1	1	1
	CPC + Dry air	1	1	1	1
	CPC + Water vapor	1	1	1	1

The MTS 810 universal testing machine is used to perform the required test. A PC is coupled to the MTS machine to provide constant amplitude loads with MTS TestStar Version 4.0E and Function Generator Version 4.0E software. The crack growth rate is monitored by crack propagation strain gage (TK-CPA01-005). The data is recorded by strain smart (Data Acquisition System). In this study the humid-air tests is performed at around 95 ~ 100% humidity. The humid-air circulates the transparent plastic corrosion chamber. The corrosive environment (humid-air) is produced with *Ultrasonic Humidifier*. The humidifier produces soothing cool mist into the corrosion chamber through clean tube.

Surface analysis and SEM micrograph are conducted on the specimens to understand the mechanism by which CPC affect crack growth. Standard methods for conducting fatigue crack growth tests have been developed, notably ASTM Standard E647. The experimental work involved in data reduction, analysis, plotting of crack growth rate, comparison with literature results are described in detail in ASTM E647 and Saxena, 1996. Crack growth tests are most commonly conducted using zero-to-tension loading, R = 0, or tension-to-tension loading with a small R, such as R = 0.1. Variations of R in the range 1 to 0.1 have little effect on most materials. Therefore, stress ratio R = 0.2 is selected.

4.1.1 Effect of Periodic Overloads on Fatigue Life

The specific objective of this task is to study the influence and interactions of periodic overloads damage on fatigue life on Al-2024-T3. The research focused on the fatigue life and crack growth behavior of Al-2024-T3. By varying the number of low cycle fatigue (LCF), the degree of fatigue damage was changed. This study provides a more reliable basis for fatigue life predictions for various loading conditions. This will also give us recommendations for service life extension and develop improved fatigue life assessment tools.

One major difficulty in fatigue analysis and life assessment for metal is that the commonly used linear cumulative damage law does not always apply for fatigue under varying loading conditions. Since most metal structures are subjected to different loading conditions, the loading history dependence has a profound influence on fatigue life. Also, using SEM, damage could be visualized in the material where the overload occurs. The intended work will include (1) modeling of overload damage during low constant amplitude cycles; (2) modeling of overloading effects on fatigue crack growth; and (3) formulating equations for life time prediction for industrial applications. The test matrix is given below in Table 4.2 to perform the task #2.

Table 4.2 Test matrix for periodic overloads on fatigue life

Spacing cycles between overloads	50	100	200	400	800	2000	4000
OLR = 1.7	1	1	1	1	1	1	1

4.2 Corrosion Fatigue Crack Growth Test Method

Laboratory fatigue test can be classified as crack initiation or crack propagation. In crack initiation testing, specimens are subjected to the number of stress cycles required for a fatigue crack to initiate. In crack propagation testing, fracture mechanics methods are used to determine the crack growth rates of preexisting cracks under cyclic loading. In general, fatigue life testing is stress controlled (SN) or strain controlled (ε -N). The test specimens are described primarily by the mode of loading, such as axial stress, plane bending, rotating beam, or alternating torsion. Testing machine is defined by several classifications: (a) the controlled test parameter (load, deflection, strain, twist, torque, etc.); (b) the design characteristics of the machine (direct stress, plane bending, rotating beam, etc.); or (c) the operating characteristics of the machine (electromechanical, servo-hydraulic, electromagnetic, etc.).

Corrosion fatigue tests follow from the ASTM E 606 standard for fatigue testing in air.

The typical cell for corrosion fatigue testing includes an environmental chamber of glass or plastic that contains solution. The specimen is gripped outside of the test solution. The chamber is sealed to the specimen, and solution is circulated through the environmental chamber (corrosion chamber). Due to corrosion chamber, an extensometer cannot be mounted on the surface of the specimen to measure the gage displacement or crack opening displacement. Instead of an extensometer, crack propagation strain gage (TK-CPA01-005) is used in this study to measure the crack growth rate. When fatigue crack growth rate test data are reported for environments, test temperature, pressure of gas, waveform type, waveform frequency, and stress ratio must be reported.

4.3 Parametric Measurement, Computer Automation and Data Analysis

Generally, fatigue processes are historically viewed as cycle-dependent processes, and this approach must be broadened to avoid missing environmental enhancement. Corrosion fatigue testing requires the following recognitions:

- It is important to achieve a steady-state crack growth rate at each test condition, which requires achieving a steady-state surface condition.
- Time dependency is very important, and therefore the role of mean/maximum stress and frequency can be very large.
- Unexpected increases in crack growth rate can occur at specific loading conditions (e.g., associated with achieving critical crack chemistry).

4.4 Crack Propagation Rate (da/dN) versus ΔK Approach to Corrosion Fatigue

While there is a strong reliance on low- and high-cycle fatigue testing, which is designed to characterize stress or strain amplitude vs. cycles to failure, there is an increasing emphasis on characterizing crack propagation using a fracture mechanics approach. This results from the ambiguities associated with defining or identifying crack "initiation", as well as increasingly successful efforts to unify the two approaches by predicting "initiation" and short crack behavior from a thorough understanding of crack propagation. The advantage of this approach is that corrosion fatigue crack growth (da/dN vs. ΔK) data from testing is in many cases useable in stress intensity solutions for practical prediction of component life.

The fracture mechanics approach isolates crack propagation from initiation and in terms of a precise near-tip mechanical driving force, ΔK. However, the fracture mechanics approach to corrosion fatigue can be compromised by various factors. In addition to the complications arising from crack-tip plasticity (which may affect the assumption of linear, elastic conditions for K) and crack closure effects (which can be accounted for if ΔK_{eff} is known), environmental effects can complicate the requirement of similitude. Another disadvantage of the fracture mechanics approach is that it may not provide a meaningful description of crack "nucleation" especially in cases where cracks are observed to nucleate by processes (e.g., pitting, and corrosion or cracking) that are unrelated to crack advance.

Standard methods of fatigue crack growth (as defined in ASTM E 647) are generally applicable to corrosion fatigue crack growth tests. Some general aspects of corrosion fatigue crack growth are described below, and additional background is provided in *Proc. Int. Symp. On Plan Aging and Life Prediction of Corrodible Structures*, 1995. First, the environment must be contained about the cracked specimen without affecting loading, crack monitoring, or specimen-environment composition. Secondly, load-control and crack-monitoring electronics and environment composition must be stable throughout long-term testing. Thirdly, crack length must also be measured for calculations of stress intensity and crack growth rate.

4.5 Crack Growth Test Methods for Vacuum and Gas

One of the most critical considerations for fatigue tests in vacuum and gaseous environments is the maintenance of the purity of the test environment. Maintaining an ultra-clean test system is important, because even a small amount of impurity can either significantly reduce or accelerate the fatigue crack growth rate, depending on the material and the types of impurity. A clean environmental test chamber that provides a very low background pressure and quantifiable impurity levels (below 10^{-7} to 10^{-6} Pa, or $7.5*10^{-10}$ to $7.5*10^{-9}$ torr) is essential, even if the tests are to be carried out in gaseous environments at relatively high pressures (i.e., above the background).

4.5.1 Corrosion Chamber

Stainless steels or plastics are suitable materials for the environmental tests chamber, with copper used as the gasket material. The test chamber usually is equipped with a glass view that enables the operator to visually monitor the progress of the experiment. A complete sealing between specimen and corrosion chamber is needed. High effective seals between plastic and metal surfaces are made with silicon rubber caulking compounds or latex rubber. Since, normal specimen movement or any sudden fracture event should be accommodated without catastrophic consequences. The decision to circulate the environment depends on the application and the extent of any problems in controlling the environmental gases. The corrosion chamber is shown below in Figure 4.1.

4.5.2 Corrosion Environment

Only high-purity, laboratory-grade gases should be used. Additional purification and dehumidification of the gas is recommended by passing it through a molecular-sieve purifier and a cold trap (-196 ºC, or –321 ºF) before allowing the gas to enter the test chamber. De-ionized distilled water in the reservoir should be purified further while subjecting it to repeated freezing/pumping/thawing cycles in order to remove residual dissolved gases in the water.

The prevailing water chemistry in the environment is an essential factor in any simulation environment. Accelerated fatigue cracking can occur in a number of environments, including seawater, salt water/salt spray, and body fluids. These must be reproduced as closely as possible in the laboratory. Substitute ocean water, as described in ASTM D -

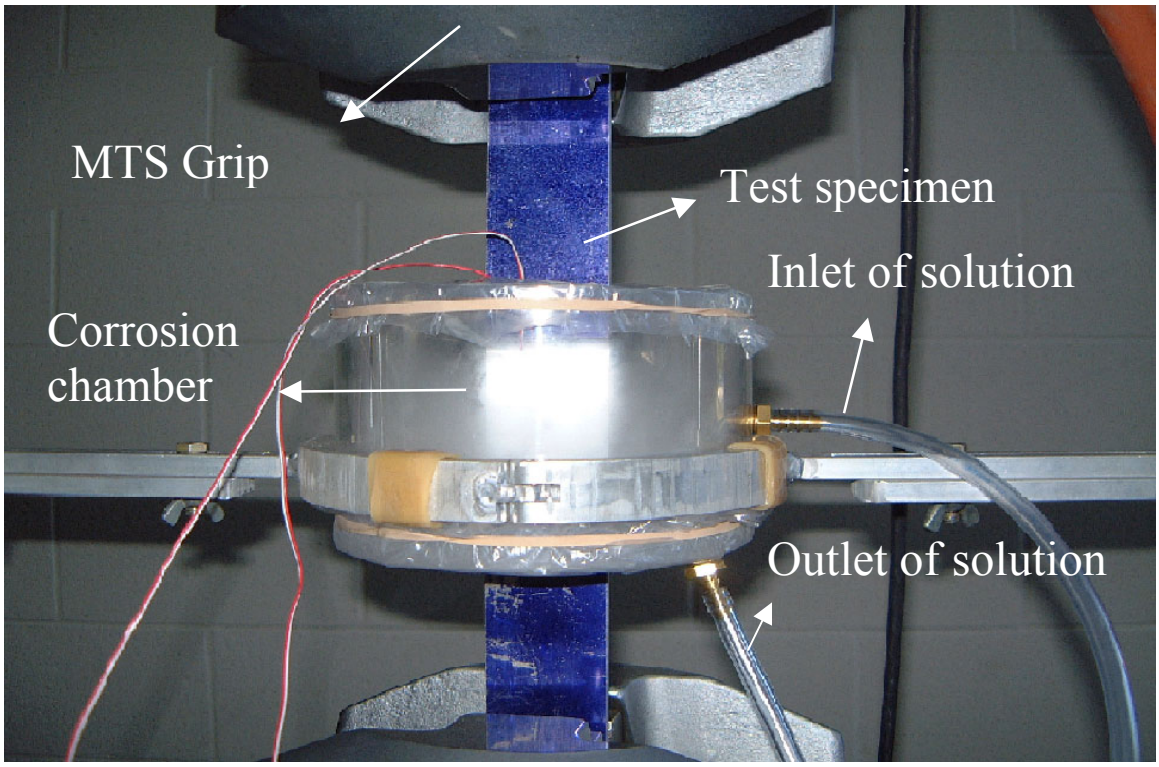

Figure 4.1 Environment chamber with specimen mounted in MTS-810 universal testing machine

1141, usually is a satisfactory substitute for seawater, but in this study, sea-water (3.7% NaCl) is produced by just mixing water with NaCl. Laboratory solutions are prepared using the purest chemicals available in distilled or de-ionized water. Concentrations at the level of parts per million can have profound effects on corrosion. Also, several variables must be measured and controlled when simulating a corrosive environment; solution purity, composition, temperature, pH, dissolved oxygen content, and the flow circulation rate of the solution.

4.6 Analysis of Fracture Surface

It is crucial to ensure accuracy of the crack monitoring technique, to identify branching and out-of-plane cracking, and to determine crack morphology. Accurate determination of crack growth on a cycle or time basis requires an understanding of the resolution of the monitoring technique under the actual test conditions. Fracture surfaces of fatigue-fractured test specimens usually are examined by scanning electron microscopy (SEM) to determine the fracture path and the fracture mode of the test material in relation to its microstructure. Such information is valuable in identifying the fracture mechanism in certain environment and material combinations and is used to assess the severity of the deleterious environment and to aid in analyzing service failures.

Fatigue in inert environments generally produces different fracture modes or fracture paths than does fatigue in deleterious environments. Also, the SEM micrograph is taken

continuously from the crack front initiation to the end of failure. Therefore, the variation of crack surface is investigated in sequence from the crack initiation to the end of crack failure.

A characteristic observation on the growth of macro-cracks is the occurrence of striations on the fatigue fracture surface. The striations are supposed to be remainders of micro-plastic deformations, but the mechanism need not be the same for all materials. Moreover, striations are not observed in all materials. The visibility of striations also depends on the severity of the load cycle. Furthermore, microscopic photography of a macro-crack has shown that the crack front is not a simple straight line and that the crack tip is not necessarily a very sharp crack. The crack tip is rounded. Apparently, the geometry of the macro-crack level does not agree with the classical concept of a crack on elementary fracture mechanics (perfectly flat, straight, or elliptical crack front). However, for these cracks, fracture mechanics applications have been proven to be possible.

4.7 Test Specimen

In-plane yielding must be limited to the crack tip by guaranteeing that the net section stress is below yield strength. Also, the maximum plastic zone size, defined as ~ 0.2 $(K_{max} / \sigma_{ys})^2$, is much less (e.g., 10- to 50-fold) than the un-cracked ligament. Specimen thickness, as it influences the degree of plane-strain constraint, and crack size, as it influences the chemical driving force, may affect corrosion fatigue crack speeds. Specimen thickness and crack geometry must be treated as variables. Specimen thickness may affect crack growth rate, because transport of the environmental gases to the crack tip may be the rate-limiting factor.

For general economy, compact tension specimens are frequently used. Such specimens minimize the applied load required to achieve a given crack tip stress intensity, thus permitting the use of low load capacity and less expensive test machines. However, due to the unavailability for the compact tension specimen, center pre-crack Al-2024-T3 is used as a test specimen. Center pre-crack tension is also commonly used, because it is relatively easy to maintain the specimen gage section at uniform temperature. As a substantial part of the total fatigue life is attributed to the early state of fatigue crack growth, the crack starter is made by saw cutting at the edge of the center hole. So, crack will start easily at the edges of the hole. Then, the fatigue crack initiation life can be ignored when the fatigue crack growth life is calculated. In corrosion fatigue, the electrochemistry within the crack is mass transport dependent and can vary with crack depth, and possibly also with specimen geometry and with accessibility of solution in the through-thickness direction via the crack sides. These factors can also influence crack growth rates. So, in reports of test data, information regarding crack depth or thickness should be quoted. In addition, in applying load to specimens in a corrosion chamber, chamber friction must not affect load in sealed systems. This is generally not a significant factor in most tests. The geometry and dimension of test specimen are shown below in Figure 4.2.

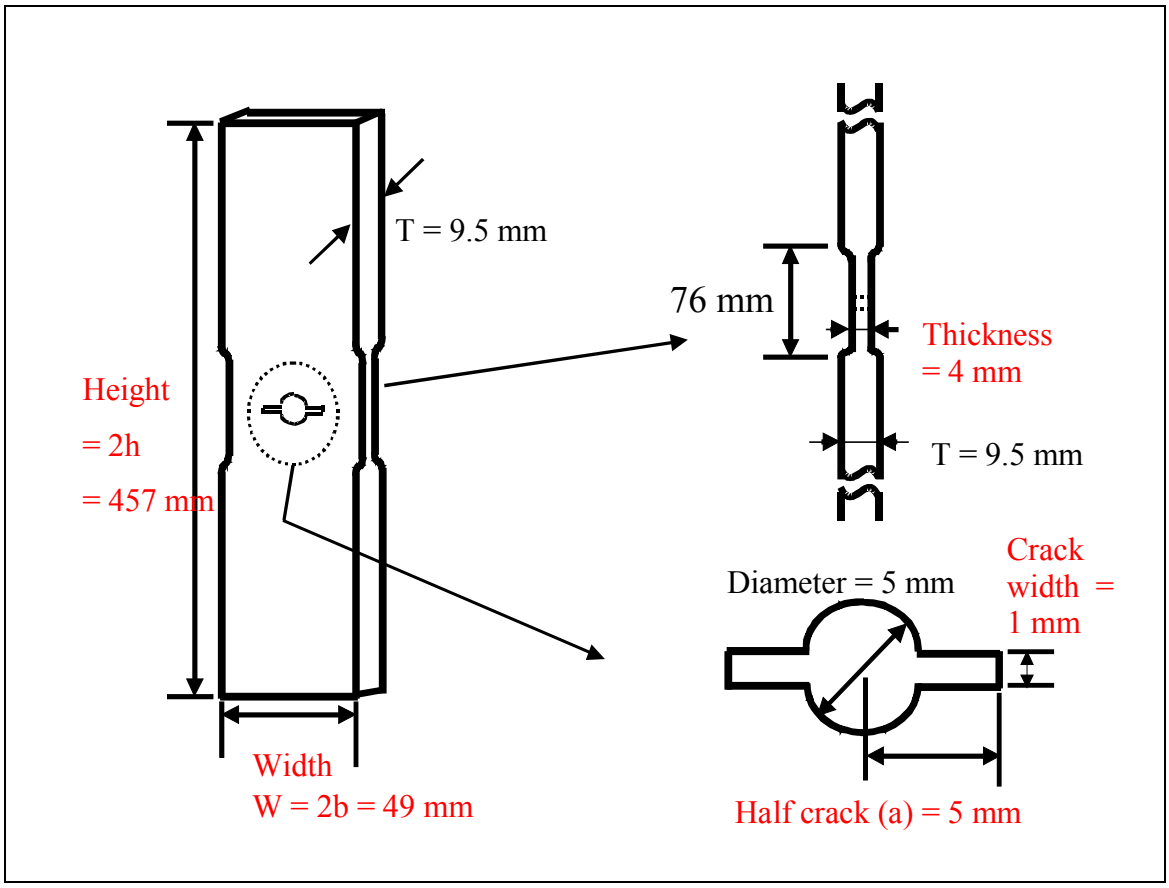

Figure 4.2 Geometry and dimension of test specimen-ASTM E647

4.7.1 Recommendation of Specimen Configuration & Size

In order for results to be valid according to this test method it is required that the specimen be predominantly elastic at all values of applied load. The minimum in-plane specimen sizes to meet this requirement are based primarily on empirical results and are specific to specimen configuration. For the center pre-crack specimen the following is required.

1) $(W-2a) \geq 1.25\, P_{max} / (B\sigma_y)$
2) $B \leq (W/8)$

where (W-2a) = specimen's un-cracked ligament
W = Width
B = specimen thickness.

For the center pre-crack specimen, the thickness and width is varied independently, which are based on specimen buckling and through-thickness crack-curvature considerations. ASTM E647 recommends that the upper limit on thickness in the center pre-crack specimens is W/8. The minimum thickness necessary to avoid excessive lateral

deflections or buckling in the center pre-crack specimens is sensitive to specimen gage length, grip alignment, and load ratio, R. The machined notch for the center pre-crack specimen should be made by electrical-discharge machining (EDM), milling, broaching, or saw-cutting. The recommended width of pre-crack starter slot at the edge of hole is 0.2 mm (0.008 in). To make this per-crack starter slot, EDM is recommended. Unfortunately, due to the limit of cost, saw-cutting is used. According to ASTM E647, saw-cutting is recommended only for aluminum alloys. So, in this research, the center pre-crack starter is produced by narrow saw. But, the width cannot be made with a width of 0.2 mm. If saw-cutting is used, the minimum width of pre-crack starter slot is 1 mm.

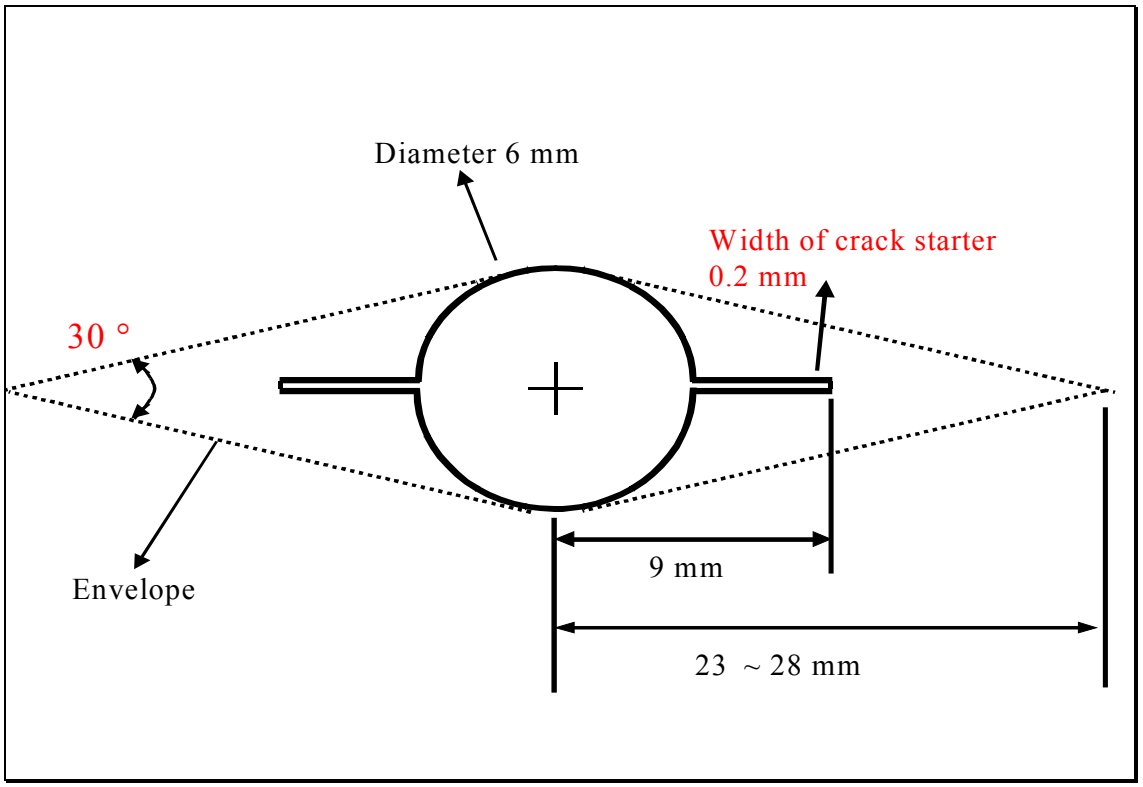

Figure 4.3 Suggested design for center pre-crack starter

The suggested design for center fatigue pre-crack starter is shown below in Figure 4.3. The crack starter must lie within the envelope defined by the 30˚ included angles having their apexes at the ends of the fatigue cracks. From the basic fracture mechanics, the overall requirement for plane strain is

$t, a, (b-a), h \geq 2.5 (K/\sigma_y)^2$
where a = half crack length
b = half width
h = half height

This requirement for plane strain is obviously not met for this case. So, in this research, the state of specimen is between plane-stress and plane strain. As the thickness increases,

the transition happens from the plane stress to plane strain. Also, stress intensity factor K value changes from K_c =110 MN/$m^{3/2}$ (plane stress) to K_{IC} = 34 MN/$m^{3/2}$ (plane strain) according to the thickness. For plane stress, ductile fracture mode dominates the fatigue crack growth on the other hand, for plane strain brittle fracture mode dominates the mechanism of fatigue crack growth.

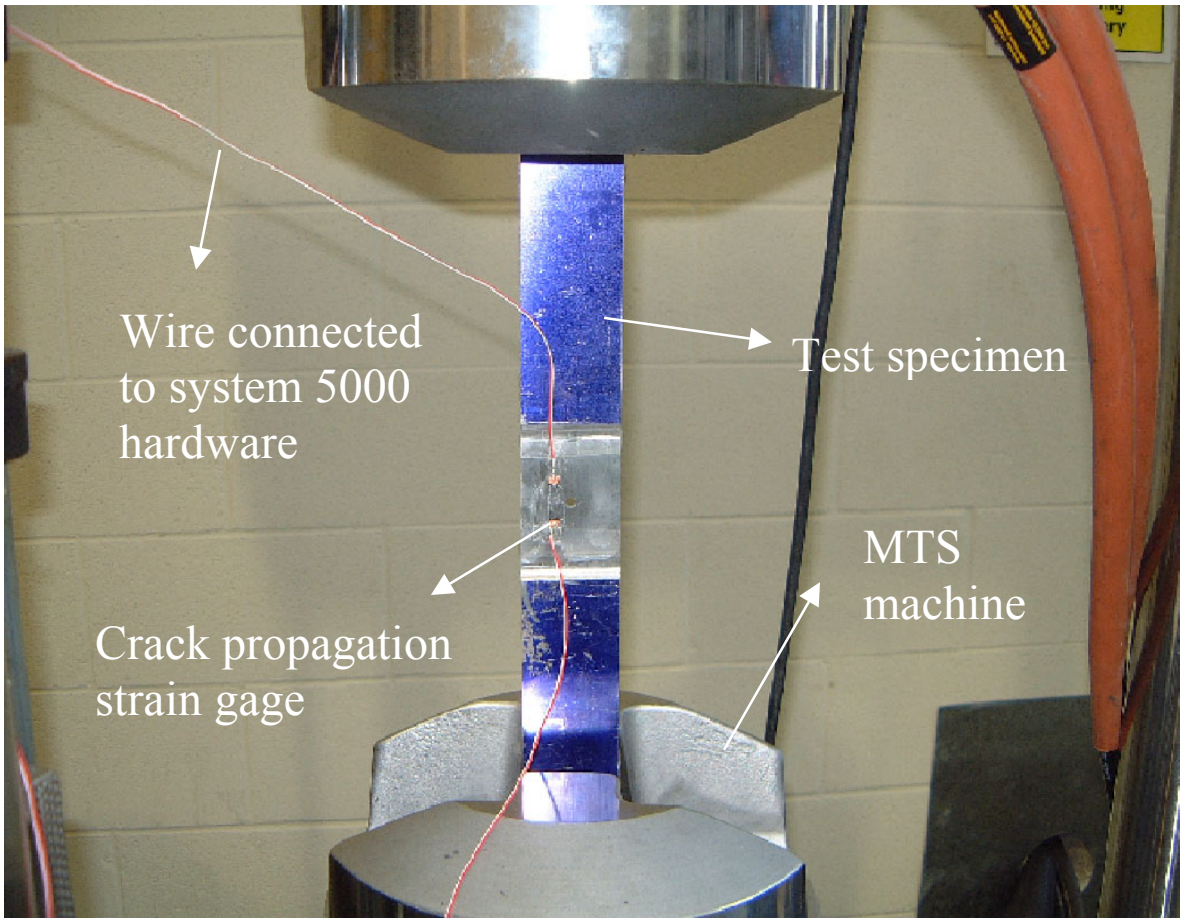

Figure 4.4 Specimen with crack propagation strain gage

4.8 Surface Preparation & Installation of Crack Propagation Strain Gage

The purpose of surface preparation is to develop a chemically clean surface having a roughness appropriate to the gage installation requirements, a surface alkalinity corresponding to a pH of 7 or so, and visible gage layout lines for locating the strain gage. Basically, the surface preparation includes six basic operations. Solvent degreasing, abrading, gage layout lines, conditioning and neutralizing, finally gage bonding. The procedures are given below. GAK-2-200 (M-Bond 200 Application Kits) is used to install the strain gage. Kits are provided from Vishay Micro-Measurements, Inc.

General procedures about surface preparation and gage bonding:

1. Thoroughly degrease the gage area with solvent, such as CSM-1A Degreaser. All degreasing should be done with uncontaminated solvents, thus the use of “one way” containers, such as aerosol cans, is highly advisable.

2. Dry abrading with 220- or 320-grit silicon-carbide paper is generally required. Final abrading is done by using 320 or 400-grit silicon carbide paper on surface wetted with “M-prep conditioner A”. This is followed by wiping dry with a gauze sponge. Repeat this wet abrading process. Then, dry by wiping through with a gauze sponge.

3. Now apply a liberal amount of M-Prep Neutralizer 5A and scrub with a cotton-tipped applicator. Do not wipe back and forth because this may allow contaminants to be deposited again.

4. Place the gage (bonding side down) on a chemically clean plate. Place a 4- or 6-inch (100- or 150-mm) piece of Micro-Measurements No. PCT-2A cellophane tape over the gage. Carefully life on end of the tape at a shallow angle, then realign the gage/tape assembly properly on the specimen.

5. Lift the gage end of the tape/gage assembly, tuck the loose end of the tape under and press to the specimen surface so that the gage and terminal lie flat, with the bonding surface exposed.

6. M-Bond 200 catalyst can now be applied to the bonding surface of the gage. Set the brush down on the gage and swab the gage backing. Do not stroke the brush in a painting style, but slide the brush over the entire gage surface. Allow the catalyst to dry at least one minute.

7. Lift the tucked-under tape end of the assembly, and holding in the same position, apply one or two drops of M-Bond 200 adhesive at the fold formed by the junction of the tape and specimen surface.

8. Immediately rotate the tape to a 30-degree angle. While holding the tape slightly taut, slowly and firmly make a single wiping stroke over the gage/tape assembly with a piece of gauze. Use a firm pressure with your fingers when wiping over the gage. Firm thumb pressure must be applied to the gage area. This pressure should be held for at least one minute. A very thin, uniform layer of adhesive is desired for optimum bond performance.

9. Remove the tape slowly.

4.8.1 Crack Propagation Strain Gage and Circuitry

Strain gage and circuitry to input of system 5000 hardware is composed of Scanner: Model 5100 Scanner, Sensor Cards: Model 5110 Strain Gage Card and Software: StrainSmart Software provided from Vishay Micro-Measurements, Inc. System 5000 hardware is intended to help measure the strain, temperature, force, displacement and other engineering parameters. Strainsmart software (Version 4.0 Beta) is designed to

function with system 5000 hardware and a variety of measurement sensors. This Strainsmart software also takes into account other parameters, such as temperature, lead-wire resistance, inherent non-linearity in the circuitry. Vishay Micro-Measurements Strainsmart software and System 5000 Hardware is used with crack propagation strain gage (TK-CPA01-005) to monitor the crack growth rate. The connecting the lead-wires from the gage into the signal inputs on the Model strain gage card (Model 5110 strain gage card) is done. This card is located into the slots on the back of the Model 5100 Scanner (System 5000 hardware). A complete measurement system consists of sensor (strain gage) connected to System 5000 hardware, a PC running Strainsmart software (Figure 4.5). Making external connections to strain gage card from the rear end connector is necessary to complete the circuitry. Strainsmart software can be used to obtain a step curve of strands broken versus time. So, Strainsmart is used to monitor a step curve of output due to the increase in resistance with successive broken strands as crack grows through the specimen. The curve can be plotted with time. If the frequency of the test is given, the cycles can be obtained by multiplying with time. For each broken strand, the crack grows 0.01in (0.25mm). There are totally twenty grid lines at each 0.01in (0.25mm) between strands. The increments of crack growth with cycles obtained by the time and frequency can be used to find out the crack growth rate. Until the specimen is broken totally, the time is monitored in order to get the fatigue life cycles.

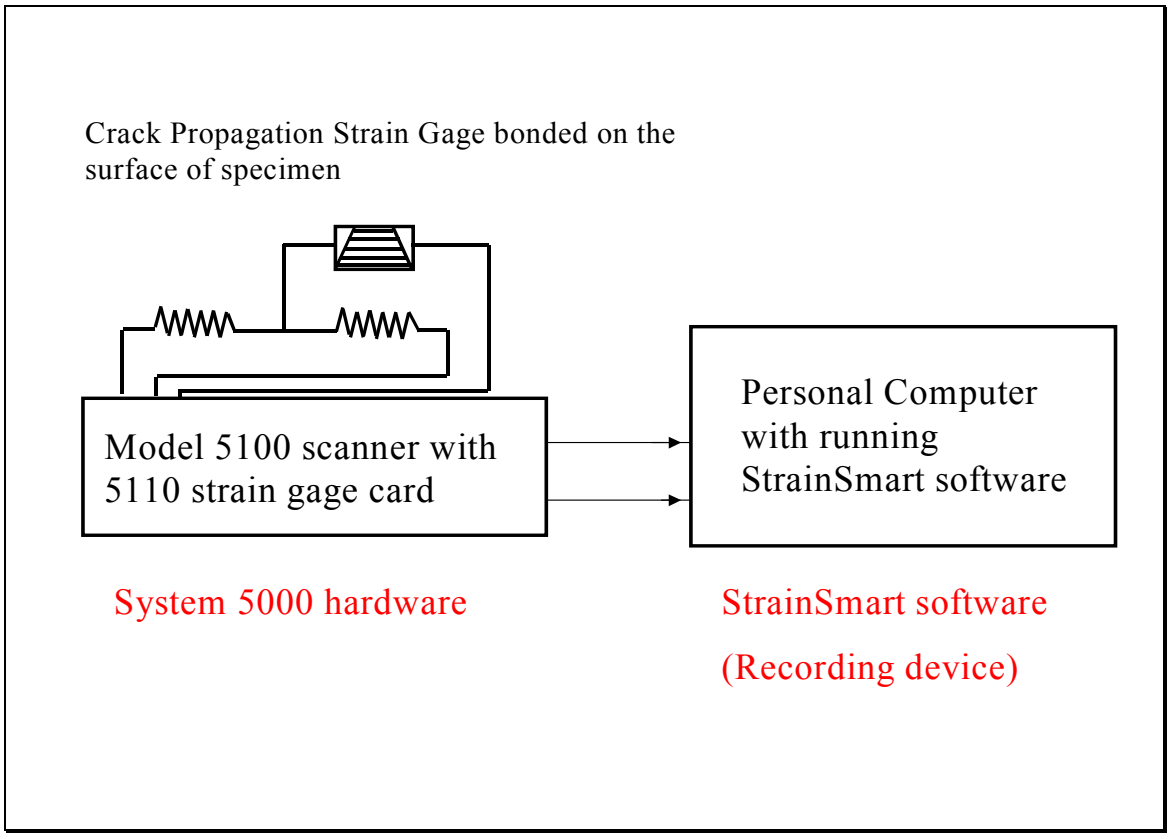

Figure 4.5 Complete measurement system with strain gage, system 5000 hardware & "Strainsmart" software with PC

The details about making the external connections to strain gage card necessary to complete crack propagation strain gage circuitry is shown in Figure 4.6 and 4.7. The setting for strainsmart software is also mentioned below.

1. A uniaxial strain gage should have been selected as sensor with a gage factor 2. The crack propagation strain gage itself has an initial resistance 5 ohm.

2. A wire has been soldered between pins 6 and 2 on the input connector to a 5110 Strain Gage Input Card.

3. Excitation voltage is set to 2V. This input should be connected to a 5110 Strain Gage Input Card.

4. Use foil or wire-wound resistors; not carbon resistor.

5. This circuitry is similar to a quarter-bridge connection.

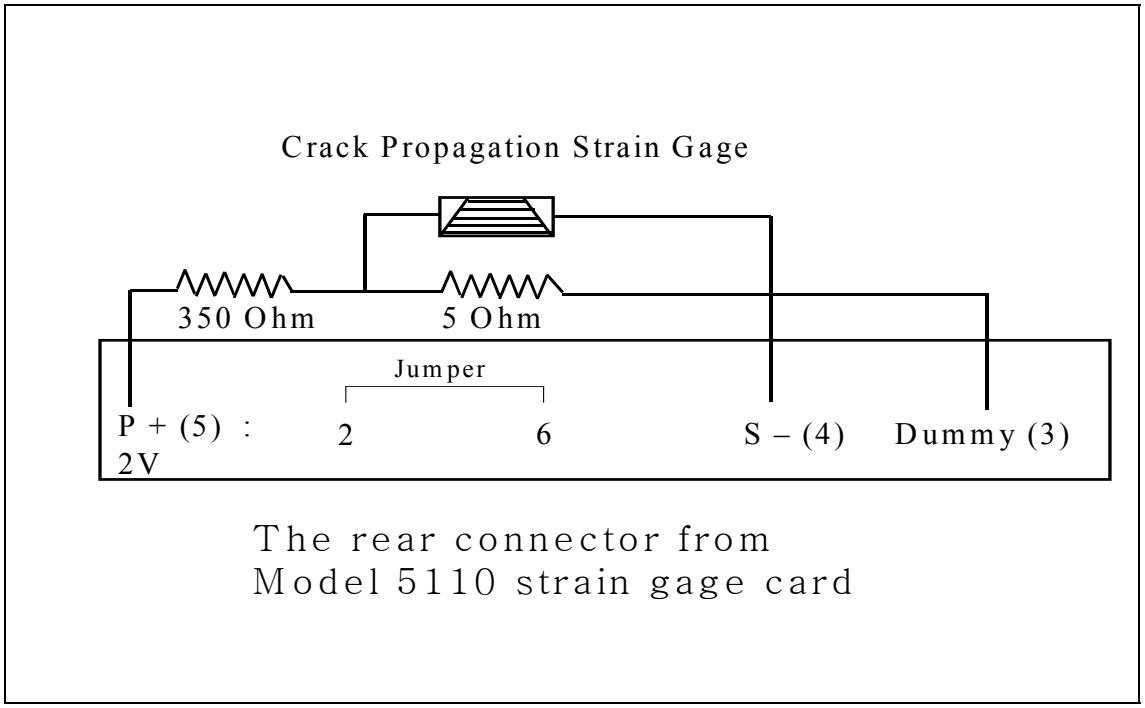

Figure 4.6 External connection to model 5110 strain gage card from the rear connector

4.8.2 Crack Propagation Strain Gage Characteristics

Crack propagation gages have a nominal gage thickness of only 0.0017in (0.043mm). The high-endurance K-alloy foil grid has a single cycle strain range of up to ±1.5% with a fatigue life of greater than 107 cycles at ±2000 micro-strain. The standard backing is a glass-fiber-reinforced epoxy matrix. The resistance of gage is 5 Ohm when there are no

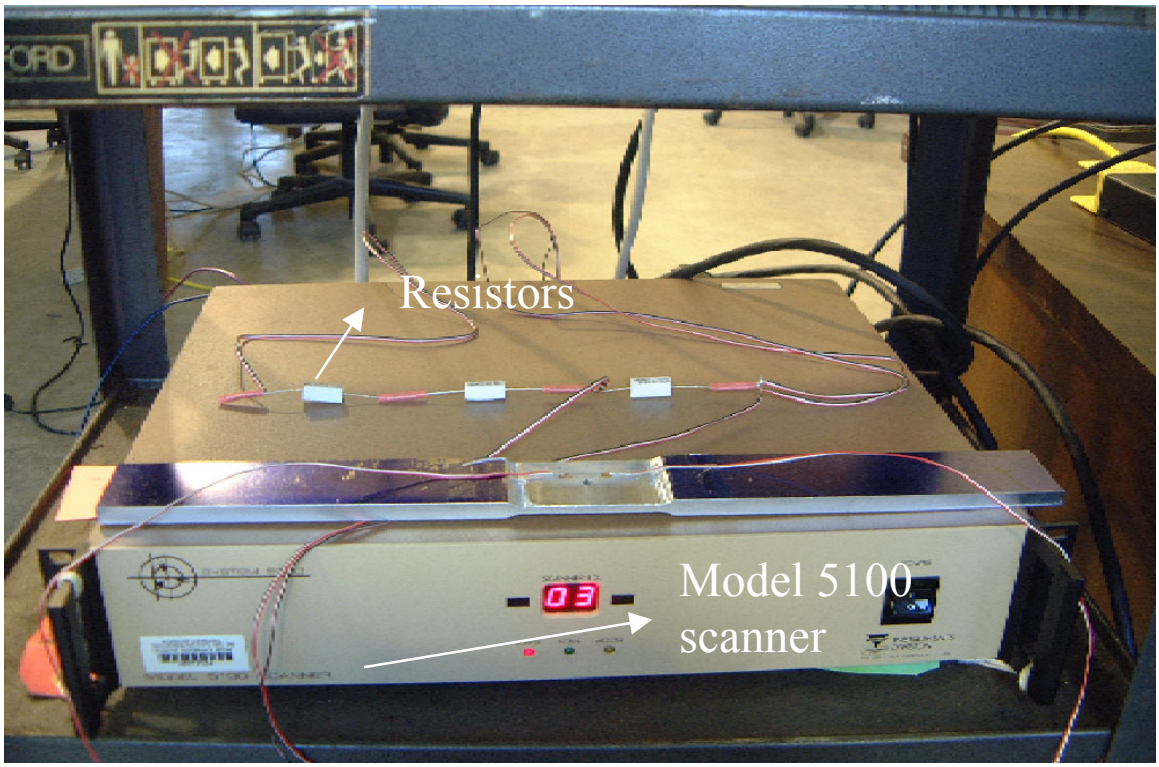

Figure 4.7 Measurement system with strain smart software & system 5000 hardware

fracture strands. Crack propagation gages provide a convenient method for indicating rate of crack propagation in a test part or specimen. The crack propagation gage consists of a number of resistor strands connected in parallel. When bonded causes successive open circuit of the strands, resulting in an increase in total resistance. The CPA01 pattern incorporates 20 resistor strands. The CPA01 produce stepped increases in resistance with successive open circuit (Figure 4.8). Then, due to the increase in resistance, there is a voltage jump for each broken strand. The output is plotted with time. So, we can calculate the cycle (ΔN) by multiplying time with frequency. If the cycle is known, crack growth rate average ($\Delta a/\Delta N$) for each broken strand ($\Delta a = 0.25$ mm) can be obtained.

1. Description (CPA 01) - TK-CPA01-005

There are twenty grid lines – 0.01in (0.25mm) between strands. Crack propagation gages have a K-alloy foil grid on a glass-fiber-reinforced epoxy matrix.

4.8.3 Monitoring the Crack Length

Indirect methods, based on specimen compliance or electrical potential technique, have been applied successfully to monitor crack growth. in a wide variety of hostile environments. Visual methods generally are not practical. Visual methods are often precluded from the test chamber. The electrical potential technique is preferred over the compliance method for use inside a corrosion chamber, because the compliance gage is a potential source of test environment contamination. Its use in a corrosion chamber is also unsuitable. However, the electric potential technique is non-contaminating and can be

used in most environments. These methods are described in more detail in ASTM E647 or Andresen, 1996. In this study, crack propagation strain gage (TK-CPA01-005) is used to measure the crack growth rate.

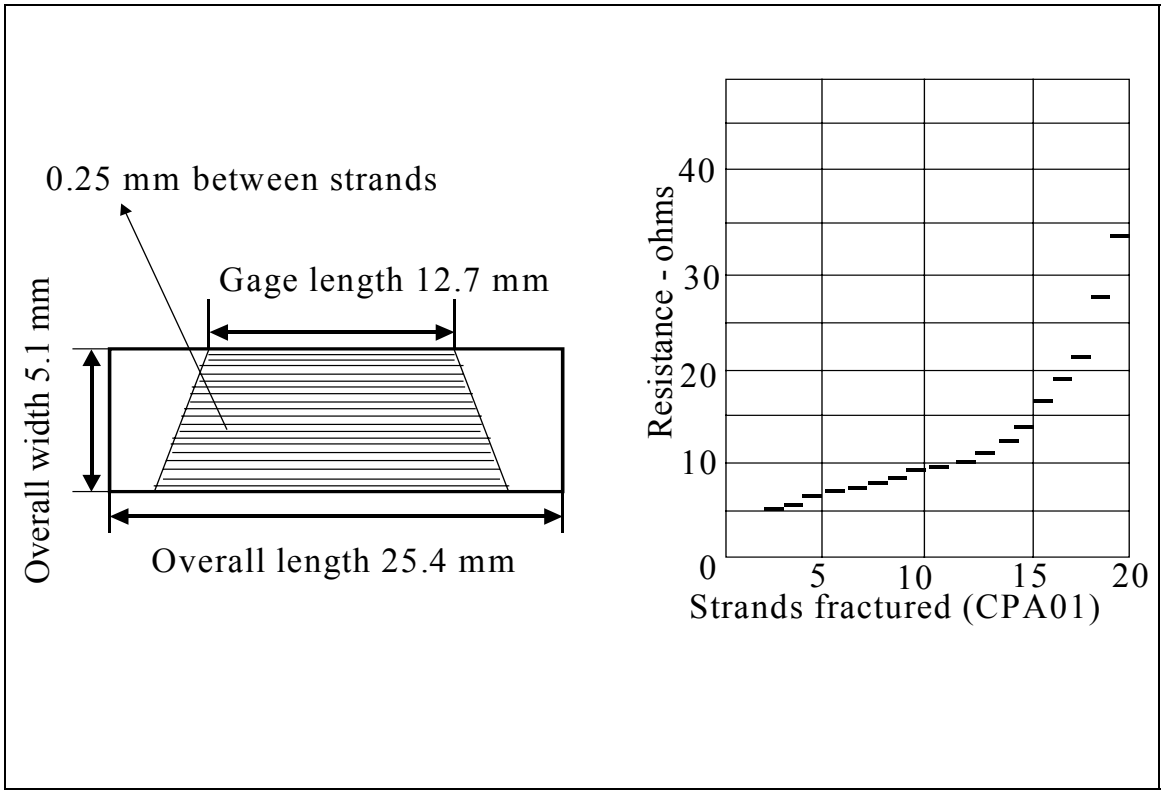

Figure 4.8 Dimensions of crack propagation strain gage and plot of resistance-ohms versus strands fractured

4.8.4 Calculation of Crack Growth

Crack growth rate is calculated from crack length versus cycle number (da/dN) data. Crack growth rate can be calculated by the secant and incremental methods, which are described in ASTM E 647. Another method is, as mentioned above, using Strainsmart. The Strainsmart software is used to monitor a step curve of output due to the increase in resistance with successive broken strands as crack grows through the specimen. The curve can be plotted with time. If the frequency of the test is given, the cycles can be obtained by multiplying with time. For each broken strand, the crack grows 0.01in (0.25mm), because there are twenty grid lines at each 0.01in (0.25mm) between strands. The increments of crack growth with cycles (obtained by the increment time and frequency) can be used to find out the crack growth rate.

4.9 Characteristics of LPS-3 Heavy-Duty Inhibitor (CPC)

As stated above, LPS 3 Heavy-Duty Inhibitor is used in this study. It is provided from LPS Laboratories, Atlanta Headquarters, Illinois Tool Works Company. There are many

kinds of CPC. For example, LPS-2™ and 3™, Boeshield T-9™, WD 40 ™, CRC 3-36 ™, Ardrox 3961 ™ and so on. But, for multi-year protection and water-displacing properties, LPS 3 Heavy-Duty Inhibitor (LPS 3) is chosen as CPC. The properties are shown below.

1. Multi-year protection
2. Penetrating and water-displacing properties
3. Stops rust and corrosion
4. Provides non-sling lubrication
5. Self-healing, waxy film
6. Provides anti-seize coating

4.10 Experimental Methodology for Overloads Test

Four millimeter thick 2024-T3 is used in this experiment. The tensile strength and yield are reported in literature as 495 and 325 MPa, respectively. The specimen geometry is the center pre-crack specimen, with 457 mm length and 49 mm width. All specimen dimensions are the same like task #1. All specimens were pre-cracked. Load is applied perpendicular to the crack growth direction. MTS closed loop electro-hydraulic testing machine is used to apply loads. A PC is coupled to the system to provide constant amplitude load periodic overloads (TestWare-SX Version 4.0D). Under constant amplitude loading, periodic overloads are applied until a failure. Overload Ratio of 1.7 is used. The periodic spacing cycles between overloads (Figure 4.9) are varied roughly between 20 and 5000. For all tests of Task #2, the stress ratio is 0.2, and the frequency is 0.5 except the periodic overloads. The frequency of overload is chosen as 0.2 due to the hydraulic control error during the demonstration. So, the main objective of task 2 is to find out the optimum spacing cycles between overloads for overload ratio of 1.7 in order to get a maximum fatigue life until failure. Then, the number of cycles for each test required to grow the crack from the initial size to failure is recorded. Overall experimental facility is shown in Figure 4.10.

4.11 Specimen Material (Aluminum alloy 2024-T3)

(1) Mechanical Properties of aluminum alloy 2024-T3

Tensile Strength	Yield Strength	Shear Strength	Fracture Toughness
485 MPa	345 MPa	285 MPa	34 $MN/m^{3/2}$

(2) Chemical Compositions Limits of aluminum alloy 2024-T3

Compositions	Si	Fe	Cu	Mn	Mg	Cr	Ni	Zn	Ti + Zr	Al
Weight (%)	0.5 max	0.5 max	4.4	0.6	0.45	0.1 max	0.05 max	0.2 max	0.2 max	93.5

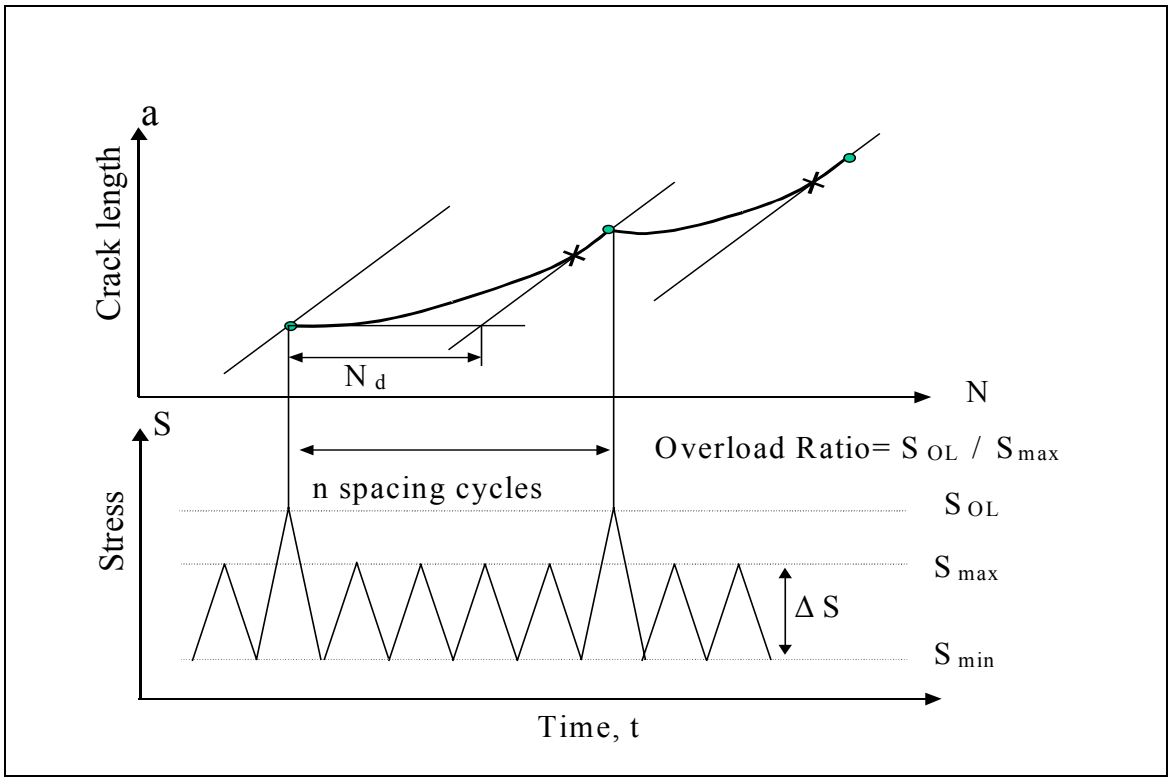

Figure 4.9 Typical behavior of crack length as function of number of cycles at constant ΔS, which results from overloads

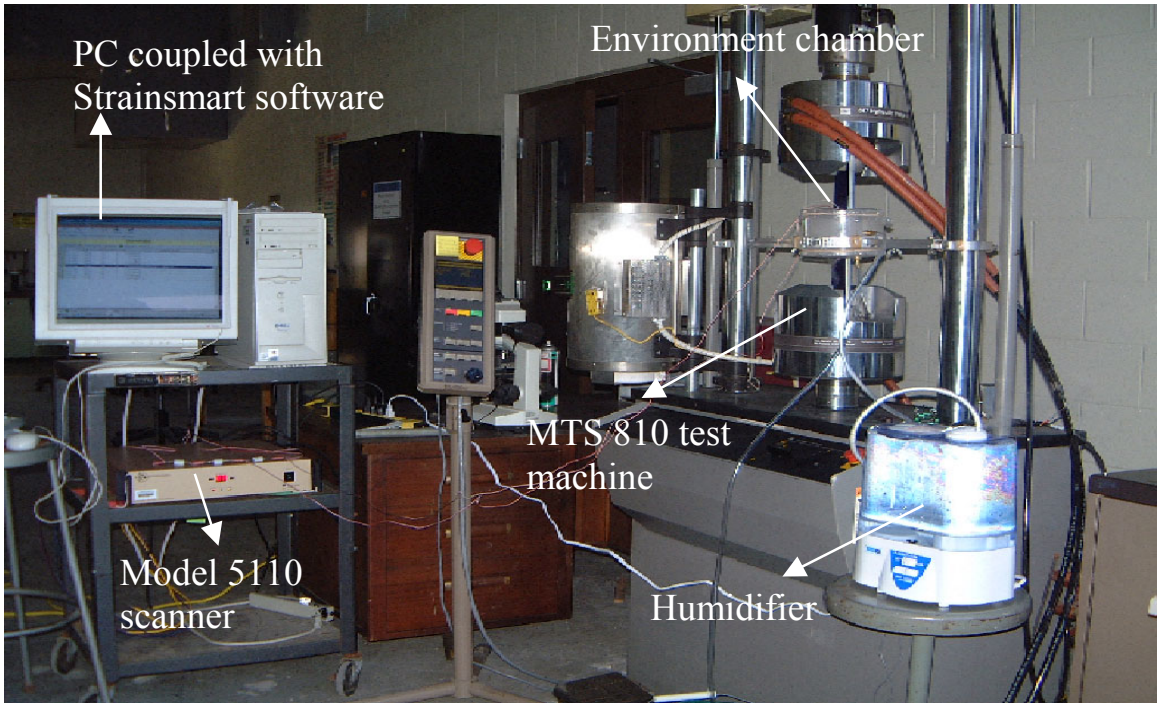

Figure 4.10 Overall experimental facility (MTS-810, Strain smart software, environment chamber)

CHAPTER 5. RESULT, DISCUSSION & EVALUATION

5.1 Corrosion Fatigue Test

The first aim of this work is to develop the further understanding of fatigue phenomena to predict the fatigue life and to understand the effect of periodic overloads on fatigue life. The emphasis is the effect of environments (dry air, water vapor with or without Corrosion Prevention Compounds (CPC)) and loading conditions (different frequencies, stress ratios) on the fatigue life of Al-2024-T3. The effect of CPC (LPS-3 Heavy duty corrosion inhibitor) on fatigue life under corrosive environment is carried out. The above work has been carried out experimentally.

The combined effect of treatment with CPC on the corrosion fatigue life would be a compromise between the beneficial effect (exclusion of moisture and prevention of oxidation at the crack tip) and the detrimental effect of the reduced friction between fraying surfaces (due to lubrication effect of the corrosion prevention itself). These studies about the synergistic actions of corrosion and fatigue, however, have produced diverse and wide range results. The reason is partly due to the large number of variables involved with type of material behavior. The exact degree to which corrosion affects fatigue life depends on the factors that influence fatigue such as stress level, frequency, stress amplitude, stress ratio and stress history, as well as on corrosion parameters such as the type of environments (vacuum, dry air, water vapor, salt vapor) and exposure time. Their mutual interactions on fatigue life are studied in this research. But, in general the exposure to corrosive environment either prior to fatigue or during the cyclic loading significantly reduces the life of the component. The primary characteristics of corrosion fatigue life are that the crack growth rates can be substantially higher in the corrosive environment. Because, it reduces the fatigue life of crack initiation or it increases the crack growth rate or both. The following factors are crucial in most investigations of corrosion fatigue life.

1. Stress Intensity Amplitude (ΔK)
2. Effect of Fatigue Frequency
3. Effect of stress ratio
4. Effect of Environment

5.1.1 Results from Corrosion Fatigue Testing

Generally, the results shown in Table 5.1 show that the increasing stress ratio has a bad effect on fatigue life for any environment conditions. The increasing frequency didn't show the clear trend like increasing stress ratio. Also, water vapor has detrimental effects on fatigue life. The water vapor truly reduces the fatigue life except at R = 0.5 with freq. 1.0 Hz. Because in this case of R = 0.5 with freq. 1.0 Hz, the stress conditions (mechanical loading condition) are superior to the water vapor condition (environmental condition). The water vapor tends to reduce the surface friction between crack faces during the fatigue cyclic loading. It is observed that the effect of water vapor is not

prominent during the crack initiation process. But, the water vapor dramatically reduces the fatigue life during the crack propagation process, especially at the instant of failure.

Table 5.1 Test result for various fatigue tests

Test Program	Freq. 0.5 Hz		Freq. 1 Hz	
	R = 0.2	R = 0.5	R = 0.2	R = 0.5
Dry air	7 hours 30 min 13466 cycles	4 hours 30 min 8550 cycles	4 hours 45 min 17164 cycles	1 hours 58 min 7114 cycles
Water vapor	7 hours 12648 cycles	3 hours 56 min 7108 cycles	3 hours 31 min 12681 cycles	2 hours 7259 cycles
CPC + Dry air	7 hours 45 min 13955 cycles	3 hours 56 min 7085 cycles	4 hours 1 min 14482 cycles	1 hours 56 min 6927 cycles
CPC + Water Vapor	8 hours 27 min 15231 cycles	4 hours 46 min 8576 cycles	4 hours 23 min 15831 cycles	1 hours 44 min 6212 cycles

The result of the tests with Corrosion Prevention Compounds (LPS-3) & water vapor generally show the beneficial effect of LPS-3 on fatigue life. LPS3 does not protect the effect of water vapor on crack faces completely during the crack growth phase of the test. If LPS3 can be treated frequently during the test, it might improve the fatigue life more than the test result obtained if it is treated only once. The fatigue life (CPC + Water Vapor at Freq. = 0.5 & R = 0.2), 8 hours 27 minute is greater than the fatigue life, 7 hours at water-vapor even when the initial crack length is the same.

There might be some small errors due to the small difference of the initial crack length, the surface finish or the misalignment when the specimen is fabricated or gripped in the testing machine. Generally, the tests with CPC (LPS3) & water vapor truly show the 20 ~ 24 % increase of fatigue life than the test with just water vapor except the case of R = 0.5, and frequency = 1.0 Hz. Also, in order to see the effects of CPC on water vapor clearly,

the frequency needs to be decreased to allow more time to take place for protecting corrosion effect. More tests should be run to validate the test results and draw a complete S-N plot.

In this study, the test is done at maximum time interval of 9 hours due to the limitation of time. The effect of only LPS-3 on fatigue life is done in order to investigate the effect of LPS-3 itself on the fatigue life. If the results are compared between dry air and CPC + dry air, there is not a clear trend. The fatigue life is increased only in case of R=0.2 and Freq.=0.5 Hz.

5.2 Effect of Overloads on Fatigue Life

Service loads are mostly random in nature. This load fluctuation can lead to fatigue crack propagation, the rate of which depends on the interaction of loads. High peak overload can cause large immediate incremental growth, but sometimes disturb the crack tip parameters leading to retarded growth in the following cycles. The underlying mechanisms of this retardation need to be discovered to investigate the fatigue life effectively.

The phenomenological behavior under various load combinations need to be studied. Single overload and interactions between periodic overloads are such cases. The retardation associated with the interaction between overloads controlled by the periodicity (spacing cycles between overloads) of the overloads is examined. The periodicity is varied roughly between 50 cycles and 4000 cycles for the overload ratio of 1.7. Typically, crack closure does play a predominant role, but other mechanisms also contribute to retardation such as residual compressive stresses ahead of the crack tip, shear lip effects, strain hardening etc. This approach needs to be assessed to investigate the total fatigue damage on fatigue life. The periodic tensile overloads are superposed on constant amplitude load cycles in this study. Overload ratio of 1.7 is used in this research. The interaction between overloads is controlled by spacing cycles (50, 100, 200, 400, 800 and so on) between overloads. The objective of this part is to investigate the optimum spacing cycles of the overload ratio of 1.7 for maximum fatigue life of the test specimen Al-2024-T3.

Specifically, the technical objectives can be summarized as follows: Study of the significance of periodic overloads and interactions between low and high cycle fatigue.

For this task, the same type test specimen is used which is used for the corrosion test. The retardation associated with periodic overloads controlled by the periodicity spacing cycles between overloads is examined for overload ratio ($OLR = S_{ol} / S_{max} = 1.7$). From available literature, the maximum interaction, and thus the maximum fatigue life, is observed when overload spacing is around half of the delay cycles of single overload application. In this thesis work, overload is taken as 255 MPa, the maximum stress of base constant cycling loading is S_{max} = 150 MPa, and the minimum stress of base constant cycling loading is S_{min} = 30 MPa. Therefore, the stress ratio $R = S_{min} / S_{max} = 0.2$. The frequency is 0.5 Hz except at overload. During the overload, the frequency is

reduced to 0.2 Hz due to the limitation of hydraulic control mechanisms. Periodic overload experiments are carried out under load control, keeping the load range constant for the constant amplitude cycling loading. The number of cycles for each test that is required to grow the crack from the initial size to failure is recorded.

5.2.1 Results from Overloading Testing

The test result obtained from task #2 is shown in Table 5.2. Generally, a group of single overload experiments should be performed to provide the basic information. The spacing cycle between overloads leading to the maximum fatigue life is associated with the behavior of the material to single overloads. Also, these single overload results should be compared with periodic overloads experiments. Unfortunately, the single overload experiment couldn't be carried out due to experimental limitation. In further works, a group of single overload tests needs to be run.

Table 5.2 Test result for periodic overloads tests

Spacing cycles between overloads	50	100	200	400	800	2000	4000
Overload Ratio 1.7	86700 cycles 24 hour 42 min	102513 cycles 28 hour 53 min	219894 cycles 61 hour 31 min	336840 cycles 93 hour 54 min	400500 cycles 111 hour 27 min	340170 cycles 94 hour 33 min	296074 cycles 82 h our 16 min

From the above results, when overloads are applied periodically, interactions between overloads become possible. Therefore, crack growth retardation, in other words, the total fatigue life is enhanced dramatically when periodic overloads are superposed during the constant amplitude cycling loading if these results are compared with the results obtained in task #1 described earlier. Results from overload test have produced interesting observation. When the overloads are too close, for the densely applied spaced overloads, in case of spacing cycles n = 50, and 100, the total fatigue life is shorter than that of the remotely applied spaced overloads (spacing cycles, n = 800, 2000, 4000). The reason is that the interaction between overloads changes as the crack grows. In this work, there is a large range in between where the best enhanced retardation has occurred. To determine the longest total fatigue life for different spacing cycles needs more specific test results.

It was reported, (Tür and Vardar, 1996) that the maximum fatigue life at overload ratio = 1.65 occurred every 5000 spacing cycles. For overload ratio = 1.3 the longest fatigue life occurred every 600 spacing cycles. The maximum interaction, and thus the maximum

total fatigue life, was observed when overload spacing was around half of the delay cycles (N_d) of single overload application in this literature. The same trend is observed for 2024-T3 in this study. The retardation for an overload is measured in various ways, N_d is shown in Figure 9 (chapter4). The implication of this is that the minimum growth rate following single overload occurs just before N_d / 2 was reached, such that repeated applied overloads at this spacing led to the maximum fatigue life, thus maximum retardation effect.

Generally, the total fatigue life increases as periodicity is increased until a peak is reached, followed by a decrease in total fatigue life afterwards. The immediate conclusion from the above table 5.2 is that the overload interactions go through a maximum as the spacing cycles between overloads increases. At the peak total fatigue life, it starts decreasing. The best spacing cycles between overloads is in the range of 400 to 2000 cycles. In further work, more test specimens should be used to find out the best spacing cycles between overloads. Also, these periodic overloads tests need to be done for various different overload ratios (OLR). The trend of result is the same at different overload ratios as OLR = 1.7. But, the different retardation mechanisms are expected depending on the overload ratio.

The total fatigue life increases as spacing cycle between overloads is increased until a peak in the total fatigue life is reached, followed by a decrease in total fatigue life afterwards. But, another concern of this thesis work is that the total fatigue life is composed of fatigue crack initiation life and fatigue crack growth life. It is not clear to tell the transition from fatigue crack initiation to fatigue crack growth by naked eyes. Attention should be paid to distinguish this transition. In the task #1, around 70% of the total fatigue life is spent on fatigue crack initiation life. Thus, the other 30% of the total fatigue life is used for fatigue crack growth life. This range is changed for different loading conditions. Also, for periodic overloads tests, this fatigue crack growth life range is varied roughly from 25% to 40%. In case of spacing cycles n=50, the fatigue crack growth life is approximately 30% of the total fatigue life, 86700 cycles. In case of spacing cycles n=100, the fatigue crack growth life is roughly 40% of the total fatigue life, 102513 cycles. In case of spacing cycles n=800, the fatigue crack growth life is roughly 25% of the total fatigue life, 400500 cycles. The trend of this data is not known explicitly.

5.3 Results of Periodic Overloads Test in terms of Crack Length

The spacing cycles between overloads can be associated with the measure of crack length. In this work, Scanning Electron Microscope (SEM) is used to measure the incremental crack length “da” between overloads. The incremental crack length “da” is the retarded crack growth length between overloads. This retarded crack length is compared with the plastic zone size at the crack tip. The overload induced plastic zone is expressed by the following equation in case of plane strain.

$$2r_y^{OL} = \frac{1}{3\pi}\left(\frac{K_{OL}}{S_y}\right)^2$$

It was reported by Mills and Hertzberg; in 1976 that the maximum retardation occurs at "da / $2r_y^{OL}$ "= 0.2 (independent of the overload ratio applied). This level of maximum retardation occurring at da = 0.2 * (overload induced plane strain plastic zone size) for 2024-T3 is also reported by, Tür and Vardar, 1996. The overload induced plastic zone at the crack tip governs the retardation behavior. The SEM micrograph is used to find out the crack length "da" between overloads in case of n = 800 cycles. If S_y (Yield stress) is taken as 345 MPa, and K_{OL} is varied roughly from 28 MN/$m^{3/2}$ (crack length a=5mm at point 1 in Figure 5.1) to 38 MN/$m^{3/2}$ (crack length a=9mm at point 2 in Figure 5.1) and finally 48 MN/$m^{3/2}$ (crack length a=12mm at point 3 in Figure 5.1) as the crack grows through the test material. Then, theoretically 0.2*$2r_y^{OL}$ is varied from 0.14 mm (at point 1) to 0.24 mm (at point 2) and finally 0.41 mm (at point 3). The tested incremental crack length between overloads "da" from the SEM micrograph observation is shown in the following Figure 5.2, 5.3, 5.4, 5.5. It is varying form 0.02 mm (at point 1) to 0.05 mm (at point 2) and finally 0.15 mm (at point 3). The results from theories and SEM figures are not the same to verify the test results in Table 5.2. The reason is that this SEM micrograph is taken at spacing cycle of n = 800. Therefore, it was found that the maximum retardation between overloads is not yet achieved at n = 800 cycles. It is expected that the maximum retardation will be at higher spacing cycles, but less than 2000 cycles.

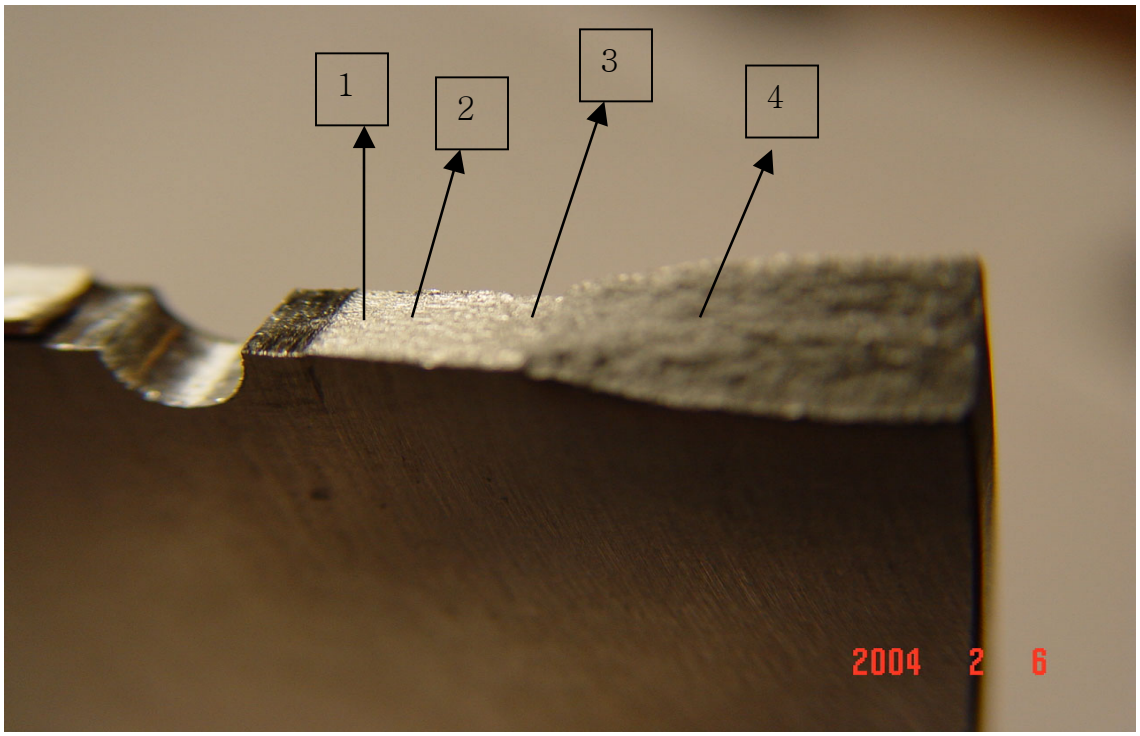

Figure 5.1 Test Specimen crack surface with R=0.2, frequency=0.5, OLR=1.7, n= 800 Label [1: crack start, 2: ductile mode, 3: intermediate mode, 4: brittle mode]

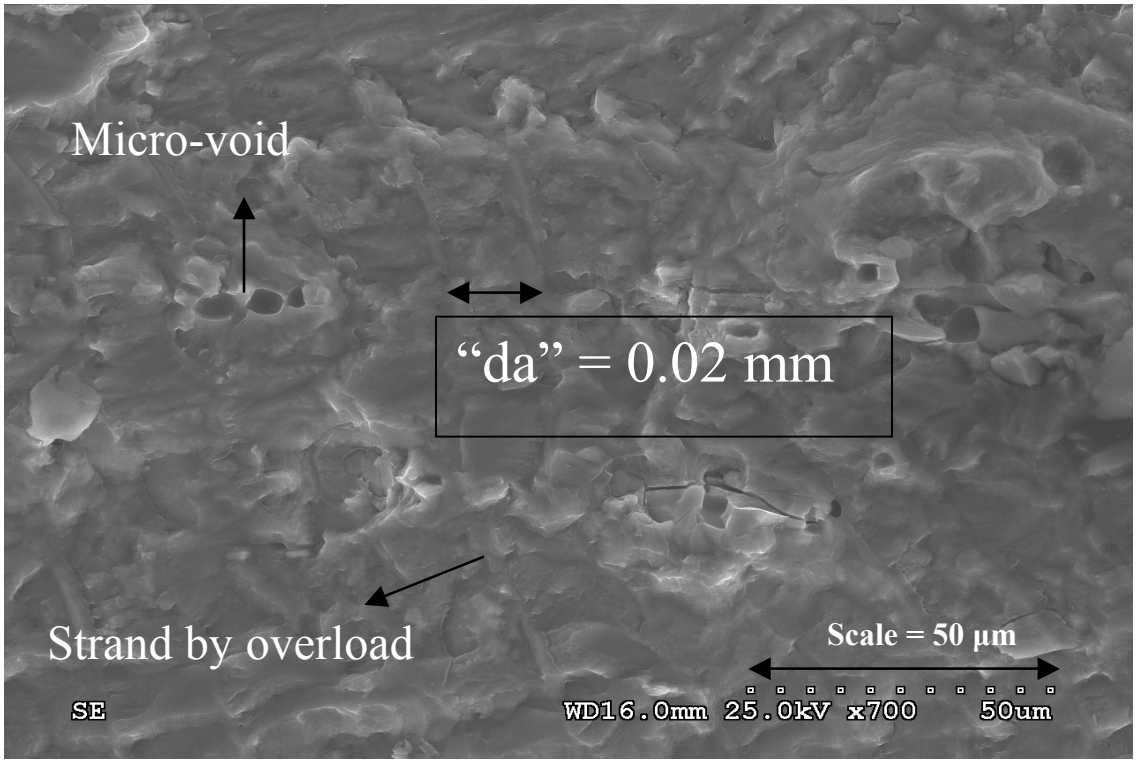

Figure 5.2 SEM micrograph of the above specimen at point 1 (Refer figure 5.1)

In Figure 5.2, instead of striations, crack surface shows that the dimple pattern is initiated at particles in 2024-T3, and several strands are deformed at the overloads. The distance between overloads, "da" = 0.02 mm is measured from the scale in Figure 5.2. Tear dimples in this figure result from non-uniform applied stresses. This tear dimples pattern is observed in the region of crack growth surface. The aluminum alloy exhibits a ductile rupture type of failure with micro-voids nucleating on the particles or precipitates. This micro-void coalescence consists of three sequential steps; (a) void nucleation by particle, (b) void growth by joining with isolated voids, (c) and (d) void coalescence with more plastic deformation.

The distance between overloads, "da" = 0.05 mm is measured from the scale in Figure 5.3. Tear dimples pattern is also observed in the region of crack growth surface at point 2. The distance between overloads, "da" = 0.15 mm is measured from the scale in Figure 5.4. Tear dimples pattern is also observed in the region of crack growth surface at point 3.

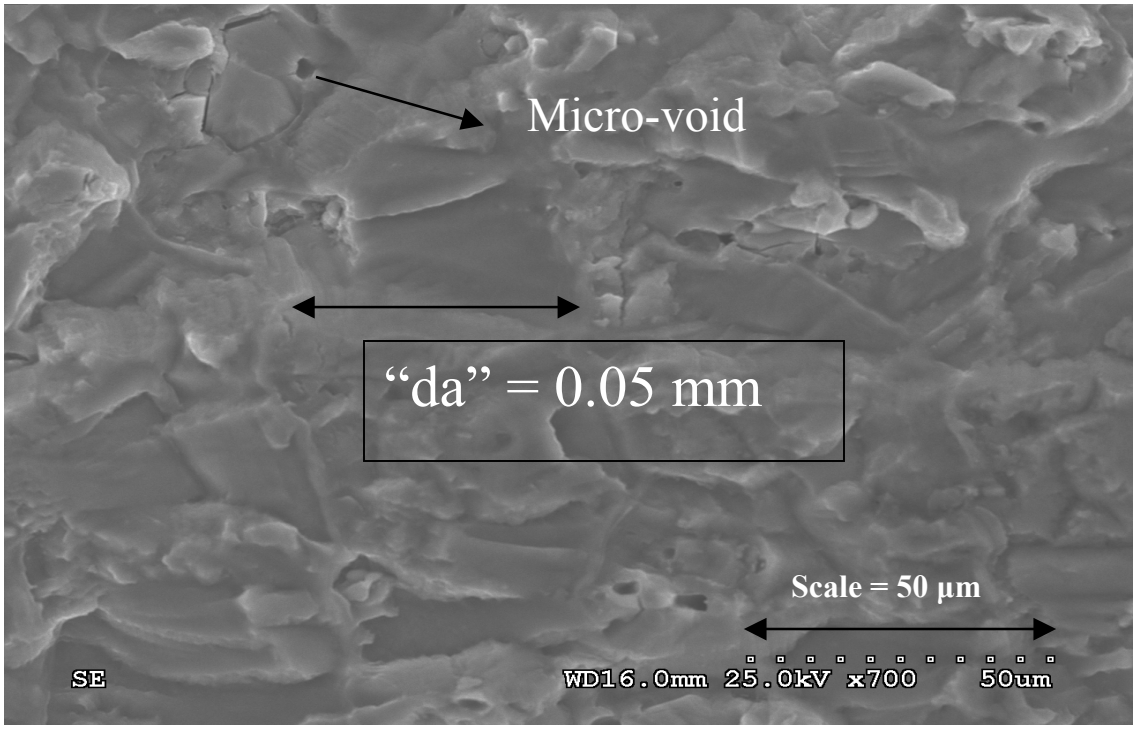

Figure 5.3 SEM micrograph of the above specimen at point 2 (Refer figure 5.1)

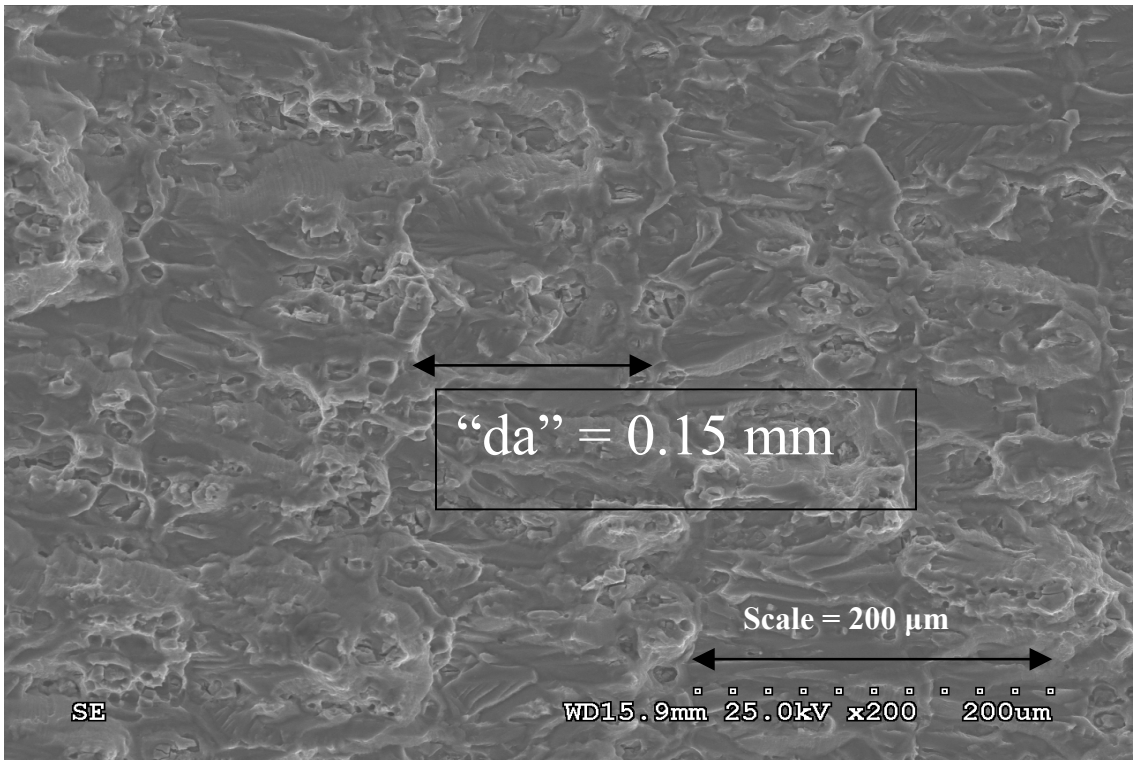

Figure 5.4 SEM micrograph of the above specimen at point 3 (Refer figure 5.1)

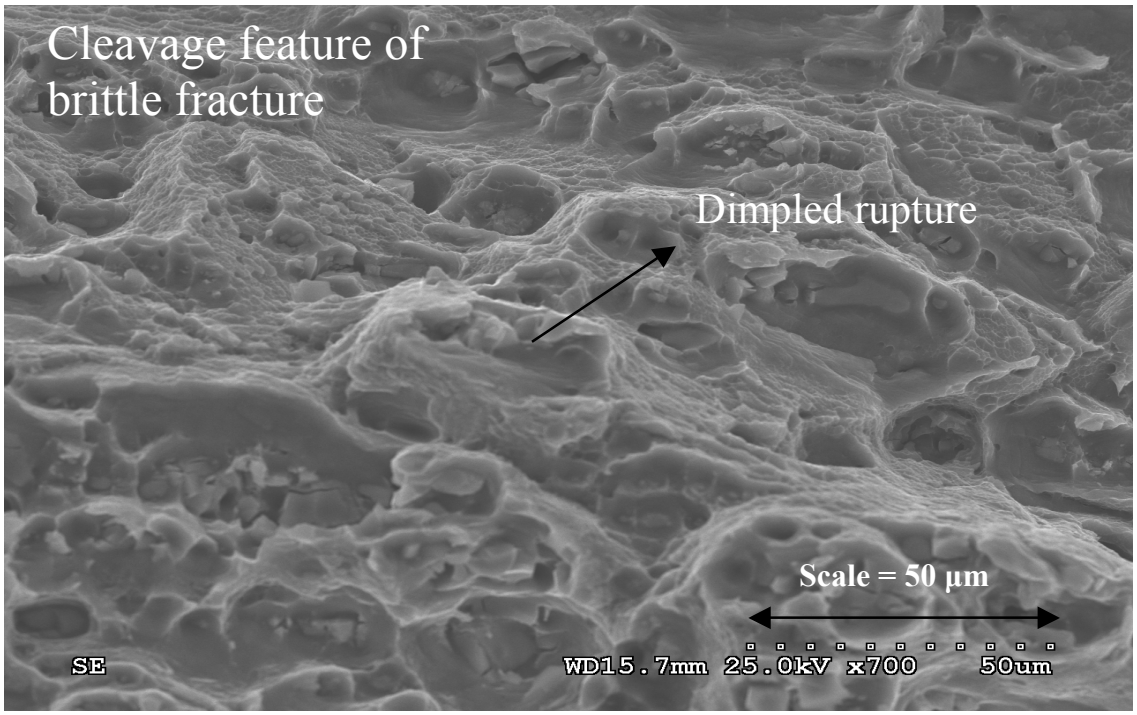

Figure 5.5 SEM micrograph of the above specimen at point 4 (Refer figure 5.1)

The cleavage feature in Figure 5.5 is characterized by the dimpled rupture. These features of dimpled rupture are predominant in the brittle fracture during the fast fracture.

5.4 Results of Crack Growth by Crack Propagation Strain Gage

The crack growth rate needs to be measured with fatigue life. The crack propagation strain gage output voltage (this data is done without specimen) is shown in Figure 5.6. This data is obtained by cutting each strand of strain gage one by one with a sharp knife purposely to check the output voltage. If time for each voltage jump is known from real test result, the number of cycles can be known from frequency for each crack growth, 0.25 mm. Since the distance between each strand is 0.25 mm. Then, the average crack growth rate per cycle (da/dN = 0.25 mm / number of cycles) can be known. The test data for crack propagation strain gage output voltage (at R=0.2 & frequency=0.5 with dry air) is also shown in Figure 5.7. Each voltage jump cannot be distinguished due to noisy signal. This experimental difficulty has to be overcome in the future work. The noisy signal is removed by taking the average data from the plot as shown in Figure 5.7.

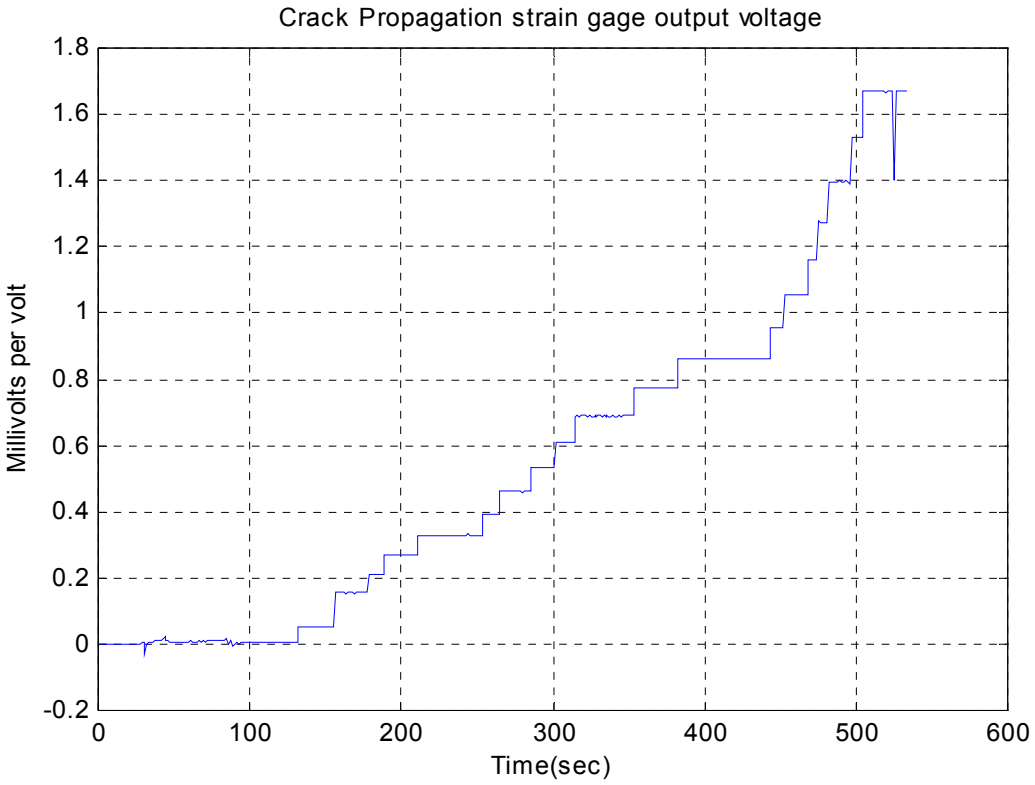

Figure 5.6 Crack propagation strain gage output voltage

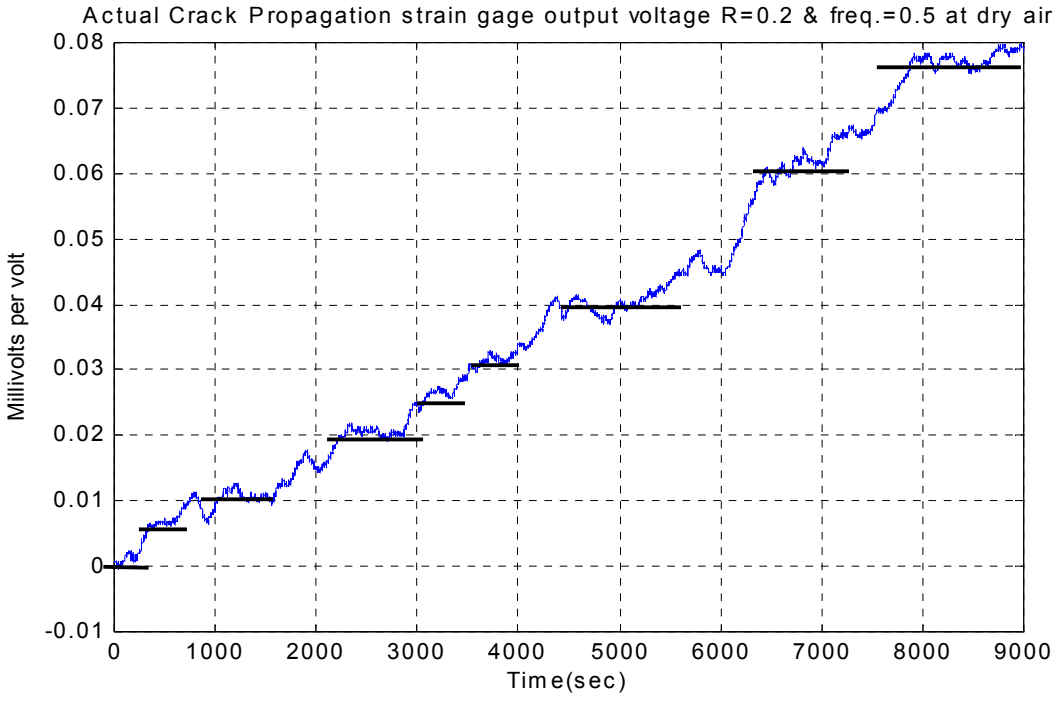

Figure 5.7 Test data for crack propagation strain gage output voltage

5.5 Results from Scanning Electron Microscope (SEM)

The fracture surfaces of test specimens of 2024-T3 have been examined by a Scanning Electron Microscope (SEM) to characterize the failure processes and to establish correlations with the previous studies of fatigue crack growth along the crack surfaces. The SEM observations show two significantly different types of behavior that are ductile fracture and brittle fracture. It is explained in terms of the differences in materials processing history. The microstructure of engineering alloys is complex as shown in Figure 5.8. The fracture surfaces of the test specimen need to be investigated in order to see the effects of fatigue damage on the crack surface. Crack growth surfaces at several locations from the crack starter to the specimen failure should be observed continuously in sequence. Several pictures were taken using SEM along the crack surface in sequence.

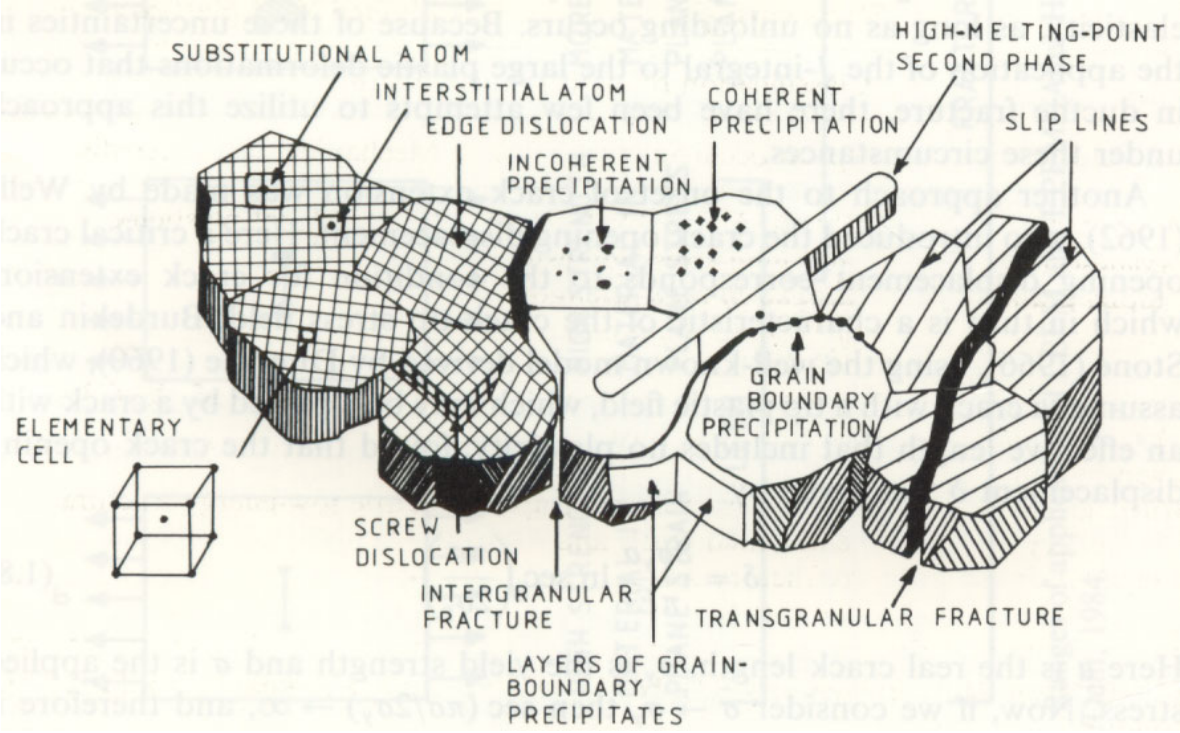

Figure 5.8 Microstructure features in metallic materials (Dodd and Bai, 1987)

The boundaries between grains are the weakest regions in the material, so that the crack grows along grain boundaries. This is called inter-granular fracture. Inter-granular fatigue cracking occurred in case of brittle fracture. Figure 5.14 and Figure 5.23 show cleavage feature of a brittle fracture. The cleavage feature is characterized by the dimpled rupture. These features are created during the fast fracture. Figure 5.9 shows the fracture crack surfaces and indicates each part in detail.

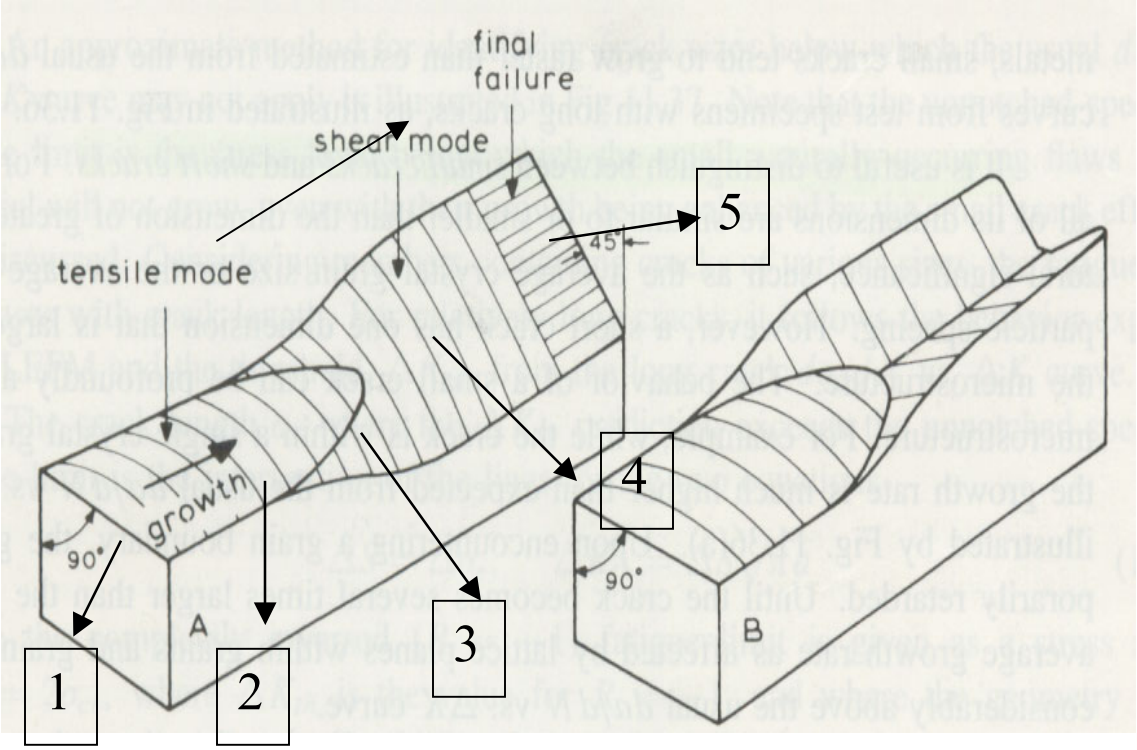

Figure 5.9 Schematic of fatigue crack surfaces showing transition from a flat tensile mode to an angular shear mode. The shear growth (A) occurs on a single sloping surface, or (B) forms a V-shape. (Dowling, 1993)

A typical mode of ductile fracture is by void growth. Ductile fracture is normally trans-granular. Void coalescence is the final stage in void-controlled ductile fracture. Plasticity is localized between voids. This localized deformation leads to final coalescence of voids and complete failure. These three sequential steps for fracture by voids is one of the major features of ductile fracture.

Figure, 5.10, 5.11, 5.12 and 5.13 show micro-void coalescence that is indicative of a ductile fracture. Figure 5.10 is taken at point 1, that is the crack starting point. Figure 5.11 is taken at point 2, that is the entire tensile mode. Tear dimples and micro-voids are found on the crack surface. Figure 5.12 is taken at point 3, that is the mixed mode of tensile and shear. Figure 5.13 is the entire shear mode. Dimpled rupture that is indicative of cleavage feature of brittle fracture is found partly on the surface.

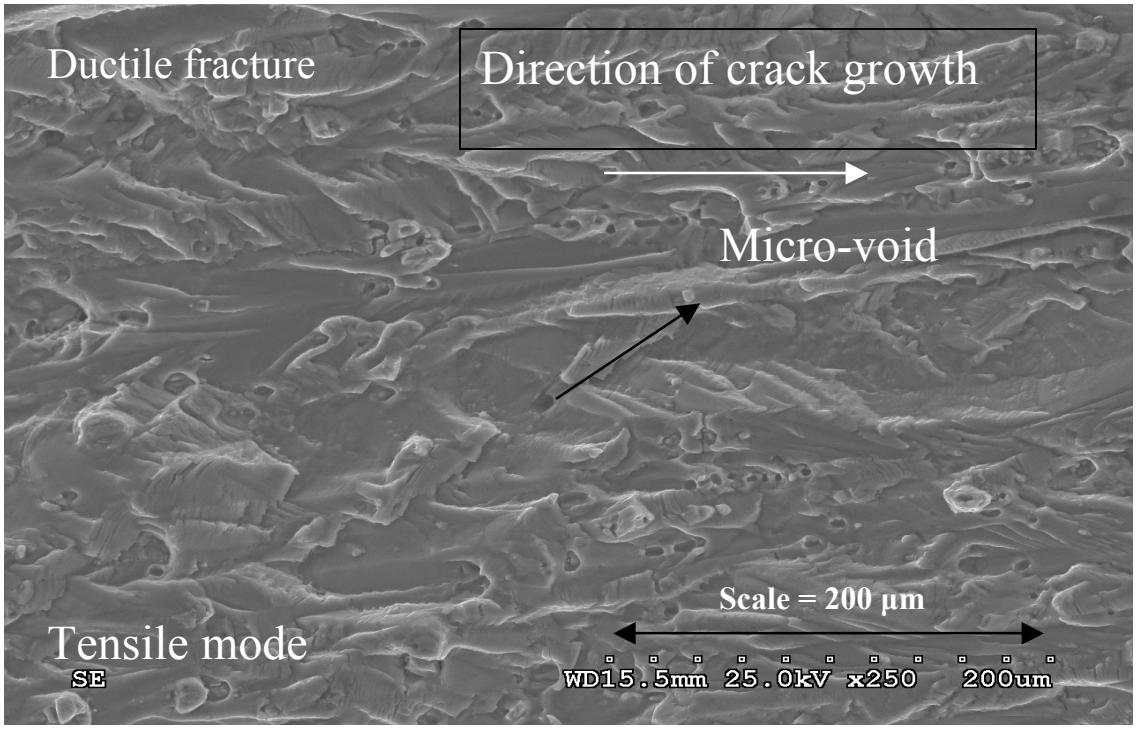

Figure 5.10 SEM micrograph (tested at stress ratio=0.2, frequency=0.5 with dry air, refer to figure 5.9 for identification of location point 1)

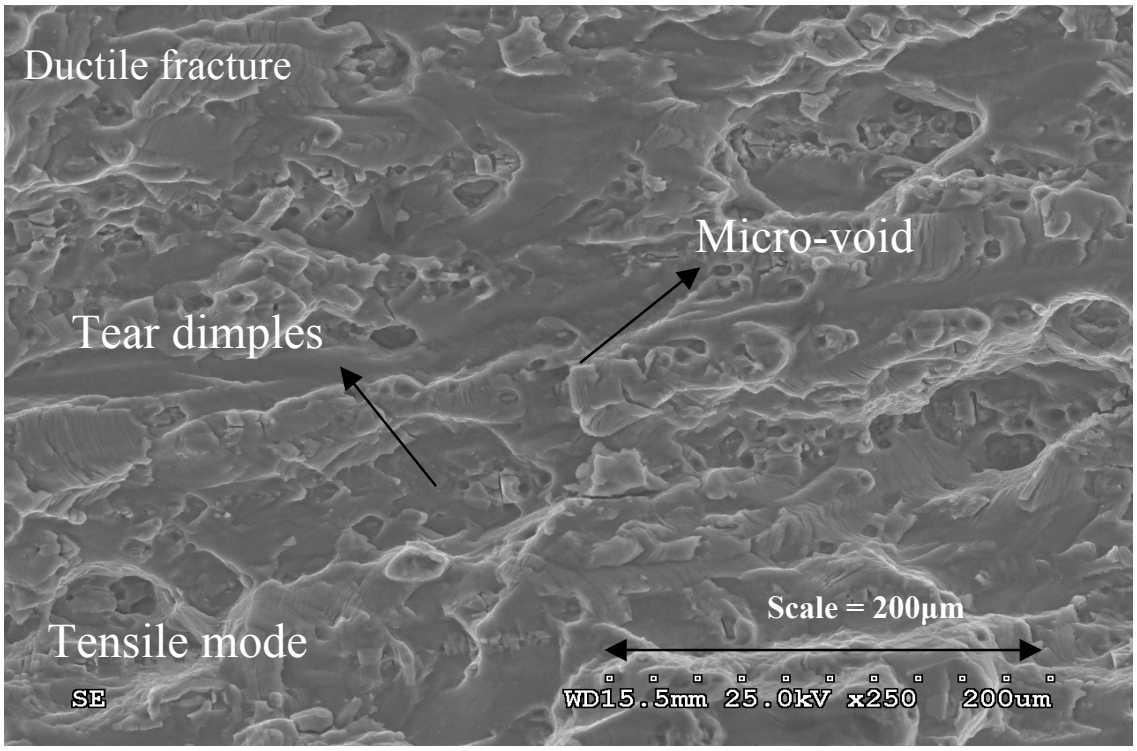

Figure 5.11 SEM micrograph (tested at stress ratio=0.2, frequency=0.5 with dry air, refer to figure 5.9 for identification of location point 2)

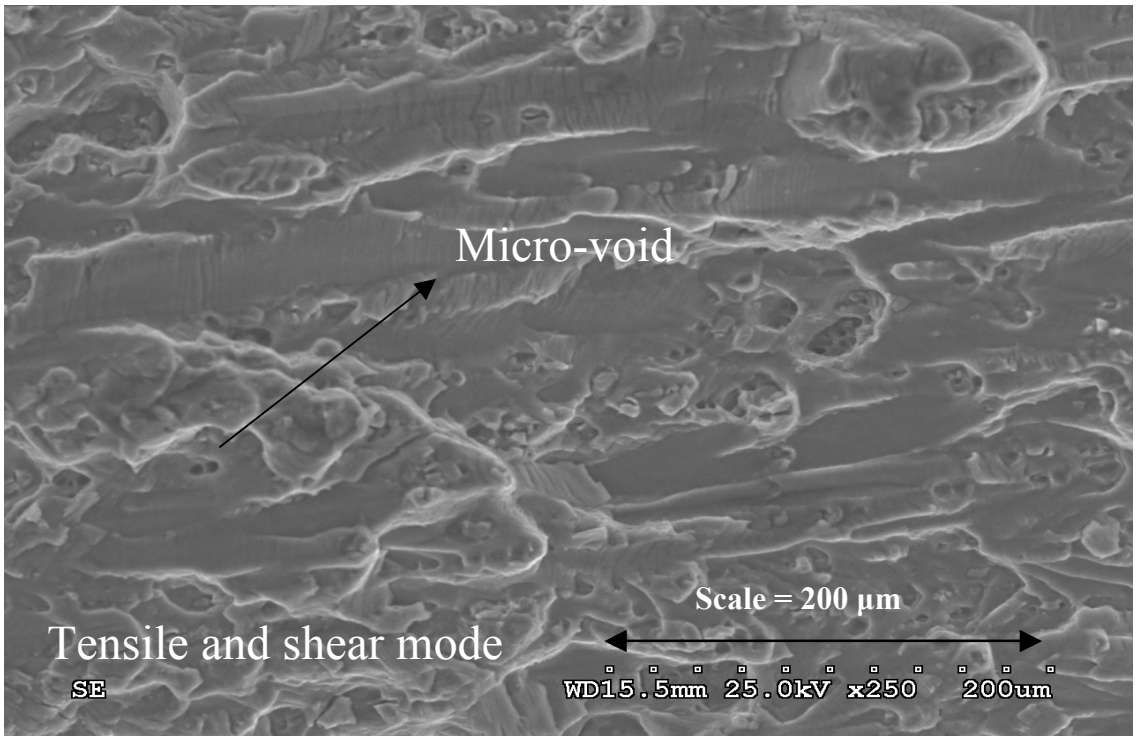

Figure 5.12 SEM micrograph (tested at stress ratio=0.2, frequency=0.5 with dry air, refer to figure 5.9 for identification of location point 3)

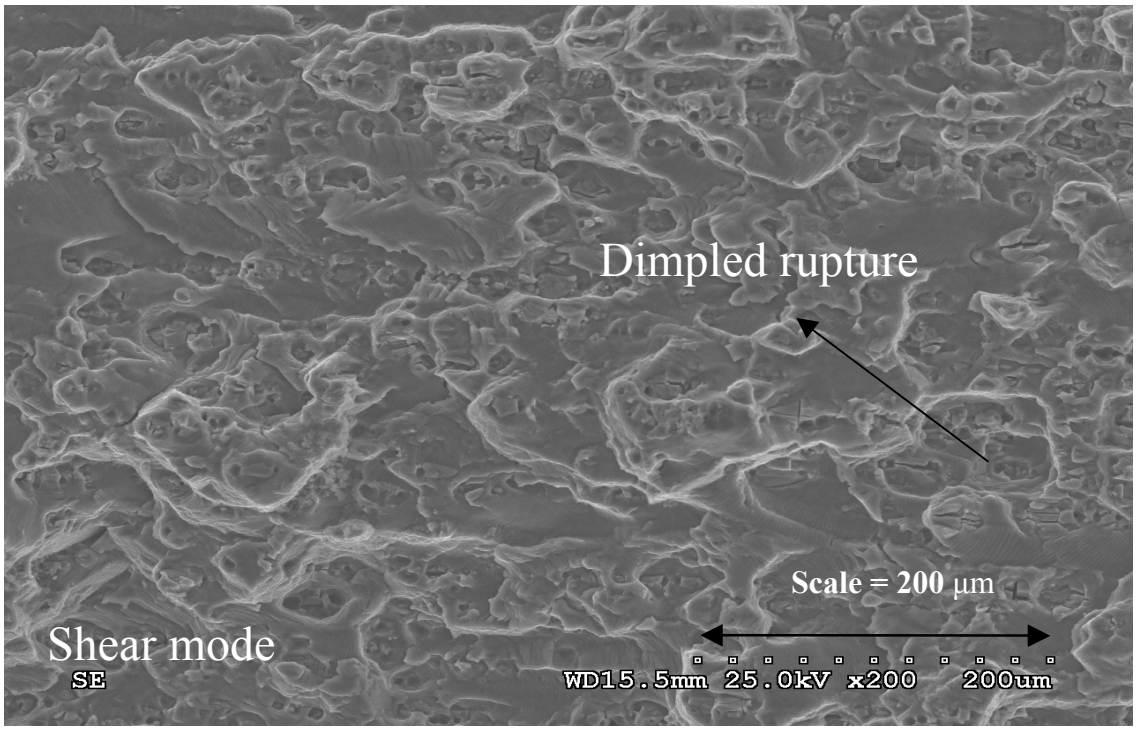

Figure 5.13 SEM micrograph (tested at stress ratio=0.2, frequency=0.5 with dry air, refer to figure 5.9 for identification of location point 4)

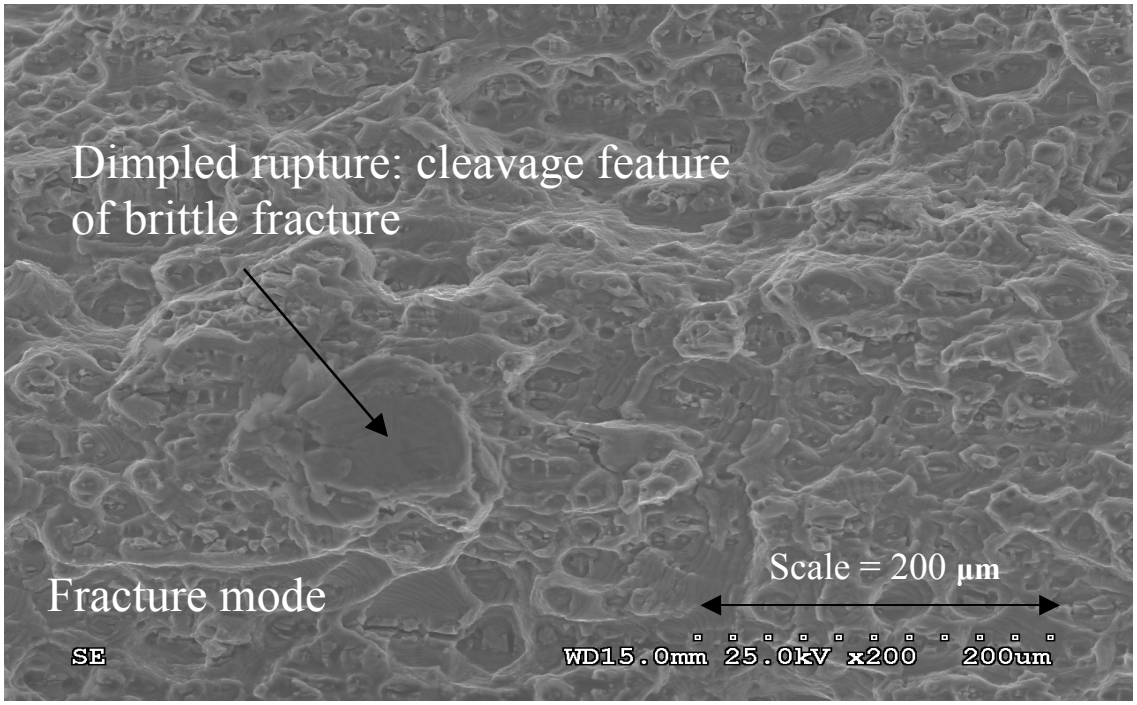

Figure 5.14 SEM micrograph (tested at stress ratio=0.2, frequency=0.5 with dry air, refer to figure 5.9 for identification of location point 5)

In task #1, the striation that is indicative of a ductile failure is not deformed. The fatigue striation that is indicative of ductile failure usually occurs in steels. In this work, instead of striations, crack surface shows that the dimple pattern is initiated at particles in 2024-T3. Figure 5.15 shows tear dimples result from non-uniform applied stresses. This tear dimples pattern is observed in the region of crack growth surface in this thesis work.

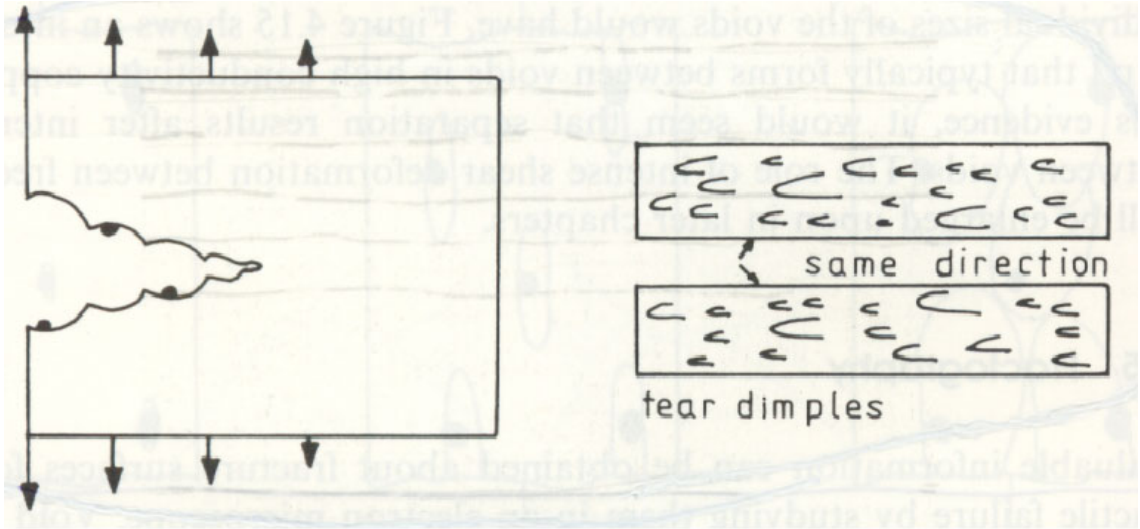

Figure 5.15 Tear dimples according to the applied stresses (Dodd, and Bai, 1987)

This mechanism is called micro-void coalescence, which is also indicative of a ductile failure in case of Al-2024-T3. The aluminum alloy exhibits a ductile rupture type of failure with micro-voids nucleating on the particles or precipitates (Figure 5.16). In task #2, the strands are formed by overloads.

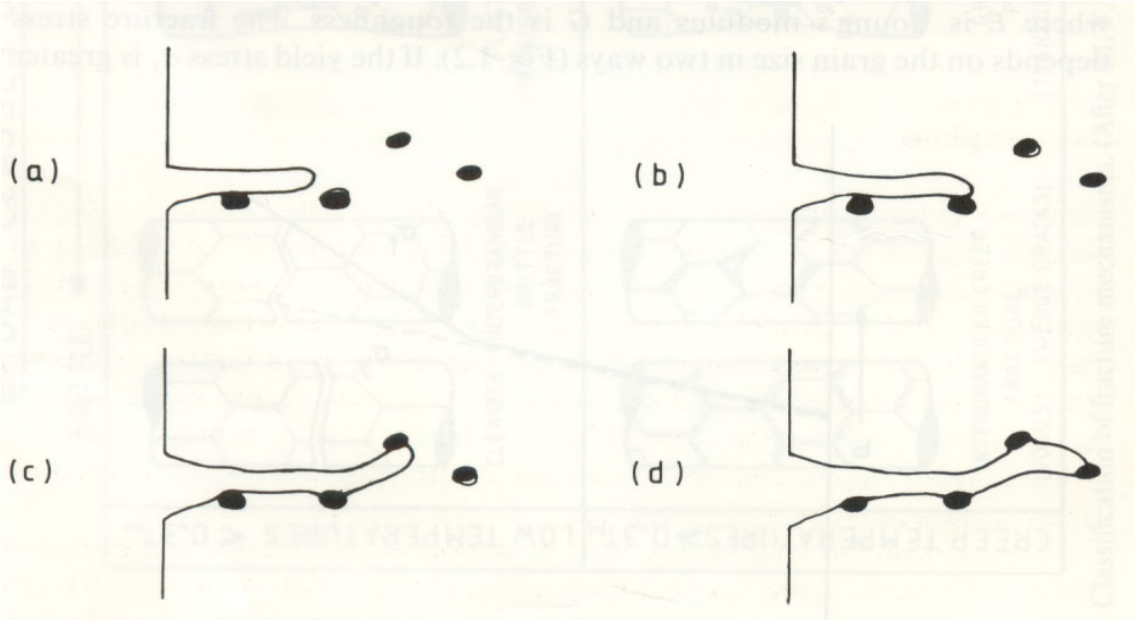

Figure 5.16 Nucleation, growth and coalescence of voids (Dodd, and Bai, 1987)

The trans-granular fracture by striation formation is used to distinguish it from the inter-granular. Also, trans-granular failure mode with fatigue striations is indicative of a ductile failure process. Figure 5.20 show a gradual transition in failure mode from tensile mode (ductile) to brittle mode (brittle) and an increase in crack growth rate. It is interesting to note that a careful examination of the crack surface along the entire crack surface shows no indication of a change in deformation mode as the crack length propagates.

It is also reported in Dodd and Bai, 1987, that the grain boundary embrittlement caused by water vapor ahead of crack tip produces partial inter-granular failure mode and an acceleration of crack growth rate. But, it is not clear from Figure 5.17, 5.18 and 5.19 alone whether the transition from transgranular failure to intergranular failure is caused from the environmental attack (water-vapor). In Figure 5.18, dimpled rupture (cleavage feature of brittle fracture) is observed on the crack surface due to water-vapor even at point 2 which is tensile mode. In metals, generally, inter-granular cracking is likely to occur if there is a hostile environmental influence. To evaluate the possibility of grain boundary embrittlement due to water vapor into the material, a qualitative calculation should be made in the future work. In Figure 5.19, the cleavage feature of brittle fracture is predominant even in shear mode due to water-vapor.

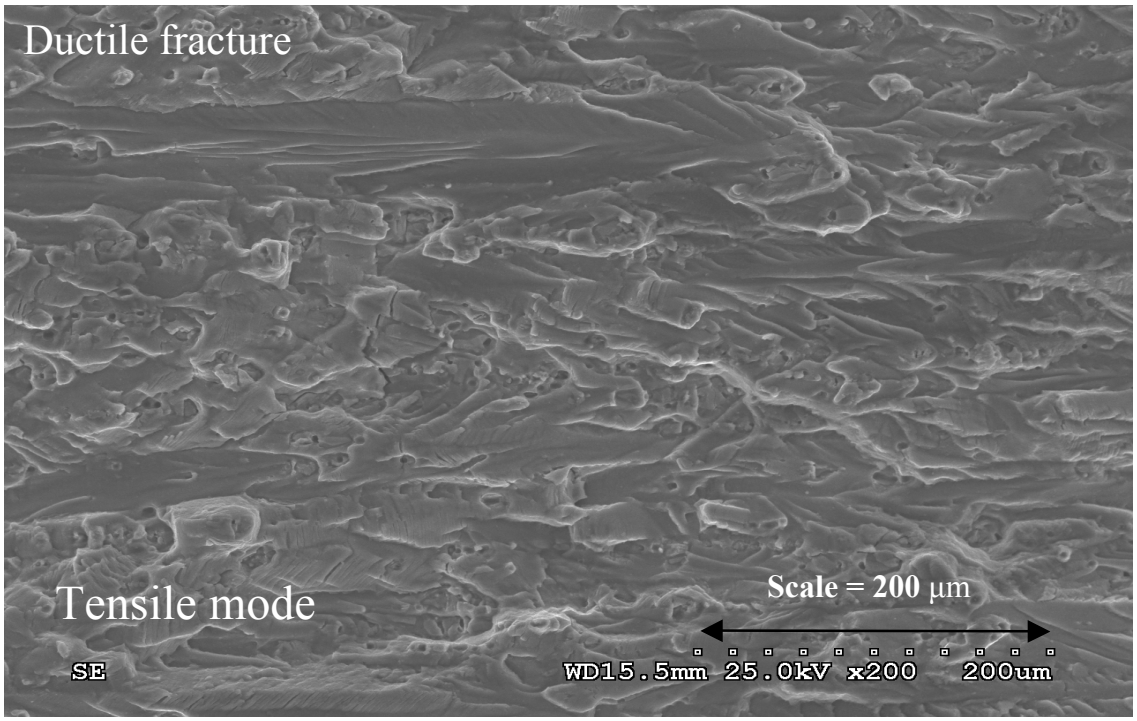

Figure 5.17 SEM micrograph (tested at stress ratio=0.2, frequency=0.5 with water, refer to figure 5.9 for identification of location point 1)

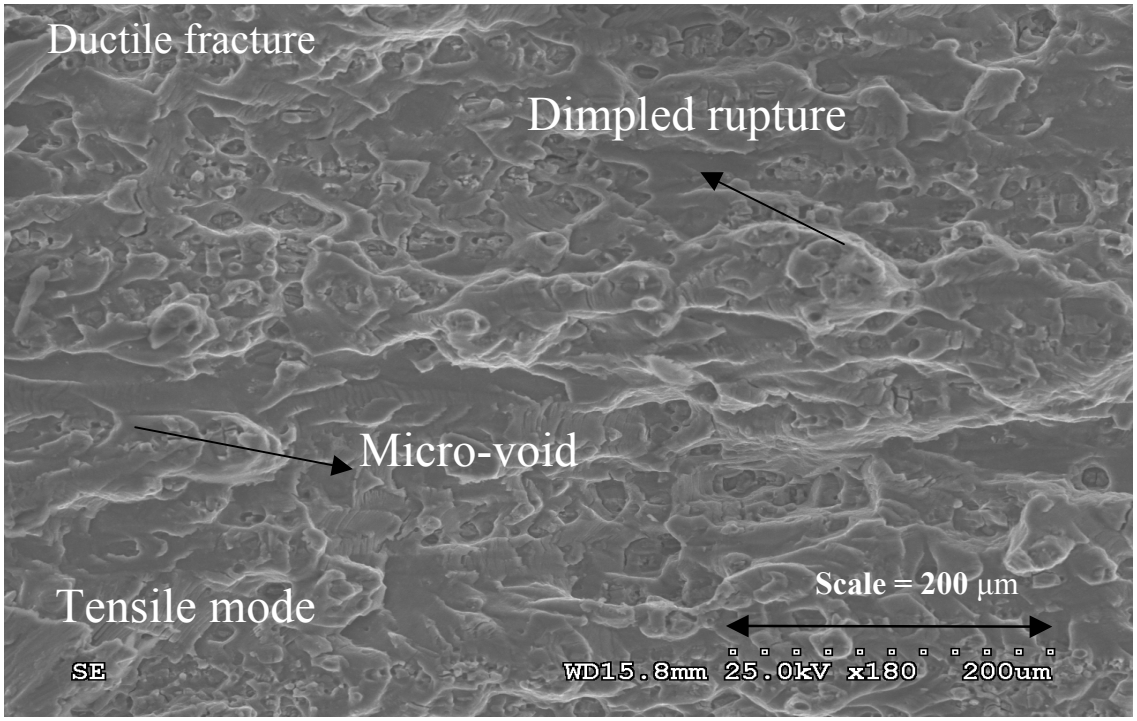

Figure 5.18 SEM micrograph (tested at stress ratio=0.2, frequency=0.5 with water, refer to figure 5.9 for identification of location point 2)

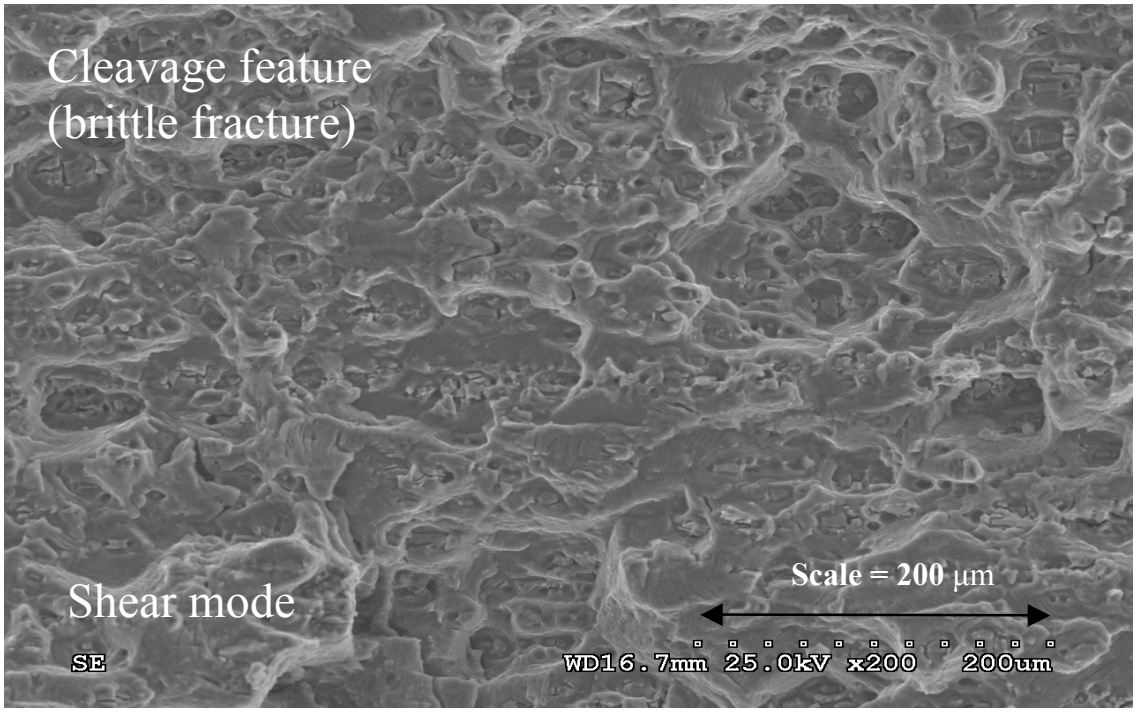

Figure 5.19 SEM micrograph (tested at stress ratio=0.2, frequency=0.5 with water, refer to figure 5.9 for identification of location point 4)

The observations in this thesis work provide some useful insights and basis for explaining the crack growth behavior on the fatigue tests of 2024-T3. A gradual transition in failure mode from tensile mode (ductile) to brittle mode (brittle) is observed on the crack surface by SEM micrograph. The SEM observations in this work also show that a ductile failure mode is prominent as the crack grows transgranularly through the materials.

SEM micrograph is also taken in lesser magnitude in the Figures, 5.21, 5.22 and 5.23 to investigate the large region. In Figure 5.21, a long strand is observed in tensile mode due to non-uniform applied stress at stress ratio=0.2, frequency=0.5 Hz with dry air. In Figure 5.22, more plasticity deformation is observed on the crack surface due to water-vapor at stress ratio = 0.2, frequency = 0.5 Hz.

5.6 Summary of Experimental Results

Generally, the result from corrosion test showed that the increasing stress ratio has a bad effect on fatigue life for any environment conditions. The water-vapor truly reduces the fatigue life (except at R = 0.5, frequency = 1.0 Hz). The reason is that the water-vapor tends to reduce the surface friction between crack faces during the fatigue cyclic loading. The result with corrosion-prevention-compounds (LPS-3) & water-vapor generally show the beneficial effect of LPS-3 on fatigue life. The tests with CPC (LPS3) & water vapor showed a 20 ~ 24 % increase of fatigue life than the test with just water vapor.

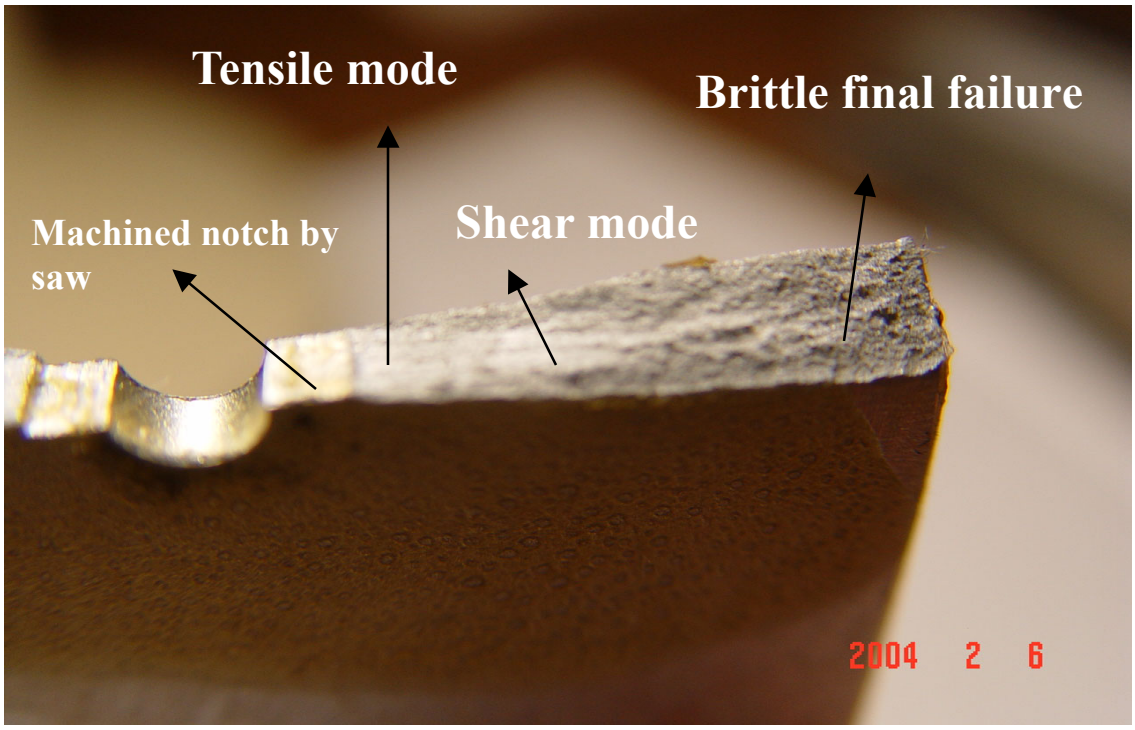

Figure 5.20 Fatigue crack surface showing transition from a flat tensile mode to an angular shear mode (at stress ratio=0.5, frequency=1 with LPS3)

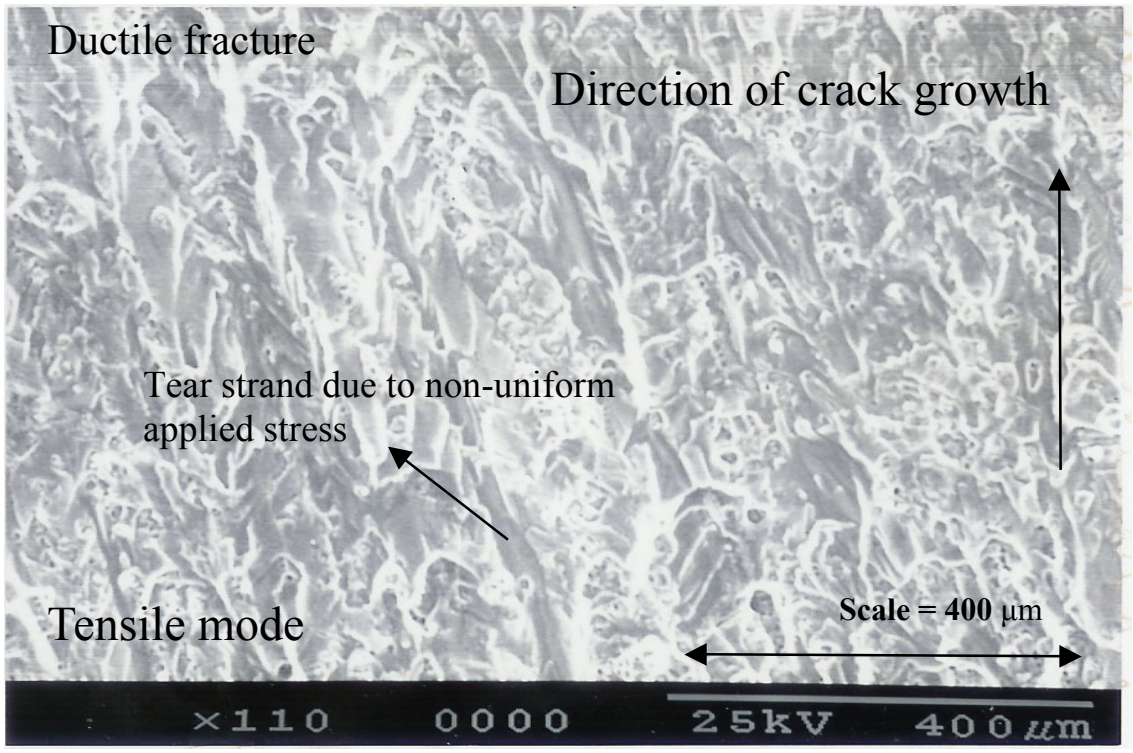

Figure 5.21 SEM micrograph (tested at stress ratio=0.2, frequency=0.5 with dry air, refer to figure 5.9 for identification of location point 2)

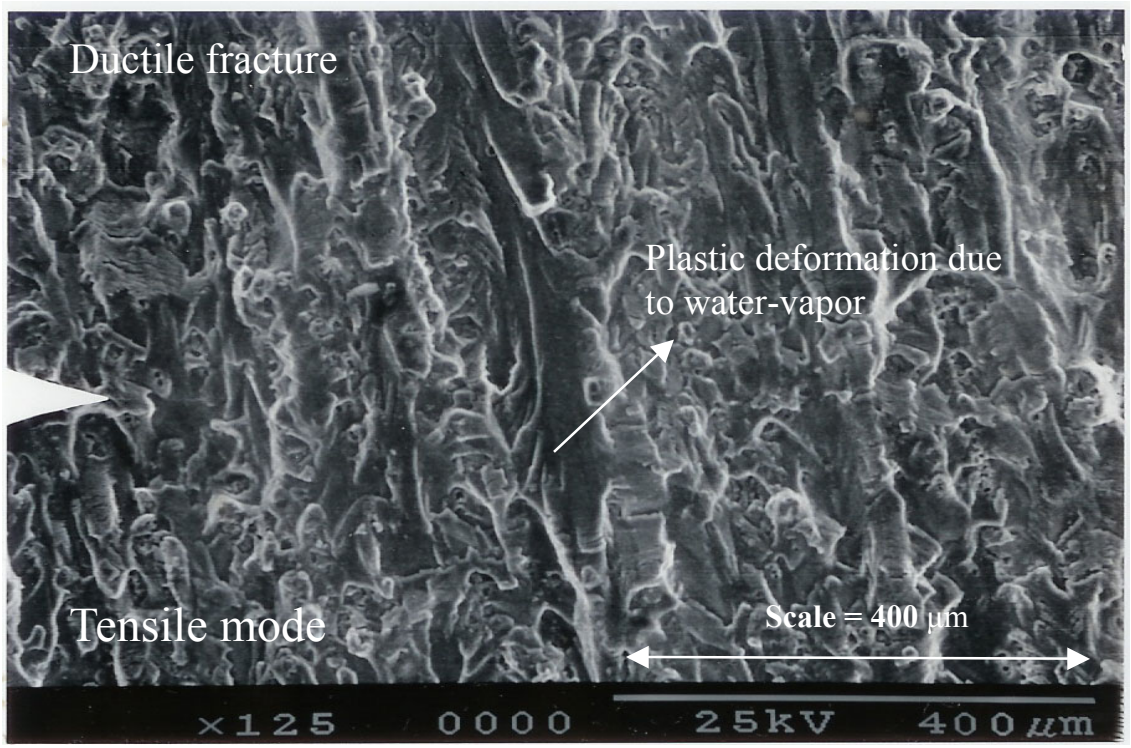

Figure 5.22 SEM micrograph (tested at stress ratio=0.2, frequency=0.5 with water, refer to figure 5.9 for identification of location point 2)

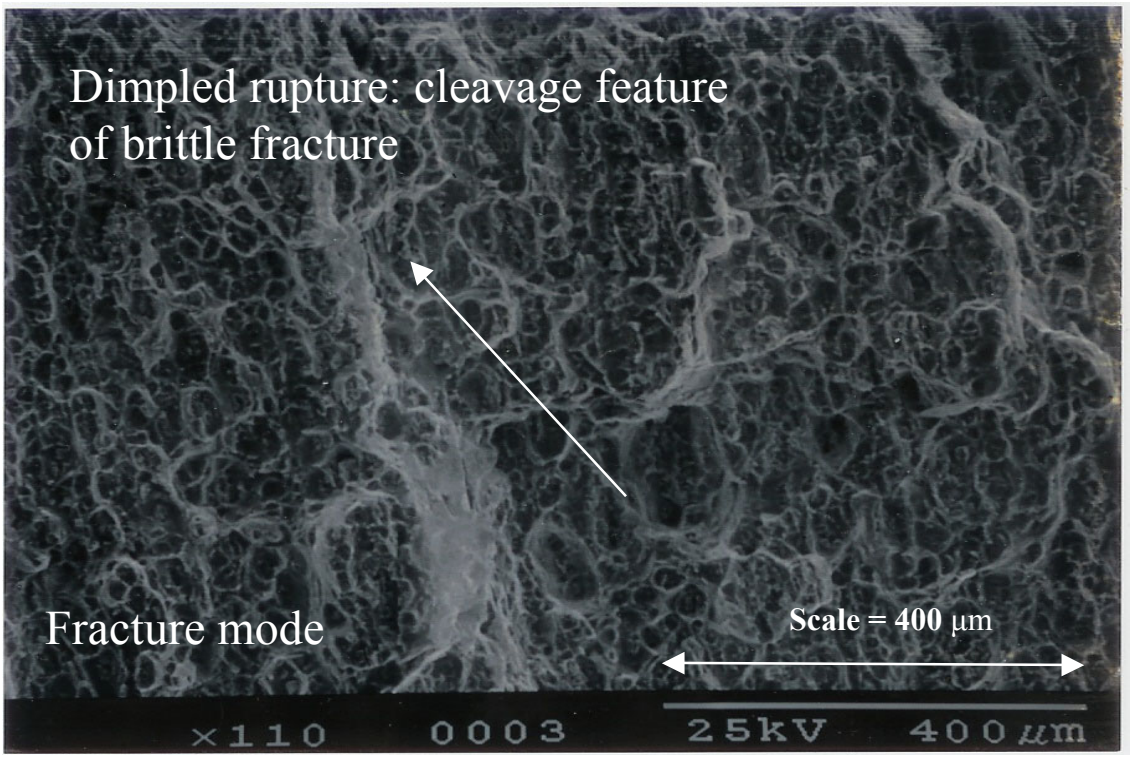

Figure 5.23 SEM micrograph (tested at stress ratio=0.5, frequency=1 with dry air, refer to figure 5.9 for identification of location point 5)

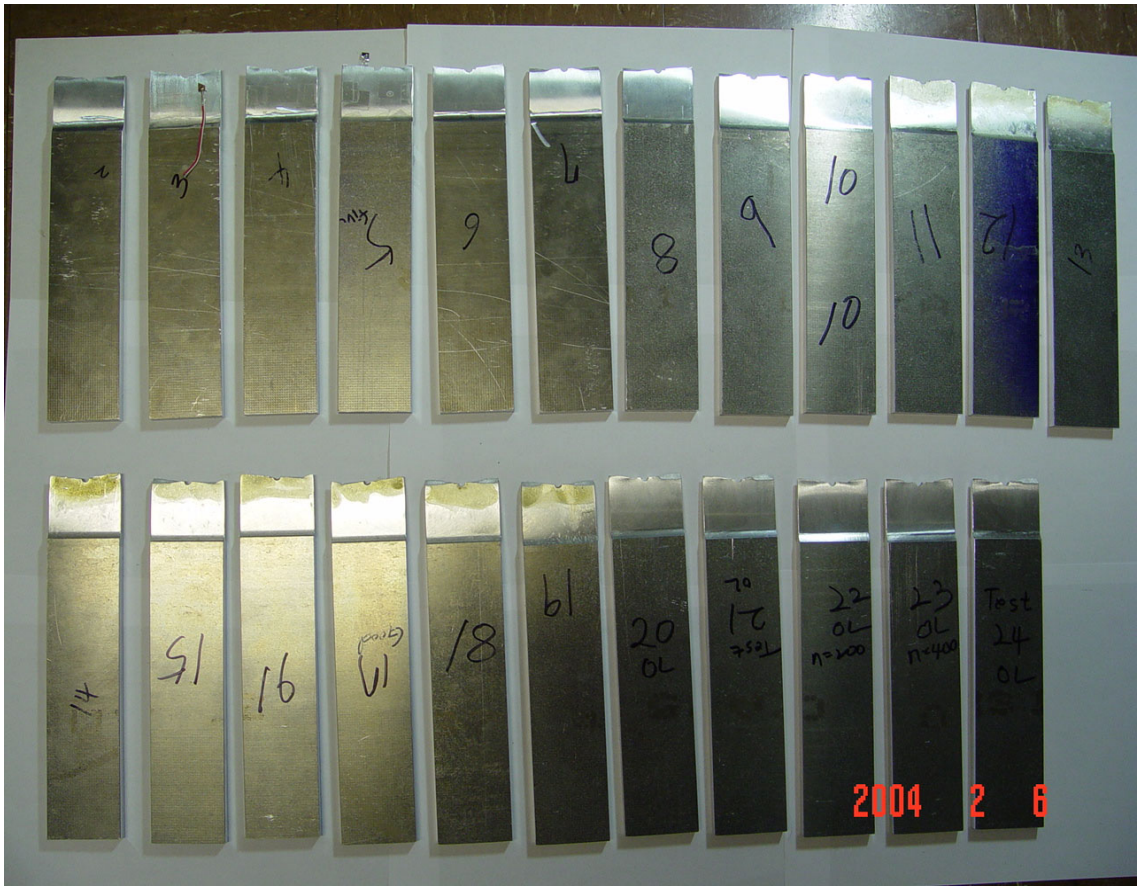

Figure 5.24 Test specimens after failure

In periodic overloads test, the total fatigue life increases as spacing cycles between overloads is increased until a peak is reached, followed by a decrease in total fatigue life afterwards. At the peak total fatigue life, it starts decreasing. The best spacing cycles between overloads to get a maximum fatigue life is in the range of 400 to 2000 cycles. In terms of crack length, it is reported in Mills and Hertzberg, 1976 that the maximum retardation occurs at $da / 2r_y^{OL} = 0.2$ (independent of the overload ratio applied). This level of maximum retardation occurring at da = 0.2 * (overload induced plane strain plastic zone size) for 2024-T3 is also reported by, Tür and Vardar, 1996. The SEM micrograph is used to find out the crack length "da" between overloads in case of n = 800 cycles. The measured "da" from SEM micrograph for n = 800 cycles was not well matched with the results of da = 0.2 * (overload induced plane strain plastic zone size). The maximum retardation between overloads is not yet achieved at n = 800 cycles.

A gradual transition in failure mode from tensile mode (ductile) to brittle mode (brittle) is observed on the crack surface by SEM micrograph. A careful examination of the crack surface along the entire crack surface shows no indication of a change in deformation mode as the crack length propagates with dry air. But, cleavage feature (which is indicative of brittle fracture) was partly observed in tensile mode due to the fast fracture with water-vapor.

CHAPTER 6. CONCLUSIONS & RECOMMENDATIONS FOR FUTURE WORK

6.1 Conclusions

The main objective of this research (task #1) is to determine the effect of Corrosion-Prevention-Compounds (CPC) on fatigue life for various stress ratios (R = 0.2, 0.5), frequencies (0.5, 1.0) with and without the CPC treatment, and under constant amplitude fatigue loading in water vapor. The following observations can be made from the results obtained from task #1.

- Increasing stress ratio has a negative effect on fatigue life.
- Increasing frequency didn't show a clear trend.
- The water vapor reduces the fatigue life. Water vapor tends to reduce the surface friction between crack faces during the fatigue loading; water vapor reduces the fatigue life during the crack propagation period, and not during the crack initiation period.
- The tests with CPC (LPS3) & water vapor show a 20 ~ 24 % increase of fatigue life than the test with just water vapor except the case of R = 0.5, and frequency = 1.0 Hz. Therefore, the tests with CPC (LPS-3) generally show the beneficial effects on fatigue life.
- Tests with crack propagation strain gage failed due to the noisy signal from the MTS 810 machine itself, vibration from the loading condition and also because of the lack of the bonding system. Tests must be carried out more carefully to avoid the above experimental errors.

The second part of this thesis work includes investigating the effect of periodic overloads on the fatigue life under constant amplitude fatigue loading. The periodic overloads increase the fatigue life dramatically. The total fatigue life is increased by 4~15 times than the fatigue life of the constant amplitude fatigue loadings depending on the spacing cycles between overloads. Due to experimental constraints, only limited number of specimen are used in this section of study. More test specimens are required to find out the optimum spacing cycles between overloads for various overload ratios. With the limited testing, it has been found that the best spacing cycles between overloads is in the range from 400 to 2000 cycles to achieve the maximum fatigue life. It was observed by earlier investigators (Mills and Hertzberg, 1976) that the maximum retardation (maximum fatigue life) occurs at $da / 2r_y^{OL} = 0.2$ (independent of the overload ratio applied). The SEM micrograph is used to determine the crack length "da" between overloads in case of n = 800 cycles. This retarded crack growth "da", between overloads is compared with the theoretical plastic zone size at the crack tip. Both results show similar trend. It was found that the maximum retardation occurred at $\Delta a = 0.2$ * (overload induced plane strain plastic zone size) for 2024-T3, which wass also reported in the literature, (Tür and Vardar, 1996).

Several pictures are taken by using Scanning Electron Microscope (SEM) along the crack surface in sequence. Most crack surfaces show that tear dimples pattern are initiated at particles on the crack propagation surface of aluminum alloy 2024-T3. Tear dimples pattern is generated from non-uniform applied stresses at the end of specimen. The tear dimples pattern is indicative of a ductile fracture mode. The aluminum alloy exhibits a ductile rupture type of failure with micro-voids nucleating on the particles or precipitates. This mechanism is called micro-void coalescence and is indicative of ductile fracture.

6.2 Recommendations for Future Work

The important aspect in this thesis work is that how to verify the results from task #1. More test specimens should be used to verify one data point, i.e. 3 to 4 specimen per data point. Then, statistical evaluation needs to be made to verify the test results with those formed other literatures. Unfortunately, due to the lack of time and cost, only limited test specimens are used in this study. Generally, the scatter in fatigue life for specimens under similar conditions is expected due to the specimen design, the location of crack initiation site, misalignment when gripped, etc. Also, salt-fog or other corrosion environments need to be used in combination with the corrosion chamber.

As mentioned in chapter 5 Results and Evaluations, test results with crack propagation strain gage failed due to the noisy signal from the MTS 810 machine itself, vibration from the loading condition and also because of the lack of a proper bonding system. To investigate the crack growth retardation after each applied overloads, the voltage jump for each broken strand need to be measured exactly to calculate the crack growth per cycle. Careful attention should be given when the test is run with crack propagation strain gage to avoid the noisy signal. If this test is done properly, the crack growth rate can be found directly. Measuring the crack growth rate is a difficult work due to the complexities relating to the measurements involved. To monitor the crack growth rate exactly, other improved methods need to be used. For example, compliance method, electric potential difference method or displacement measurement hardware is recommended. Further works should be done when considering these points. In this thesis work, by using Scanning Electron Microscope (SEM), the crack surface is investigated. The crack increment between overloads is observed by SEM micrograph.

In task #2, the objective is to determine the optimum spacing cycles between overloads for various overload ratios. More test specimens should be used to find out the exact spacing cycles between overloads for each overload ratio. In this work, only one overload ratio of 1.7 is tested with the spacing cycles from 50 to 40000 cycles. A series of overload ratios need to be used to check the different interactions of overload ratios. More research needs to be conducted to establish the ways in which fatigue life of metals is assessed and may be extended, and also to predict the fatigue life of aircraft components more accurately.

REFERENCES

Aliaga D., Davy A., and Schaff H., 1985, "A Simple Crack Closure Model for Predicting Fatigue Crack Growth under Flight Simulation Loading, Durability and Damage Tolerance in Aircraft Design", A. Salvetti and G. Cavallini, Ed., EMAS, Warley, U.K., p 605-630.

ANSYS User's Manual 5.7 : Ansys structural analysis guide.

Andresen Peter L. (GE Corporate Research & Development), 1996, "Corrosion Fatigue Testing", Fatigue and Fracture, Vol. 19. P 193-209.

Saxena Ashok and Muhlstein Christopher L., 1996, "Fatigue Crack Growth Testing", Fatigue and fracture, Vol. 19, p 168-184.

ASTM. 1995, Annual Book of ASTM Standards E647 – 95a, Am. Soc. for Testing and Materials, "Standard Test Method for Measurement of Fatigue Crack Growth rates", pp. 562-598.

Barsom J.M., E.J. Imhoff, and S.T. Rolfe, 1971, Fatigue Crack Propagation in high Yield Strength Steels, *Eng. Fract. Mech*., Vol 2, p301-324.

Baudin G. and Robert M., 1984, "Crack growth Life Time Prediction under Aeronautical Type Loading", Proc. Fifth European Conf. on Fracure, p 779.

Bellinger NC, SK Kumar, Komorowski JP, 1994, "Modeling of pillowing in aircraft lap joints due to corrosion," Canadian Aeronautics and Space Journal , Vol. 40, No. 3, p 125-130.

Boissonat J., 1963, "Experimental Research on the effects of a Static Preloading on the Fatigue Life of Structural components, Fatigue of Aircrack Structures", W. Barrois and E. Ripley, Ed., Pergamon Press, p 97-113.

Bradley Dodd and Yilong Bai, 1987, "Ductile Fracture and Ductility with Applications to Metalworking", Academic Press.

Bradshaw F.J. and Wheeler C., 1969, "The Effect of Gaseous Environment and Fatigue Frequency on the Growth of Fatigue Cracks in Some Aluminium Alloys", Int. J. Fract., Vol. 6, p 225.

Broek D., 1988, "The Practical Use of Fracture Mechanics", Kluwer Academic Publishers.

Broek D., 1972, "Fatigue Crack Growth and Residual Strength of Aluminium Sheet at Low Temperature, Report TR 72096, National Aerospace Laboratory, Amsterdam.

Cullen W., Gabetta G., and Hanninen H., Dec. 1985, "A review of the Methods and Mechanisms for the Environmentally-assisted Crack Growth of Pressure Vessel and Piping Steels in PWR Environments," NUREG/CR-4422 MEA-2078, U.S. Nuclear Regulatory Commision.

Dahl W. and Roth G., 1979, "On the Influence of Overloads on Fatigue Crack Propagation in Structural Steels," Tech. Un. Aachen.

Broek David, 1988, The Practical Use of Fracture Mechanics, Kluwer Academic Publishers.

De Koning A.U. and Dougherty D.J., 1981, "A Simple Crack Closure Model for Prediction of Fatigue Crack Growth Rates under Variable Amplitude Loading, Fracture Mechanics", R. Roberts, Ed., STP 743, ASTM, p 63.

De Koning A.U. and Dougherty D.J., 1989, " Prediction of Low and High Crack Growth Rates under Constant and Variable Amplitude Loading, Fatigue Crack Growth under Variable Amplitude Loading", J. Petit et al., Ed., Elsevier, p 208-217.

De Koning A.U., Dougherty D.J., and Hillberry B.M., 1992, "Modelling High Crack Growth Rates under Variable Amplitude Loading, Advances in Fatigue Lifetime Predictive Techniques", STP 1122, ASTM, p 214-233.

Dowling N.E., 1993, "Mechanical Behavior of Materials: Engineering Methods for Deformation, Fracture, and Fatigue", Prentice-Hall.

Elber W., 1970, "Fatigue Crack Closure under Cyclic Tension," Engineering Fracture. Mechanics, Vol. 2(1), pp. 37-45.

Elber W., 1971, "The significance of Fatigue Crack closure," Damage Tolerance in Aircraft Structures, STP 486, ASTM, American Soc. for Testing and Materials, Philadlephia, PA. pp 230-242.

Endo K. and Miyao Y., 1958, "Effects of cyclic Frequency on the Corrosion Fatigue Strength", Bulletin Japan, Soc. Mech. Engineers, Vol. 1, p 374-380.

Ford F.P., 1988, Status of Research on Environmentally Assisted Cracking in LWR Pressure Vessel Steels, Trans. ASME, J. Pressure Vessel Technology, Vol. 110, p 113-128.

Führing H. and Seeger T., 1979, "Structural Memory of Cracked Components under Irregular Loading, Fracture Mechanics", C.W. Smith, Ed. STP 677, ASTM, p 1144-1167.

Führing H. and Seeger T., 1979, "Dugdale Crack Closure Analysis of Fatigue Cracks under Constant Amplitude Loading", Eng. Fract. Mech., Vol. 11, p 99-122.

Gangloff R.P. and Wei R.P., 1977,"Metall. Trans. A", Vol 8A, p 1043.

Gangloff R.P., 1984, Exxon Research and Engineering Co., unpublished research.

Gill S.J. and Crooker T.W., 1990, *Marine Tech*., Vol. 27, p 221.

Hartman A., 1965, "On the Effect of Oxygen and Water Vapor on the Propagation of Fatigue Cracks in 2024-T3 Alclad Sheet", Int. J. Fract. Mech., Vol. 1, p 167.

Heywood R.B., 1956, "The effect of High Loads on Fatigue, Colloquium on Fatigue", W. Weibull and F.K.G. Odquist, Ed., Springer Verlag, p 92-102.

Heuler P. and Schütz W. 1985, "Fatigue Life Prediction in the Crack Initiation and Crack Propagation Stages, Durability and Damage Tolerance in Aircraft Design", A. Salvetti and G. Cavallini, Ed., EMAS, Warley, U.K., p 33-69.

Hinton B, Shankar K, Trathen P, Salagaras M, Wilson L, Devereaux G, 1996, "Control of corrosion on Aluminum alloys with corrosion prevention compounds", Paper #335, 13th International Corrosion Congress, Melbourne, Australia, 25-29 November.

Irwin, G.R., 1960, "Plastic zone near a crack and fracture toughness" In Proceedings of the Seventh Sagamore Ordnance Materials Conference, Vol. IV, pp. 63-78. New York: Syracuse University.

Ogura Keiji & Ohji Kiyotsugu, 1977, "FEM analysis of crack closure and delay effect in fatigue crack growth under variable amplitude loading", Engineering fracture mechanics, Vol. 9, pp.471-480.

Komorowski JP, K Shankar, Gould RW, et al., 1993, "Corrosion detection in aircraft structures,", 1993 USAF Structural Integrity Program Conference, San Antonio, Texas, 30.

Komorowski JP., Kumar S K, Gould RW, Bellinger NC, Karpala F, Hageniers OL, 1996, "Double pass retroflection for corrosion detection in Aircraft structures." Materials Eva. Lu. Vol. 54, No. 1, p 80-86.

Shankar Krishnakumar, Dhamari Rudy, 2002, "Fatigue behavior of aluminum alloy 7075 bolted joints treated with oily film corrosion compounds", Materials and Design 23, Elsevier, p 209-216.

Kumar R., 1992, "Review on Crack Closure for Constant Amplitude Loading in Fatigue", Eng. Fract. Mech., Vol. 42, p 389-400.

Mills W.J. and Hertzberg R.W., 1975, "The Effect of Sheet Thickness on Fatigue Crack Retardation in 2024-T3 Aluminum Alloy", Eng. Fract. Mech., Vol. 7, p 705-711.

Mills W.J. and Hertzberg R.W., 1976, “Load Interaction Effects on Fatigue Crack Propagation in 2024-T3 Aluminum Alloy”, Eng. Fract. Mech., Vol. 8, p 657-667

Miner M.A., 1945, “Cumulative Damage in Fatigue”, Journal of Applied Mechanics, Vol. 12, p A159 - A164.

Naumann E.C., Hardrath H.R., and Guthrie E.C., 1959, “Axial Load Fatigue Tests of 2024-T3 and 7075-T6 Aluminum Alloy Sheet Specimens under Constant- and Variable Amplitude Loads,” Report TN D-212, NASA Fatigue Crack Growth under Spectrum loads, 1976, STP 595, ASTM.

Newman Jr. J.C., Amen H., 1975, “Elastic-Plasticity Analysis of a Propagating Crack under Cyclic Loading”, AIAA J., Vol. 13, p 1017-1023.

Newman Jr. J.C., 1981, “A Crack-closure model for Predicting Fatigue Crack Growth under Aircraft Spectrum Loading, Methods and models for Predicting Fatigue Crack Growth under Random loading”, J.B. Chang and C.M. Hudson, Ed. STP 748, ASTM, p 53-84.

Newman Jr. J.C., Dawicke D.S., 1989, “Prediction of Fatigue-Crack Growth in a High-Strength Aluminum Alloy under Variable-Amplitude Loading”, NASA Technical Memorandum 101544, The Seventh International Conference on Fracture, March 20-24, Feb. 1989.

Newman Jr. J.C., 1997, “Prediction of Crack Growth under Variable-Amplitude Loading in thin-Sheet 2024-T3 Aluminum Alloys”, NASA Langley Research Center, Hampton, Virginia, USA, Engineering Against Fatigue, University of Sheffield.

Barsom J.M., Imhoff E.J., and Rolfe S.T., 1971, “Fatigue Crack Propagation in high Yield Strength Steels”, Eng. Fract. Mech., Vol 2,, p301-324

Ohji K., Ogura K., and Ohkubo Y., 1975, “Cyclic Analysis of a Propagating Crack and its Correlation with Fatigue Crack Growth”, Eng. Fract. Mech., Vol. 7, p 457-463.

Padmadinata U.H., 1990, “Investigation of Crack-Closure Prediction Models for Fatigue in Aluminum Sheet under Flight-Simulation Loading,” Ph.D. dissertation, Delft University of Technology.

Pao P.S., Wei W., and Wei R.P., 1979, “Environment-sensitive Fracture of Engineering Materials”, TMS-TIME, p 565.

Pao P.S., (Materials Science and Technology Division, Naval Research Laboratory), 1996, “Mechanisms of corrosion fatigue”, Fatigue and Fracture, Vol. 19, P 185-192.

Paris P.C., 1964, “The Fracture Mechanics Approach to Fatigue,” Fatigue-An Interdisciplinary Approach, J.J. Burke, et al., Proc. of the 10th Sagamore Army Materials Research Conf.3, Syracuse University Press, Syracuse, NY, pp. 107-127.

Proc. Int. Symp. On Plan aging and Life Prediction of Corrodible Structures, 1995, National Association of Corrosion Engineers.

Proc. Int. Symp. On Plan aging and Life Prediction of Corrodible Structures, 1995, Corrosion Fatigue, Corrosion Tests and Standards: Application and Interpretation, R. Baboian, Ed., ASTM.

McClung R.C., & Sehitoglu H., 1989, “On the finite element analysis of fatigue crack closure-1. Basic modeling issues, Engineering fracture mechanics”, Vol. 33, pp.237-252

Sanford R.J., 2002, “Principles of fracture mechanics”, Prentice-Hall.

Rolfe S.T. and Barsom J.M., 1977, “Fracture and Fatigue Control in Structures”, Prentice-Hall.

Dhamari Rudy, Shankar Krishnakumar and Wei Riyu, 1999, “Effect of Corrosion Prevention Compounds on Fatigue Life of Double Lap Joints” University College, UNSW, ADFA, ACT 2600 Australia, ACAM 99, The Second Australasian Congress on Applied Mechanics, 10-12 February 1999, Canberra, Ausralia.

Schijve J., 1970, “Cumulative Damage Problems in Aircracft Structures and Materials”, Aero. J., Vol. 74, p 517-532.

Schijve J., 1972, “The Accumulation of Fatigue Damage in Aircraft Materials and Structures, AGARDograph 157.

Schijve J., 1972, “Effects of Test Frequency on Fatigue Crack Propagation under Flight-Simulation Loading”, Symp. On Random Load Fatigue, AGARD CP 118..

Schijve J., 1973, “Effect of Load Sequences on Crack Propagation under Random and Program Loading”, Eng. Fract. Mech., Vol. 5, p 269-280.

Schijve J., 1976, “Observations on the Prediction of Fatigue Crack Propagation under Variable-Amplitude Loading”, Fatigue Crack Growth under Spectrum Loads, STP 595, ASTM, p 3-23.

Schijve J., 1979, “Four Lectures on Fatigue Crack Growth”, Eng. Fract. Mech., Vol. 11, p 176-221.

Schijve J., 1985, “The Significance of Flight Simulation Fatigue tests, Durability and

Damage Tolerance in aircraft Design", A. Salvetti and G. Cavallini, Ed., EMAS, Warley, U.K., p 71-170.

Schijve J., Vlutters A.M., Ichsan S.P., and ProvoKluit J.C., 1985, "Crack Growth in Aluminum Alloy Sheet Material under Flight-Simulation Loading", Int. J. Fatigue, Vol. 7, p 127-136.

Schijve J., 1992, "Fundamental Aspects of Predictions on Fatigue Crack Growth under Variable Amplitude Loading, Theoretical Concepts and Numerical Analysis of Fatigue", A.F. Blom and C.J. Beevers, Ed., EMAS, Warley, U.K., p 111-130.

Schijve J. (Delft University of Technology), 1996, "Fatigue Crack Growth under Variable-Amplitude Loading", Fatigue and Fracture, Vol. 19, P110-133.

Schütz W., 1979, "The Prediction of Fatigue Life in the Crack Initiation and Propagation Stages: A State of the Art Survey", Eng. Fract. Mech., Vol. 11, p 405-421

Scott P.M. and Truswell A.E., 1983, "Corrosion Fatigue Crack Growth in Reactor Pressure Vessel Steels in PWR Primary Water", J. Pressure Vessel Tech., Vol. 105, p 245-254.

Tür Yahya K., et al., 1996, "Periodic Tensile Overloads in 2024-T3 Al-Alloy", Engineering Fracture Mechanics, Vol. 53, No. 1, p 69-77.

Tür Y.K. and Vardar Ö., 1996, "Periodic Tensile Overloads in 2024-T3 Aluminum Alloy", Engineering. Fracture. Mechanics., Vol 8, p 657-667.

Van Der Sluys W. and Emanuelson R., May 1985, "Overview of Data Trends in Cyclic Crack Growth Results in LWR Environments", Proc. 2nd IAEA Specialists' Meeting on Subcritical Crack Growth (Sendai, Japan), U.S. Nuclear Regulatory Commission, p 15-17.

Walker K., 1970, "The Effect of Stress Ratio During Crack Propagation and Fatigue for 2024-T3 and 7075-T6 Aluminum," Effects of Environment and Complex Load History on Fatigue Life, ASTM STP 462, Am. Soc. for Testing and Materials, West Conshohocken, PA, pp. 1-14.

Wang G.S. and Blom A.F., 1991, "A Strip Model for Fatigue Crack Growth Predictions under General Load Conditions", Eng. Fract. Mech., Vol. 40, p 507-533.

Willenborg J., Engle R.M., and Wood H.A., 1971, "A Crack Growth Retardation Model Using as Effective Stress Concept," Report TR71-1, Air Force Flight Dynamic Laboratory, Wright-Patterson Air Force Base.

Wheeler O.E., 1972, "Spectrum Loading and Crack Growth", J. Basic Eng., Vol. 94, p 181-186.

APPENDIX A1: "ANSYS" PROGRAM COMMAND CODES

1. Crack retardation due to two overloads (80MPa – 100MPa)

```
/TITLE, Crack Retardation Simulation (Mapped Mesh for two overloads: 80MPa - 100MPa)
/PREP7
!*
ET,1,PLANE82
!*
KEYOPT,1,3,0
KEYOPT,1,5,0
KEYOPT,1,6,0
!*
TOFFST,273
MPTEMP,,,,,,,,
MPTEMP,1,0
MPDATA,EX,1,,70000
MPDATA,PRXY,1,,0.33
TB,BISO,1,1,2,
TBTEMP,20
TBDATA,,200,0.0,,,,
/AXLAB,X,Total Strain
/AXLAB,Y,Stress
/GTHK,AXIS,1
/GRTYP,0
/XRANGE,DEFAULT
/YRANGE,DEFAULT,,1
!*
WPSTYLE,,,,,,,,1
wpstyle,10,10,0,100,0.003,0,0,,5

FLST,3,9,8
FITEM,3,0,0,0
FITEM,3,10,0,0
FITEM,3,50,0,0
FITEM,3,50,20,0
FITEM,3,10,20,0
FITEM,3,0,20,0
FITEM,3,0,60,0
FITEM,3,10,60,0
FITEM,3,50,60,0
K, ,P51X
LSTR,      1,      2
LSTR,      2,      3
LSTR,      3,      4
```

```
LSTR,      2,      5
LSTR,      1,      6
LSTR,      6,      5
LSTR,      5,      4
LSTR,      4,      9
LSTR,      5,      8
LSTR,      6,      7
LSTR,      7,      8
LSTR,      8,      9
FLST,2,4,4
FITEM,2,5
FITEM,2,4
FITEM,2,6
FITEM,2,1
AL,P51X
FLST,2,4,4
FITEM,2,4
FITEM,2,7
FITEM,2,2
FITEM,2,3
AL,P51X
FLST,2,4,4
FITEM,2,12
FITEM,2,9
FITEM,2,8
FITEM,2,7
AL,P51X
FLST,2,4,4
FITEM,2,10
FITEM,2,11
FITEM,2,9
FITEM,2,6
AL,P51X
FLST,2,4,5,ORDE,2
FITEM,2,1
FITEM,2,-4
AGLUE,P51X
WPSTYLE,,,,,,,,0
LPLOT
FLST,5,3,4,ORDE,3
FITEM,5,2
FITEM,5,7
FITEM,5,12
CM,_Y,LINE
LSEL, , , ,P51X
CM,_Y1,LINE
```

```
CMSEL,,_Y
!*
LESIZE,_Y1, , ,80, , , , ,1
!*
FLST,5,3,4,ORDE,2
FITEM,5,3
FITEM,5,-5
CM,_Y,LINE
LSEL, , , ,P51X
CM,_Y1,LINE
CMSEL,,_Y
!*
LESIZE,_Y1, , ,40, , , , ,1
!*
FLST,5,3,4,ORDE,3
FITEM,5,1
FITEM,5,6
FITEM,5,11
CM,_Y,LINE
LSEL, , , ,P51X
CM,_Y1,LINE
CMSEL,,_Y
!*
LESIZE,_Y1, , ,20, , , , ,1
!*
FLST,5,3,4,ORDE,2
FITEM,5,8
FITEM,5,-10
CM,_Y,LINE
LSEL, , , ,P51X
CM,_Y1,LINE
CMSEL,,_Y
!*
LESIZE,_Y1, , ,20, , , , ,1
!*
MSHAPE,0,2D
MSHKEY,1
!*
FLST,5,4,5,ORDE,2
FITEM,5,1
FITEM,5,-4
CM,_Y,AREA
ASEL, , , ,P51X
CM,_Y1,AREA
CHKMSH,'AREA'
CMSEL,S,_Y
```

```
!*
AMESH,_Y1
!*
CMDELE,_Y
CMDELE,_Y1
CMDELE,_Y2
!*
SAVE
FINISH
/SOLU
!*
FLST,2,3,4,ORDE,3
FITEM,2,2
FITEM,2,5
FITEM,2,10
DL,P51X, ,SYMM

FLST,3,1,1
FITEM,3,2961
MONITOR,VAR1,P51X,UX
FLST,3,1,1
FITEM,3,2961
MONITOR,VAR2,P51X,UY
FLST,3,1,1
FITEM,3,2961
MONITOR,VAR3,P51X,FY
FINISH
/POST1
FINISH
/SOLU
!*
TIME,0
AUTOTS,-1
NSUBST,5,25,3,1
KBC,0
!*
TSRES,ERASE
FLST,2,2,4,ORDE,2
FITEM,2,11
FITEM,2,-12
/GO
!*
SFL,P51X,PRES,-30,
/STATUS,SOLU
SOLVE
EPLOT
```

```
FLST,2,2,4,ORDE,2
FITEM,2,11
FITEM,2,-12
/GO
!*
SFL,P51X,PRES,30,
/STATUS,SOLU
SOLVE
EPLOT
FLST,2,2,4,ORDE,2
FITEM,2,11
FITEM,2,-12
/GO
!*
SFL,P51X,PRES,-30,
/STATUS,SOLU
SOLVE
EPLOT
FLST,2,2,4,ORDE,2
FITEM,2,11
FITEM,2,-12
/GO
!*
SFL,P51X,PRES,30,
/STATUS,SOLU
SOLVE
EPLOT
FLST,2,2,4,ORDE,2
FITEM,2,11
FITEM,2,-12
/GO
!*
SFL,P51X,PRES,-80,
/STATUS,SOLU
!*
TIME,0
AUTOTS,-1
NSUBST,10,50,5,1
KBC,0
!*
TSRES,ERASE
/STATUS,SOLU
SOLVE
EPLOT
FLST,2,2,4,ORDE,2
FITEM,2,11
```

```
FITEM,2,-12
/GO
!*
SFL,P51X,PRES,80,
/STATUS,SOLU
SOLVE
!*
TIME,0
AUTOTS,-1
NSUBST,5,25,3,1
KBC,0
!*
TSRES,ERASE
EPLOT
FLST,2,2,4,ORDE,2
FITEM,2,11
FITEM,2,-12
/GO
!*
SFL,P51X,PRES,-30,
/STATUS,SOLU
SOLVE
EPLOT
FLST,2,2,4,ORDE,2
FITEM,2,11
FITEM,2,-12
/GO
!*
SFL,P51X,PRES,30,
/STATUS,SOLU
SOLVE
EPLOT
FLST,2,2,4,ORDE,2
FITEM,2,11
FITEM,2,-12
/GO
!*
SFL,P51X,PRES,-30,
/STATUS,SOLU
SOLVE
EPLOT
FLST,2,2,4,ORDE,2
FITEM,2,11
FITEM,2,-12
/GO
!*
```

```
SFL,P51X,PRES,30,
/STATUS,SOLU
SOLVE
EPLOT
FLST,2,2,4,ORDE,2
FITEM,2,11
FITEM,2,-12
/GO
!*
SFL,P51X,PRES,-30,
/STATUS,SOLU
SOLVE
EPLOT
FLST,2,2,4,ORDE,2
FITEM,2,11
FITEM,2,-12
/GO
!*
SFL,P51X,PRES,30,
/STATUS,SOLU
SOLVE
EPLOT
FLST,2,2,4,ORDE,2
FITEM,2,11
FITEM,2,-12
/GO
!*
SFL,P51X,PRES,-30,
/STATUS,SOLU
SOLVE
EPLOT
FLST,2,2,4,ORDE,2
FITEM,2,11
FITEM,2,-12
/GO
!*
SFL,P51X,PRES,30,
/STATUS,SOLU
SOLVE
EPLOT

FLST,2,2,4,ORDE,2
FITEM,2,11
FITEM,2,-12
/GO
!*
```

```
SFL,P51X,PRES,-100,
/STATUS,SOLU
!*
TIME,0
AUTOTS,-1
NSUBST,20,70,10,1
KBC,0
!*
TSRES,ERASE
/STATUS,SOLU
SOLVE
EPLOT
FLST,2,2,4,ORDE,2
FITEM,2,11
FITEM,2,-12
/GO
!*
SFL,P51X,PRES,100,
/STATUS,SOLU
SOLVE
!*

TIME,0
AUTOTS,-1
NSUBST,5,25,3,1
KBC,0
!*
TSRES,ERASE
EPLOT
FLST,2,2,4,ORDE,2
FITEM,2,11
FITEM,2,-12
/GO
!*
SFL,P51X,PRES,-30,
/STATUS,SOLU
SOLVE
EPLOT
FLST,2,2,4,ORDE,2
FITEM,2,11
FITEM,2,-12
/GO
!*
SFL,P51X,PRES,30,
/STATUS,SOLU
SOLVE
```

```
EPLOT
FLST,2,2,4,ORDE,2
FITEM,2,11
FITEM,2,-12
/GO
!*
SFL,P51X,PRES,-30,
/STATUS,SOLU
SOLVE
EPLOT
FLST,2,2,4,ORDE,2
FITEM,2,11
FITEM,2,-12
/GO
!*
SFL,P51X,PRES,30,
/STATUS,SOLU
SOLVE
EPLOT
FLST,2,2,4,ORDE,2
FITEM,2,11
FITEM,2,-12
/GO
!*
SFL,P51X,PRES,-30,
/STATUS,SOLU
SOLVE
EPLOT
FLST,2,2,4,ORDE,2
FITEM,2,11
FITEM,2,-12
/GO
!*
SFL,P51X,PRES,30,
/STATUS,SOLU
SOLVE
EPLOT
FLST,2,2,4,ORDE,2
FITEM,2,11
FITEM,2,-12
/GO
!*
SFL,P51X,PRES,-30,
/STATUS,SOLU
SOLVE
EPLOT
```

```
FLST,2,2,4,ORDE,2
FITEM,2,11
FITEM,2,-12
/GO
!*
SFL,P51X,PRES,30,
/STATUS,SOLU
SOLVE
EPLOT

FINISH
/POST1
FINISH
/POST26

FORCE,TOTAL
SHELL,TOP
LAYERP26,0
ESOL,2,801,2961,S,Y,
!*
FORCE,TOTAL
SHELL,TOP
LAYERP26,0
ESOL,3,801,2961,EPEL,Y,
!*
FORCE,TOTAL
SHELL,TOP
LAYERP26,0
ESOL,4,801,2961,EPPL,Y,
!*
!*
ADD,5,3,4, , , , ,1,1,1,
VARNAM, ,
!*
/AXLAB,X,Total Strain(Elastic+Plasric)
/AXLAB,Y,Stress(FY)
!*
PLTIME,0,0
XVAR,5
SPREAD,0
PLCPLX,0
!*
PLVAR,2, , , , , , , , , ,
!*
FINISH
```

2. Stress intensity factor in 2-D modeling

```
/prep7
smart,off
/title,Fracture mechanics stress intnesity factor 2-D modeling
/com,
et,1,plane82,,,2
mp,ex,1,70e9
mp,nuxy,1,0.3
*set,a,0.004
*set,b,0.02
*set,c,0.005
*set,h,0.025
csys,0
k,1
k,2,b
k,3,b,h
k,4,-c,h
k,5,-c
l,1,2
l,2,3
lesize,2,,,16
l,3,4
lesize,3,,,16
l,4,5
lesize,4,,,24,0.2
l,5,1
esize,,,0.001
KSCON,1,0.00075,0,12
al,1,2,3,4,5
dl,1,1,symm
dl,4,1,symm
sfl,3,pres,-100e6
amesh,1
outpr,all
finish
/com
/output,scratch
/solu
solve
finish
/output
/post1
etable,sene,sene
etable,volu,volu
nsel,s,loc,y,0
```

```
nsel,r,loc,x,0
*get,nod1,node,,num,min
nsel,a,loc,y
nsel,r,loc,x,-0.000025,-0.000725
*get,nod2,node,,num,min
nsel,a,loc,y
nsel,r,loc,x,-0.000725,-0.000775
*get,nod3,node,,num,min
nsel,all
path,KI1,3,,48
ppath,1,nod1
ppath,2,nod2
ppath,3,nod3
kcalc,,,1
*get,KI1,kcalc,,k,1
*status
```

3. Stress intensity factor in 3-D modeling

```
/PREP7
SMART,OFF
/TITLE,FRACTURE MECHANICS STRESS INTENSITY-CRACK IN A FINITE WIDTH PLATE in 3-D modeling
antype,static
et,1,solid95
mp,ex,1,70e9
mp,nuxy,1,0.3
csys,1
*SET,a,0.0038
*SET,b,0.02
*SET,c,0.005
*SET,h,0.025
*SET,t,0.005
n,1
ngen,9,20,1
n,11,a
n,171,a,180
fill,11,171,7,31,20
csys,0
fill,1,11,9,2,1,9,20,3
n,15,b
n,75,b,h
fill,15,75,2,35,20
n,155,-c,h
fill,75,155,3,95,20
n,172,-c
```

```
fill,155,172,5,177,-1,,,.15
fill,11,15,3,,,7,20,3
ngen,2,200,1,177,,,,t
type,1
e,2,22,1,1,202,222,201,201
egen,8,20,-1
e,2,3,23,22,202,203,223,222
egen,8,20,-1
egen,9,1,-8
egen,5,1,73,78
e,171,151,173,172,371,351,373,372
e,151,131,174,173,351,331,374,373
e,131,132,175,174,331,332,375,374
egen,3,1,-1
e,134,135,155,177,334,335,355,377
SAVE
nsel,s,loc,x,-c
dsym,symm,x
nsel,s,loc,x,0,b
nsel,r,loc,y,0
dsym,symm,y
nsel,s,loc,x,-c,b
nsel,r,loc,z,0
d,all,uz
nsel,s,loc,y,h
sf,all,pres,-100e6
nsel,all
esel,all
finish
/output,scratch
/solu
solve
finish
/output
/post1
etable,sene,sene
etable,volu,volu
path,ki1,3,,48
ppath,1,1
ppath,2,163
ppath,3,168
kcalc,,,1
*get,ki1,kcalc,,k,1
*status
```

APPENDIX A2: COPIES OF THE PAPER PUBLISHED

(1) "**Finite Element Analysis on the Influence of Overload Induced Residual Stress Field on Fatigue Crack Growth in Aluminum Alloy**", Dr. M.A. Wahab and J.H. Park, 10th ICCE conference in New Orleans, July 20-26, 2003.

(2) "**Experimental Study on the Influence of Overload Induced Residual Stress Field on Fatigue Crack Growth in Aluminum Alloy",** Dr. M.A. Wahab, G.R. Rohrsheim and J.H. Park, Journal of Material Processing Technology, AMPT 2003-Paper#357 in Dublin, Ireland, July 8-11, 2003.

(3) "**Effects of Overload and Corrosion Preventatives on Fatigue Life in Aluminum Alloy**", Dr. M. A. Wahab and J.H. Park, 11th ICCE conference in S. Carolina, August 8-14, 2004 (Manuscript Submitted).

VITA

Jinhee Park was born on June 30th, 1977, in South Korea. He received the degree of Bachelor of Engineering in College of Engineering from the Division of Mechanical Engineering at Andong National University, located in Andong, South Korea, in February of 2001. He worked for Language Technology in Seoul, South Korea, from March 2002 to June 2002. In August 2002, he began graduate school for a study of fracture mechanics, stress analysis, finite element analysis and fatigue analysis in the Department of Mechanical Engineering at Louisiana State University (LSU) in Baton Rouge. On completion of Louisiana State University requirements, he is expected to receive the degree of Master of Science in Mechanical Engineering from LSU in August 2004.